

THRESHOLD RESUMMATION STUDIES FOR
POLARIZED AND UNPOLARIZED HIGH- p_T HADRON
PRODUCTION AT COMPASS



Dissertation

zur Erlangung des
Doktorgrades der Naturwissenschaften
(Dr. rer. nat)
der Fakultät für Physik der
Universität Regensburg

vorgelegt von
Claudia Uebler
aus Vilshofen

im Jahr 2019

Die Arbeit wurde von Prof. Dr. Andreas Schäfer angeleitet.

Das Promotionsgesuch wurde am 22. Januar 2019 eingereicht.

Prüfungsausschuss:

Vorsitzender: Prof. Dr. C. Schüller

1. Gutachter: Prof. Dr. A. Schäfer

2. Gutachter: Prof. Dr. W. Vogelsang

Weiterer Prüfer: Prof. Dr. K. Richter

To all women in science. And to all those, who never had a chance.

Abstract

This thesis is focused on threshold resummation studies for high- p_T inclusive-hadron production in longitudinally polarized lepton-nucleon scattering $\mu N \rightarrow \mu' h X$ at COMPASS. The goal is to address threshold resummation effects to double-longitudinal spin asymmetries at COMPASS kinematics. At these kinematics, nearly all available energy is used for the production of the high- p_T parton and its recoiling counterpart. In that case, the phase space for additional radiation of partons becomes small, resulting in large logarithmic QCD corrections at every order in perturbation theory. These logarithmic contributions spoil the perturbative expansion, and thus have to be resummed. Using threshold resummation techniques in Mellin momentum N space, we are able to deal with those logarithmic corrections up to all perturbative orders in α_s at a certain logarithmic level. In our calculations we choose next-to-leading logarithmic accuracy. Further, we develop a framework to include subleading $1/N$ -suppressed logarithms into future calculations.

In our phenomenological results for COMPASS we present a detailed study of the impact of next-to-leading logarithmic threshold resummation on the spin-dependent cross section and on the corresponding double-longitudinal spin asymmetry A_{LL} for the high- p_T photoproduction process $\mu N \rightarrow \mu' h X$. We include resummation for the direct, as well as for the resolved-photon contribution. In a comparison of the spin-averaged with the spin-dependent cross sections we find out that the latter receives smaller corrections from resummation than the spin-averaged one, indicating that threshold corrections do not cancel in the double-spin asymmetry and rather tend to decrease it, yielding an overall better agreement between experiment and theory.

Finally, we reveal that the parton-to-hadron fragmentation functions have a strong impact on the size and shape of the predicted spin asymmetries.

Contents

1. Introduction	1
2. Foundations of Perturbative Quantum Chromodynamics	7
2.1. Lagrangian of Quantum Chromodynamics	7
2.2. The Group $SU(3)$	9
2.3. Asymptotic Freedom and the Running Coupling	9
2.4. Regularization and Renormalization	12
3. Parton Distribution and Fragmentation Functions	15
3.1. Factorization Theorem	15
3.2. Parton Distribution and Fragmentation Functions	17
3.3. Parton Structure of the Photon	21
4. Foundations of Threshold Resummation	25
4.1. Exponentiation for (Non-)Abelian Gauge Theories	26
4.1.1. Exponentiation of Soft Photons	26
4.1.2. Exponentiation of Soft Gluons	28
4.2. Phase Space Factorization in Mellin Moment Space	33
4.3. Threshold Resummation in Mellin Space	34
4.4. Threshold Corrections for Single-Particle Inclusive Cross Section	36
4.4.1. Refactorization	37
4.4.2. Radiative Factors	40
5. Threshold Resummation for Single-Inclusive Hadron Production	45
5.1. Theoretical Framework	46
5.2. Transformation to Mellin Moment Space	51
5.3. NLL-Resummed Hard-Scattering Function	52
5.3.1. Exponents at NLL	55
5.3.2. Hard- and Soft-Matrices	57
5.4. NLO Calculation	60
5.5. Extraction of the Coefficients	63
5.6. Inverse Mellin Transform and Matching Procedure	63
5.7. Double-Spin Asymmetry	64
6. Subleading Contributions	67
6.1. Formalism to Calculate Subleading Mellin-Contributions	67
6.2. Subleading Logarithms for NLO Cross Sections	71
6.3. Subleading Logarithms for Threshold Resummation	80

7. Phenomenological Results for COMPASS	85
7.1. Polarized and Unpolarized Resummed Cross Sections	87
7.1.1. Polarized Unidentified Hadron Production from a Deuteron	87
7.1.2. Pion and Kaon Production	94
7.2. Double-Spin Asymmetry	96
8. Conclusion and Outlook	103
A. Feynman Rules	107
B. Hard, Soft and Γ-Matrices	111
B.1. Soft Matrices	111
B.2. Anomalous Dimension Matrices	112
B.3. Hard Matrices	113
C. Coefficients	117
Bibliography	119

Nothing in life is to be feared, it is only to be understood. Now is the time to understand more, so that we may fear less.

Marie Curie

1

Introduction

In the last 100 years knowledge of the proton structure has grown a lot. The story of the proton and with that its discovery starts with Rutherford's proof that the hydrogen nucleus is present in other nuclei [1]. Then, 1922 the idea of *spin* was introduced through the Stern-Gerlach experiment [2, 3] to construe the observations. That the proton is a spin-1/2 fermion was concluded five years later [4]. A series of experiments started to deepen the knowledge of the proton structure, and with that Hofstadter and McAllister made first measurements of the RMS radius for the charge and magnetic moment of protons in 1955 [5]. Then, in the 1960s, Ne'eman [6] and Gell-Mann [7] classified hadrons through the *Eightfold Way*, a SU(3) flavor symmetry. A quark model was introduced by Gell-Mann and Zweig [8] stating that hadrons were consisting of three quark types, named up, down and strange quarks, to which one referred properties as spin and electric charge. The experimental breakthrough followed in 1968, when a deep inelastic scattering (DIS) experiment at the Stanford Linear Accelerator Center (SLAC) discovered that protons and neutrons are indeed built up by smaller constituents called partons. All the developments of experimental and theoretical work in the 1960's and 1970's led finally to the theory of Quantum Chromodynamics (QCD) as we know it today. With that, one is able to describe the dynamics of quark and gluon constituents in the hadrons. QCD, as a non-abelian quantum field theory, describes the strong interaction using the concept of color charged quarks and gluons. It is part of the standard model and exhibits the crucial properties of asymptotic freedom and confinement, whereby quarks are bound strongly in the hadrons at larger distances and behave asymptotically free at short distances. However, there are still open questions left.

A lot of effort has been applied to find answers to the question of how the gluon and quark spins and orbital angular momenta combine to generate the nucleon spin of 1/2. The familiar assumption that protons are made up of two *u* and one *d* quark constituents gen-

erate a naively expectation that the quarks carry about a third of the proton momentum. However, the proton structure and momentum distribution is another one, as protons contain additional gluons and low-momenta quarks and antiquarks called sea quarks. Lattice QCD even states that the proton mass is largely determined by the binding energy of the gluons. How the total proton spin is distributed among its quark, antiquark and gluon constituents, among the polarizations and angular momenta, is still an outstanding question. Measurements from the EMC experiment [9] in the 1980s mark the starting point of the so-called “proton spin crisis”, where a series of experiments provided increasingly precise results, revealing the surprising discovery that only about 30% of the nucleon spin is built up from the polarization of quarks and anti-quarks combined. While lattice calculations [10] give rise to the assumption that the missing 70% is not provided by the quark orbital angular momentum alone, RHIC [11, 12], a polarized proton-proton collider, even indicates that the gluon polarization contributes significantly to the total spin. The proton helicity sum rule [13–15] reads

$$\frac{1}{2} = \frac{1}{2}\Delta\Sigma + \Delta G + L_z^q + L_z^g, \quad (1.1)$$

where $1/2\Delta\Sigma = 1/2 \int_0^1 dx [\Delta u + \Delta\bar{u} + \Delta d + \Delta\bar{d} + \Delta s + \Delta\bar{s}] (x)$ denotes the quark spin contribution and $L_z^q + L_z^g$ labels the total orbital angular momenta of quarks and gluons. Further, integrating the gluon distribution $\Delta g(x)$ over all momentum fractions x (and summing over flavors), we obtain the gluon spin contribution $\Delta G = \int_0^1 dx \Delta g(x)$. This highlights that Δg is a key ingredient for solving the proton spin puzzle. One of the main tools to gain information about the gluon distribution are the *spin asymmetries*, which are directly sensitive to Δg . The COMPASS experiment [16, 17], short for *Common Muon and Proton Apparatus for Structure and Spectroscopy*, at the *Super Proton Synchrotron* SPS, considers semi-inclusive hadron production of the type

$$\mu N \rightarrow \mu' h X. \quad (1.2)$$

COMPASS has already presented results for the spin-averaged cross section a while ago [18] and more recently also data for the corresponding double-longitudinal spin asymmetry A_{LL} [19, 20]. In these reactions the hard scale is set by the transverse momentum of the produced hadron which is for COMPASS kinematics much smaller than for $\Delta g(x, Q^2)$ determinations by, e.g. inclusive jet and di-jet production at RHIC, see [12]. Both sets of experiments are complementary as one needs a large kinematic reach to analyze the evolution of polarized parton distributions. High precision is needed, as the systematic theoretical uncertainties of the analyses has to be much smaller than the experimental uncertainties. If the theoretical framework is adequate for describing the photoproduction $\gamma N \rightarrow h X$ in the kinematic regime relevant at COMPASS, analyzing the data may give reliable information on Δg . Hard photoproduction processes are well understood,

in particular the connection between *direct* and *resolved* photon contributions [21]. The quasi-real photon can interact on the one hand as pointlike particle coupling *directly* with a parton from the nucleon, on the other hand it can be *resolved* into its partonic content and it can couple through quantum fluctuations containing quarks, antiquarks and gluons. However, *threshold resummation*, which is required at COMPASS kinematics [22], is an additional feature which is less standard. For large enough transverse momentum of the observed hadron, perturbative methods and in particular threshold resummation techniques can be applied. The theoretical calculations start at order $\mathcal{O}(\alpha\alpha_s)$, which is thus what we mean with Leading Order (LO), with the electromagnetic and strong coupling constants α and α_s , while next-to-leading order (NLO) means $\mathcal{O}(\alpha\alpha_s^2)$. NLO QCD corrections without resummation are presented for the double-spin asymmetry in Refs. [23–25]. However, for COMPASS kinematics whereat one is close to kinematic threshold, large QCD corrections appear. The reason is that nearly all available energy is used for the production of the high- p_T parton and its recoiling counterpart. Then, the phase space for additional radiation of partons becomes small, and after the incomplete cancelation of infrared divergences between real and virtual diagrams large logarithmic corrections can be observed at every order in perturbation theory [26, 27], starting at NLO. At n -th order logarithmic corrections up to

$$\alpha_s^n \left[\frac{\ln^{2n-1}(1-z)}{1-z} \right]_+, \quad (1.3)$$

appear and are accompanied by lower, subleading powers of logarithms. Here, z labels the threshold region, hence when $z \rightarrow 1$ no further energy is left for additional radiation.

In every higher order of perturbation theory two additional powers of these logarithms emerge and spoil the perturbative expansion [28]. Thus, these threshold logarithms cannot be neglected and require to be resummed to all orders of perturbation theory [29–36]. Using the techniques of threshold resummation we include logarithms in our following calculations up to next-to-leading logarithmic (NLL) accuracy, containing the three leading “towers” $\alpha_s^n [\ln^{2n-1}(1-z)/(1-z)]_+$ at leading-logarithmic (LL) accuracy, as well as $\alpha_s^k [\ln^{2n-2}(1-z)/(1-z)]_+$, and further $\alpha_s^n [\ln^{2n-3}(1-z)/(1-z)]_+$ at NLL.

With this technique at hand we want to study the semi-inclusive photoproduction process $\mu N \rightarrow \mu' hX$ with hadron production at high transverse momentum p_T for both cases, direct and resolved photons, calculating spin-dependent threshold resummed cross sections involving longitudinally polarized nucleons and photons. This denotes an extension to the calculations of Ref. [22], where the unpolarized cross sections have been calculated using threshold resummation methods. There, one could find that the resummed cross section shows a markedly better agreement with the experimental results than the next-to-leading order one.

Although resolved subprocesses show an equivalent structure to hadronic scattering $pp \rightarrow hX$ which has been already investigated even for the spin-dependent case, see Ref. [27],

we will use a different framework. Ref. [27] integrates over all rapidities of the produced hadron, and therefore the cross section takes, after a transformation into Mellin moment space, the form of a complete convolution with parton distribution functions. Contrary to that we will perform in the following threshold resummation at arbitrary fixed rapidity, using techniques developed in [22, 37]. This implies that only the resummed cross section convoluted with the fragmentation function is transformed into Mellin- N space, however, the parton distribution functions stay in physical space. Our main goal is then the study of the double-longitudinal spin asymmetry A_{LL} at COMPASS kinematics, and in this instance the investigation of the relevance of higher-order QCD threshold corrections. For that we compare our theoretical calculations with the experimental results of COMPASS [19, 20]. Note that there have been assumptions that higher-order perturbative corrections cancel in the ratios of spin-dependent and spin-averaged cross sections, i.e. for spin asymmetries,

$$A_{LL} = \frac{d\Delta\sigma}{d\sigma}. \quad (1.4)$$

However, as we will see, this assumption is incorrect and higher-order threshold corrections cannot be neglected for the calculation of A_{LL} .

The thesis is organized as follows. In Chap. 2 we give a short overview of the principles of perturbative Quantum Chromodynamics. However, we refer to some standard textbooks or reviews for more details. Then, as factorization is a main ingredient for our following calculation, we will investigate in Chap. 3 the underlying ideas and illuminate further parton distribution and fragmentation functions. With that we will also shed light on the parton structure of the photon which will be needed for the resolved photon contributions. After this we are ready to review the foundations of threshold resummation in Chap. 4. We will start with an exponentiation formula for (non-)abelian gauge theories, focusing first on photons and then on gluons. This is followed by an introduction into the Mellin moment space, which is necessary for threshold resummation. We want then proceed with an explicit derivation of the radiative resummation exponents. For that, refactorization will be the underlying technique. These exponents will be needed in Chap. 5, when we arrive at the threshold resummation for single-inclusive hadron production at COMPASS. In this chapter, the theoretical framework is given, and besides the formula of the resummed hard-scattering function at next-to-leading logarithmic order, we will also consider the fixed-order case. With the help of a matching procedure we will then include full NLO results in our theoretical results, to provide highest available precision. While we are restricting ourselves for our phenomenological studies at next-to-leading logarithmic level neglecting $1/N$ -suppressed logarithms, we investigate in Chap. 6 a framework, how to compute those subleading contributions and provide them explicitly for the fixed-order calculation. Further we show which terms in the threshold resummed calculation could generate $\ln N/N$ terms. Our phenomenological results for COMPASS will then be shown

in Chap. 7 and our double-longitudinal spin asymmetries will be compared with the experimental data. We will compare our results for different fragmentation function sets and consider protons and deuterons as targets. Studying the role of higher-order QCD corrections at kinematic threshold and comparing the unpolarized with the polarized calculated cross sections, we find important conclusions concerning the double-longitudinal spin asymmetry. Finally, in Chap. 8 we finish the thesis with a conclusion and an outlook. In addition to that, an appendix is available with further details.

Note that parts of our studies are already published and can be found in our papers [38] and [39], however, the detailed calculations and many details are provided in the following.

Love of learning is the most necessary passion... in it lies our happiness. It's a sure remedy for what ails us, an unending source of pleasure.

Émilie du Châtelet

2

Foundations of Perturbative Quantum Chromodynamics

In this chapter we want to introduce the main basics of perturbative Quantum Chromodynamics (QCD), serving as a starting point for the calculations in the following chapters. As this overview will be rather short, we point to some standard text books [40–43] or to Ref. [44] for further details. In the following we want to give a brief review of the Lagrangian of QCD, which is essential to derive the Feynman rules given in the Appendix A.

2.1. Lagrangian of Quantum Chromodynamics

Quantum Chromodynamics (QCD) is a non-abelian gauge theory describing the strong force which is one of the four fundamental forces. It is part of the Standard Model and describes the interaction between quarks and gluons, which carry *color*. The gauge invariant Lagrangian,

$$\begin{aligned} \mathcal{L} &= \sum_f^{N_f} \bar{\Psi}_{f,a} (i\gamma^\mu \partial_\mu \delta_{ab} - g\gamma^\mu t_{ab}^C A_\mu^C - m_f \delta_{ab}) \Psi_{f,b} - \frac{1}{4} F_{\mu\nu}^A F^{A\mu\nu} + \mathcal{L}_{gf} + \mathcal{L}_{FP} \quad (2.1) \\ &= \underbrace{\sum_f^{N_f} \bar{\Psi}_f (i\mathcal{D} - m_f) \Psi_f}_{\mathcal{L}_{cl}} - \frac{1}{4} F_{\mu\nu}^A F^{A\mu\nu} + \mathcal{L}_{gf} + \mathcal{L}_{FP}, \end{aligned}$$

is invariant under Lorentz transformations and describes how quarks interact with each other by exchanging gluons, the latter of which are massless gauge bosons building up an octet in the adjoint representation of SU(3). It consists of the *classical* Lagrangian \mathcal{L}_{cl} , a

gauge-fixing part \mathcal{L}_{gf} and a *Faddeev-Popov ghost* part \mathcal{L}_{FP} . In \mathcal{L}_{cl} , $\Psi_{f,a}$ denotes the field spinors for quarks with flavor f , mass m_f and color a , with a running from 1 to $N_c = 3$. Further the covariant derivative is

$$D_\mu = \partial_\mu - ig t^C A_\mu^C. \quad (2.2)$$

Repeated indices are understood to be summed over and the Dirac matrices γ_μ satisfy the Dirac algebra, an anti-commutation relation reading

$$\{\gamma^\mu, \gamma^\nu\} = 2g^{\mu\nu}. \quad (2.3)$$

The field strength tensor,

$$F_{\mu\nu}^A = \partial_\mu A_\nu^A - \partial_\nu A_\mu^A - gf_{ABC} A_\mu^B A_\nu^C, \quad (2.4)$$

is constructed from the gluon fields A_μ^A , where A runs from 1 to $N_c^2 - 1 = 8$. The term $-\frac{1}{4}F_{\mu\nu}^A F^{A\mu\nu}$ describes their self-interaction as gluons carry color themselves, and differs from the field strength tensor of QED by the last term $gf_{ABC} A_\mu^B A_\nu^C$, which gives rise to the three- and four-gluon interaction. The f_{ABC} are the structure constants of the SU(3) group and g is the strong coupling constant. With f_{ABC} and the eight independent generators t^A of the SU(3) group, which correspond to 3×3 hermitian matrices, the Lie algebra is defined through the commutation relation

$$[t^A, t^B] = if_{ABC} t^C. \quad (2.5)$$

Gluon emission from a quark can be identified with the color factor $C_F \equiv (N_c^2 - 1)/(2N_c) = 4/3$, which is given by the relation $t_{ab}^A t_{bc}^A = C_F \delta_{ac}$. Further, gluon emission from a gluon is associated with the color factor $C_A = N_c = 3$, which can be found in $f^{ABC} f^{BCD} = C_A \delta_{AD}$, and finally we have the color factor $T_R = 1/2$ when a gluon splits into a quark-antiquark pair given in $t_{ab}^A t_{ab}^B = T_R \delta_{AB}$. What is still missing is on the one side the gauge-fixing term \mathcal{L}_{gf} , and on the other side the ghost-field term \mathcal{L}_{FP} . The necessity for Faddeev-Popov ghosts follows from the quantization of the classical Lagrangian. For the specific gauge $\partial_\mu A^{A\mu} = 0$, the gauge fixing term is given by

$$\mathcal{L}_{gf} = -\frac{1}{2\xi} (\partial_\mu A^{A\mu}) (\partial_\nu A^{A\nu}). \quad (2.6)$$

Here, the parameter ξ can be chosen freely without changing the physical results, which are independent of the gauge used in a calculation. A common choice is the Feynman (or Feynman-t'Hooft) gauge, where the gauge parameter is $\xi = 1$. These additional ghost fields χ^A have to be introduced to solve an overcounting issue in the quantization of the

theory. Their Lagrangian reads for the gauge $\partial_\mu A^{A\mu} = 0$:

$$\mathcal{L}_{FP} = gf_{ABC}\bar{\chi}^A\partial^\mu(A_\mu^C\chi^B) - \bar{\chi}^A\partial^\mu\partial_\mu\chi^A. \quad (2.7)$$

Note that Faddeev-Popov ghost fields do not describe physical particles and have their own Feynman rules.

2.2. The Group SU(3)

Let us now go on to classify Quantum Chromodynamics in a bit more mathematical way. It is a SU(3) gauge theory and part of the SU(3) \times SU(2) \times U(1) Standard Model, where SU(2) \times U(1) represents the unification of the weak interaction and the electromagnetic interaction. In the former leptons interact via three massive gauge bosons (W^\pm and Z^0) whereas the electromagnetic force is mediated by massless photons. In the case of the group SU(3) = SU(3)_{color} of QCD, one finds $N_c^2 - 1 = 8$ massless gauge bosons, the gluons which appear in different so called colors. In contrast to the photon in QED which is a neutral spin-1 particle carrying no electrical charge, the gluons themselves carry color charge and can thus interact with each other. The gluons are described by eight vectors A_μ^A in the adjoint representation of SU(3) and are therefore said to make up an octet. Quarks are described through spinors in the fundamental representation and build up a triplet. The independent color states of the gluons are superpositions of different color-anticolor states and read:

$$\begin{aligned} (r\bar{b} + b\bar{r})/\sqrt{2}, & & -i(r\bar{b} - b\bar{r})/\sqrt{2}, \\ (r\bar{g} + g\bar{r})/\sqrt{2}, & & -i(r\bar{g} - g\bar{r})/\sqrt{2}, \\ (b\bar{g} + g\bar{b})/\sqrt{2}, & & -i(b\bar{g} - g\bar{b})/\sqrt{2}, \\ (r\bar{r} + b\bar{b})/\sqrt{2}, & & (r\bar{r} + b\bar{b} - 2g\bar{g})/\sqrt{6}. \end{aligned} \quad (2.8)$$

The eight generators of SU(3) are related to the Gell-Mann matrices, a set of hermitian, traceless matrices collected in [43]:

$$t^A = \frac{\lambda^A}{2}. \quad (2.9)$$

The consequences of the gluon self-interaction will be discussed in the next section.

2.3. Asymptotic Freedom and the Running Coupling

Free partons that means quarks and gluons, have never been observed experimentally. Unlike in QED where the elementary particles described by the Lagrangian can be observed directly, quarks and gluons are always bound in color singlet states referred to as hadrons.

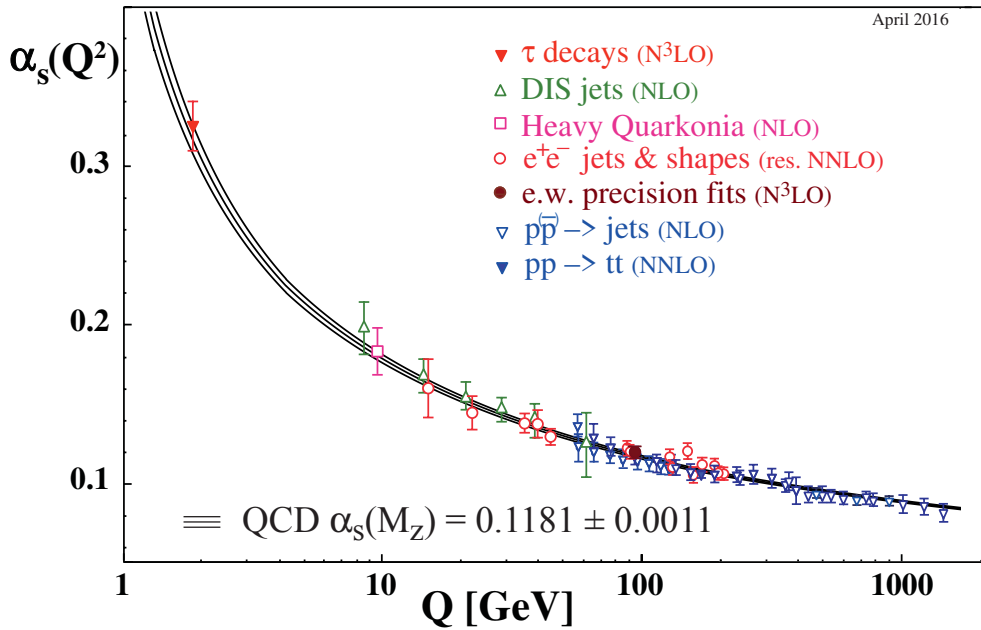


Fig. 2.1.: The coupling constant $\alpha_s(Q)$ at an energy scale Q from different measurements. The used perturbative order is declared in the brackets, with NLO standing for next-to-leading order, and res. NNLO standing for next-to NLO matched with resummed next-to-leading logarithms. The figure is taken from Ref. [44].

In the following this feature will be discussed a bit more detailed following Refs. [44–46]. The self-interaction of gluons yields a gluon vacuum polarization, resulting in *asymptotic freedom*. This means that partons, which are *confined* inside the “colorless” hadron, are treated to be asymptotically *free* in the asymptotic limit, so that perturbative methods are applicable. There, the coupling constant g or $\alpha_s = \frac{g^2}{4\pi}$, as one of the most fundamental parameters of this theory, decreases as the distance between two fields decreases, or in other words, decreases with increasing momentum transfer, see Fig. (2.1), taken from Ref. [44]. More precisely, the coupling constant can be written as a *running coupling* in terms of the β -function, satisfying the renormalization group equation (RGE):

$$\mu_r \frac{d\alpha_s(\mu_r)}{d\mu_r} = \beta(\alpha_s(\mu_r)) = -(b_0\alpha_s^2 + b_1\alpha_s^3 + b_2\alpha_s^4 + \dots), \quad (2.10)$$

with the first three coefficients of the β -function collected in [45],

$$\begin{aligned} b_0 &= \frac{11C_A}{12\pi} - \frac{N_f T_R}{3\pi} = \frac{33 - 2N_f}{12\pi}, \\ b_1 &= \frac{1}{24\pi^2} (17C_A^2 - 10T_R C_A N_f - 6T_R C_F N_f) = \frac{153 - 19N_f}{24\pi^2}, \\ b_2 &= \frac{77139 - 15099N_f + 325N_f^2}{3456\pi^3}. \end{aligned} \quad (2.11)$$

While the coefficients b_0 and b_1 are independent of the renormalization scheme, all higher-order terms have a scheme-dependence. We adopt the $\overline{\text{MS}}$ scheme, where terms containing γ_E and $\ln(4\pi)$ are subtracted, which appear together with the $(1/\epsilon)$ -poles in dimensional regularization [40]. Note that the negative sign in the β -function in Eq. (2.10) reflects the origin for asymptotic freedom: in hard processes, where the momentum transfer is large, the strong coupling becomes weak. This remains true as long as $N_f < 17$, when b_0 changes its sign. Having a prediction for $\alpha_s(\mu_r)$ at a given scale μ_r , one is able to determine the value of $\alpha_s(\mu)$ at any other scale. The behaviour described by Eq. (2.10) is an essential feature of the theory which makes it possible to use perturbation theory for the calculation of high energetic QCD processes. The main idea behind this is an expansion of physical observables in terms of the strong coupling which becomes small at high energies such that higher order terms can be neglected. Solving the differential equation in (2.10) exactly and analytically can only be done by neglecting all terms in the β -function except b_0 and b_1 . This yields:

$$\alpha_s(\mu^2) = \frac{1}{b_0 \ln(\mu^2/\Lambda_{QCD})}. \quad (2.12)$$

Here, Λ_{QCD} is an integration constant which can be thought of as marking the transition between perturbative and non-perturbative scales. In particular at $\mu = \Lambda_{QCD}$ Eq. (2.12) diverges, marking the breakdown of perturbation theory. Approximate analytical solutions can be found even at 5-loop order, including b_5 . A 3-loop solution, truncating all terms higher than b_3 is reviewed in [44],

$$\begin{aligned} \alpha_s \simeq \frac{1}{b_0 L} & \left(1 - \frac{b_1 \ln L}{b_0^2 L} + \frac{b_1^2 (\ln^2 L - \ln L - 1) + b_0 b_2}{b_0^4 L^2} \right. \\ & \left. - \frac{b_1^3 (\ln^3 L - \frac{5}{2} \ln^2 L - 2 \ln L + \frac{1}{2}) + 3b_0 b_1 b_2 \ln L - \frac{1}{2} b_0^2 b_3}{b_0^6 L^3} \right) + \mathcal{O}\left(\frac{1}{L^5}\right), \end{aligned} \quad (2.13)$$

with $L \equiv \ln(\mu^2/\Lambda_{QCD})$. Then, we can also express the coupling at a given scale k^2 in

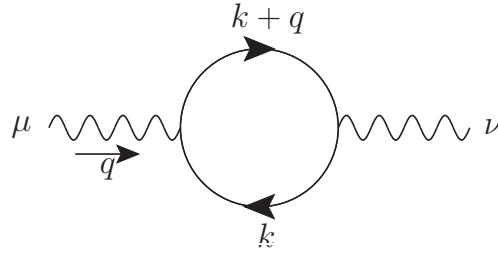


Fig. 2.2.: Virtual electron-positron pair production from the vacuum polarization of a photon.

terms of the coupling at scale μ^2 , reading at first loop order:

$$\alpha_s(k^2) = \frac{\alpha_s(\mu^2)}{1 + b_0 \alpha_s(\mu^2) \ln\left(\frac{k^2}{\mu^2}\right)} \left[1 - \frac{b_1}{b_0} \frac{\alpha_s(\mu^2)}{1 + b_0 \alpha_s(\mu^2) \ln\left(\frac{k^2}{\mu^2}\right)} \ln\left(1 + b_0 \alpha_s(\mu^2) \ln\left(\frac{k^2}{\mu^2}\right)\right) \right]. \quad (2.14)$$

2.4. Regularization and Renormalization

In the next section we want to introduce theoretical methods for higher-order calculations, in which unphysical divergent expressions appear. We distinguish between so called *infrared divergences* (IR) appearing in the low-momentum range, when $k \rightarrow 0$, and *ultraviolet divergences* in the high-momentum region, when $k \rightarrow \infty$. Further, there are collinear singularities generated by collinear emissions. At this point we will briefly discuss how these divergent contributions can be handled consistently and refer to Refs. [40–43, 47] for more details.

Once an emitted parton has momentum $k \rightarrow 0$, infrared or soft singularities appear. Those divergences cancel when all contributions or diagrams of a given process or observable are summed up, in particular they cancel against bremsstrahlung diagrams where additional final photons or gluons with soft momentum are emitted. As soft radiation cannot be observed, the cross section for soft emissions is typically added to the one without soft radiation such that these soft singularities cancel, resulting in a divergence free, infrared safe, cross section.

Collinear singularities arising from the collinear emission of partons off initial or final-state partons are factorized into the bare parton distribution or fragmentation functions. We will come later in Chap. 3 to this point.

Further, there are ultraviolet divergences, arising for example in the vacuum polarization of a photon, see Fig. (2.2). A virtual electron-positron pair is produced, so that

$$i\Pi_2^{\mu\nu}(q) \propto \int \frac{d^4k}{(2\pi)^4} \frac{1}{(k^2 - m^2)((k+q)^2 - m^2)}. \quad (2.15)$$

The internal loop momentum is not fixed and can be of arbitrary size. Therefore one integrates over the momentum and divergences appear in the upper ultraviolet integration limit. These ultraviolet divergences can be removed order by order by a modification of bare parameters called *renormalization*. However, before we can treat those contributions with the right procedure, we first have to isolate them. This method is called *regularization*. Introducing a regulator, we may regularize the divergences by a modification of the momentum integrals yielding a finite result. This result reproduces the original divergences in a certain limit. Afterwards we can perform renormalization, absorbing the divergent part into the definitions of the respective parameters. We claim a regularization method to respect Lorentz invariance and gauge symmetry, hence, a possible regularization scheme is *dimensional regularization*, introduced by [48] and [49]. The main idea here is to extend the usual four-dimensional space-time integral over loop momenta $\int d^4k/(2\pi)^4$, which is divergent, into a $D = 4 - \epsilon$ dimensional integral $\int d^Dk/(2\pi)^D$ with a small parameter ϵ . The latter integral is then finite, as the original exponent in the integrand is larger than our new chosen spacetime dimension $D = 4 - \epsilon$, and thus the integral will be analytically continued. Besides the finite result we receive for a pole $\frac{1}{\epsilon}$, so that the integral can be separated into a finite and a pole part. This pole corresponds to a logarithmic divergence and comes always together with $\ln(4\pi) - \gamma_E$, where γ_E is the Euler-Mascheroni constant. By choosing a renormalization scheme, these poles are subtracted by absorbing them into redefined quantities in the Lagrangian, followed by taking the limit $D \rightarrow 4$. Keeping the dimension of the integrals unchanged, a new momentum scale μ_r arises to absorb the dimensional changes.

Note that some other regularization schemes like the Pauli-Villars-, Cut-off-, or the Lattice-Regularization are only named here, so for further details, we recommend [40]. As the *bare* quantities appearing in the non-renormalized Lagrangian, like mass, charge or normalization of the fields do not correspond to physical observables, a redefinition is necessary, such that a finite number of renormalization constants can cancel against all appearing divergences after inserting them into the Lagrangian. The redefined fields and parameters read then:

$$\begin{aligned}
\Psi_{f,bare} &\rightarrow Z_2^{1/2} \Psi_f, \\
A_{bare,\mu}^A &\rightarrow Z_3^{1/2} A_\mu^A, \\
\chi_{bare}^A &\rightarrow \tilde{Z}_3^{1/2} \chi^A, \\
g_{bare} &\rightarrow Z_g g, \\
m_{f,bare} &\rightarrow Z_m m_f, \\
\xi_{bare} &\rightarrow Z_3 \xi.
\end{aligned} \tag{2.16}$$

The $Z_2, Z_3, \tilde{Z}_3, Z_g$ and Z_m denote the renormalization constants for the gluon, quark and ghost fields, further for the coupling constant, the mass and the gauge fixing parameter.

Note that the subtraction of terms is not restricted on infinities only, so that there exist different renormalization schemes to absorb also finite contributions besides the UV pole. A common renormalization scheme is the *modified minimal subtraction* ($\overline{\text{MS}}$) scheme [50], where the ϵ -poles are removed with the accompanying constants $-\gamma_E + \ln(4\pi)$,

$$\frac{1}{\epsilon} - \gamma_E + \ln(4\pi). \quad (2.17)$$

This renormalization scheme will be used throughout this work. Note that the renormalized quantities and the renormalization constants Z_i depend on μ_r , an introduced renormalization scale. Including all orders of perturbation theory would yield a vanishing of μ_r , so that the considered result would be a scale-independent physical observable. However, as we are only able to calculate perturbative predictions at a certain order, we have to handle and investigate the renormalization scale dependence, to which we will come later in our phenomenological studies.

Finally, we want to make clear that despite the emergence of ultraviolet infinities Quantum Field Theory does not lose its predictive power. Note that it is only a low energy limit of a full theory including gravitational effects, which come into play at the Planck scale $E_{pl} \approx 10^{19}$ GeV. Thus, to include physics at or beyond the Planck scale we need an unification of gravity with the strong, weak and electromagnetic forces [40], however, as long as we consider physics at laboratory kinematics we should be allowed to neglect infinities coming from the high momentum range.

Life need not be easy, provided only that it is not empty.

Lise Meitner

3

Parton Distribution and Fragmentation Functions

In the following chapter we want to give a short overview of a main ingredient that enables us to apply perturbative methods to the calculation of the lepton-nucleon scattering cross section in this work. How to calculate high energy cross sections is reviewed in [51–55], where it is shown that the calculation of a hadronic cross section has to cope with a combination of both, short-distance and long-distance behaviour. In momentum space, long-distance contributions correspond to those with low momentum transfer. Therefore, a cross section of a certain hadronic process is not directly computable in perturbative QCD, but has to be split up into the perturbative short-distance terms and the non-perturbative long-distance parts. While we will see in Chap. 4 how to calculate the perturbative partonic cross section with the help of threshold resummation, we dedicate ourselves in the following section to the examination of *parton distribution functions* (PDFs) and the *fragmentation functions* (FFs). For that purpose we first need to introduce a factorization theorem.

3.1. Factorization Theorem

Factorization is a main ingredient for the calculations of this work, as well as for a lot of other computations in Quantum Chromodynamics. With this tool at hand, we are able to separate long-distance terms from short-distance terms and to apply perturbative methods. Furthermore we have to deal with collinear singularities stemming from collinear emission of massless partons coming from external state partons. These singularities are removed from the partonic cross section by absorbing them into the *bare* parton distribution or fragmentation functions. Note that all those PDFs and FFs extracted from experimental data are already “renormalized” quantities which include these large collinear contributions. Following Refs. [51–55], a factorized finite hadronic cross section

$d\sigma$ depending on a hard momentum scale Q can be generally written as a convolution (\otimes) of its partonic cross section $d\hat{\sigma}^{bare}$ with the bare partonic distribution and fragmentation functions, f^{bare} and D^{bare} , of a parton in the initial or final-state hadron:

$$d\sigma(Q) = f^{bare} \otimes d\hat{\sigma}^{bare}(Q, \mu_r, \epsilon) \otimes D^{bare}. \quad (3.1)$$

The partonic counterpart to the hadronic cross section depends on a renormalization scale μ_r , and reveals collinear divergences, labeled by ϵ . All further dependences are neglected in the discussion here, like the fraction of the hadron's momentum carried by the parton. Assuming that further ultraviolet and infrared singularities are already subtracted, we want to absorb all collinear singularities coming from the partonic cross section into the bare PDFs f^{bare} and FFs D^{bare} to obtain the renormalized but scale-dependent common parton distribution and fragmentation functions f and D . As the collinear singularities arise from parton emission off the initial and final lines, we separate those contributions at the initial and final factorization scales μ_{fi} and μ_{ff} from the partonic cross section introducing the functions $d\hat{\sigma}_\epsilon$, $d\hat{\sigma}'_\epsilon$, so that we get:

$$d\sigma(Q) = f^{bare} \otimes d\hat{\sigma}_\epsilon(\mu_{fi}, \epsilon) \otimes d\hat{\sigma}(Q, \mu_r, \mu_{fi}, \mu_{ff}) \otimes d\hat{\sigma}'_\epsilon(\mu_{ff}, \epsilon) \otimes D^{bare}. \quad (3.2)$$

We use the *modified minimal subtraction* ($\overline{\text{MS}}$) factorization scheme, introduced in Eq. (2.17), where the ϵ -poles are subtracted together with some finite constants [50],

$$\frac{1}{\epsilon} - \gamma_E + \ln(4\pi). \quad (3.3)$$

With this procedure partonic cross sections $d\hat{\sigma}$ become finite. Although the physical measurable cross section $d\sigma$ is in principle independent from the arbitrary introduced factorization scales, a dependence on μ_{fi} and μ_{ff} remains in perturbation theory if we truncate the perturbative series at a certain order in α_s . The next step is to absorb the collinear singularities into the bare functions f^{bare} and D^{bare} , which result in PDFs and FFs with dependences on the factorization scales:

$$f(\mu_{fi}) = f^{bare} \otimes d\hat{\sigma}_\epsilon(\mu_{fi}, \epsilon), \quad (3.4)$$

$$D(\mu_{ff}) = D^{bare} \otimes d\hat{\sigma}'_\epsilon(\mu_{ff}, \epsilon). \quad (3.5)$$

Finally, we arrive at the common factorized expression

$$d\sigma(Q) = f(\mu_{fi}) \otimes d\hat{\sigma}(Q, \mu_r, \mu_{fi}, \mu_{ff}) \otimes D(\mu_{ff}), \quad (3.6)$$

serving as a starting point for the calculation of various processes. In the case of polarized deep inelastic scattering $lN \rightarrow l'hX$, the cross section can then be factorized into

$$\frac{p_T^3 d\Delta\sigma}{dp_T d\eta} \propto \sum_{abc} \Delta f_{a/\ell}(x_\ell, \mu_{fi}) \otimes \Delta f_{b/N}(x_n, \mu_{fi}) \otimes d\hat{\sigma}_{ab \rightarrow cX}(\hat{s}, \mu_r, \mu_{fi}, \mu_{ff}) \otimes D_{h/c}(z, \mu_{ff}), \quad (3.7)$$

with x_ℓ , x_n and z being the momentum fractions carried by the considered parton coming from the lepton and nucleon or fragmenting into the observed hadron. How the convolution looks like in detail and which further inner arguments the partonic cross section has, will be discussed in Chap. 5.

3.2. Parton Distribution and Fragmentation Functions

As we have seen in the previous section how to compose a hadronic cross section using the factorization theorem, we want to focus ourselves in the following section on the parton distribution and fragmentation functions. The parton distribution function $f_{a/h}(x_h, \mu = \mu_{fi})$ describes a parton a in a hadron h carrying a momentum fraction x_h . Further, a fragmentation function $D_{h/c}(z, \mu = \mu_{ff})$ describes the hadronization of a parton c into a hadron h , where the fraction z of the parton's momentum is carried by the hadron. They are specific to the considered hadron and universal, meaning that they are independent from the underlying hard-scattering process. Moreover, they depend on the initial or final factorization scales μ_{fi} and μ_{ff} .

Further, the helicity parton distribution function of a quark or a gluon is defined by the difference of a parton with positive and a parton with negative helicity in a nucleon with positive helicity [56]:

$$\Delta f(x, \mu) \equiv f^+(x, \mu) - f^-(x, \mu). \quad (3.8)$$

Once we have obtained the parton distribution functions at an initial scale μ_0 , we are able to make use of the DGLAP evolution equations to determine them at a different scale μ . These evolution equations are a set of differential equations deduced independently on the one hand by Dokshitzer [57], Gribov and Lipatov [58], and on the other hand by Altarelli and Parisi [59]:

$$\mu \frac{d}{d\mu} \begin{pmatrix} \Delta f_{q/h}(x, \mu) \\ \Delta f_{g/h}(x, \mu) \end{pmatrix} = \frac{\alpha_s}{2\pi} \int_x^1 \frac{dy}{y} \begin{pmatrix} \Delta P_{qq}(\frac{x}{y}) & \Delta P_{qg}(\frac{x}{y}) \\ \Delta P_{gq}(\frac{x}{y}) & \Delta P_{gg}(\frac{x}{y}) \end{pmatrix} \begin{pmatrix} \Delta f_{q/h}(y, \mu) \\ \Delta f_{g/h}(y, \mu) \end{pmatrix}. \quad (3.9)$$

The DGLAP equations are shown here for polarized splitting functions ΔP_{ij} and parton distribution functions $\Delta f_{a/h}$, however, the structure of the equation is also valid for the unpolarized case. The splitting functions $(\Delta)P_{ij}$ describe the transition of a parton j to a parton i and can be calculated perturbatively as a series in the strong coupling and

depending on a momentum fraction $\xi = \frac{x}{y}$ with $0 \leq \xi \leq 1$:

$$\Delta P_{ij} \left(\frac{x}{y} \right) = P_{ij}^{(0)} \left(\frac{x}{y} \right) + \frac{\alpha_s}{\pi} P_{ij}^{(1)} \left(\frac{x}{y} \right) + \dots \quad (3.10)$$

At LO, Eq. (3.9) describes for example the variation of a quark density to be the sum of on the one hand the quark density at a higher energy scale y convoluted with the probability of finding a quark in a quark with the momentum fraction $\frac{x}{y}$ and on the other side the gluon density at that scale y convoluted with the probability of finding a quark in a gluon with the momentum fraction $\frac{x}{y}$. This works analogously for gluons.

Due to the rare amount of experimental data compared to the unpolarized ones, polarized parton densities exhibit a lack of precision and positivity [60] is implemented for further restriction:

$$|\Delta f(x, \mu)| \leq f(x, \mu). \quad (3.11)$$

This constraint is only exact at LO, however, may be used beyond leading order if one keeps in mind that this is no longer a strict upper limit. This is due to the case that beyond leading order, PDFs can no longer be interpreted as physical probabilities.

The integral of the gluon helicity $\Delta g(x)$ over all gluon momentum fractions x , $\Delta G \equiv \int_0^1 dx \Delta g(x)$, is interpreted to be the gluon spin contribution to the proton and is a main part of the proton helicity sum rule [61],

$$\frac{1}{2} = \frac{1}{2} \Delta \Sigma + \Delta G + L_z^q + L_z^g. \quad (3.12)$$

Hence, $\Delta g(x)$ of the proton is a fundamental ingredient to describe the inner structure of the nucleon. Here, $\Delta \Sigma$ denotes the quark-antiquark spin combination and L_z^q and L_z^g are the quark and gluon orbital angular momentum contributions. The helicity distribution of quarks or gluons can be probed in high-energy scattering processes like the deep inelastic scattering (DIS) of a lepton off a polarized nucleon [62]. It was found that only a small amount of the proton spin is carried by quarks and antiquarks, so that it is crucial to gain more information about the gluon spin. The spin structure of the nucleon can be examined through the measurement on semi-inclusive double-spin asymmetries A_{LL} in deep inelastic scatterings,

$$A_{LL} \equiv \frac{d\Delta\sigma}{d\sigma} = \frac{d\sigma^{++} - d\sigma^{+-}}{d\sigma^{++} + d\sigma^{+-}}, \quad (3.13)$$

to which we will come in Chap. 7.

Fits of available data for a set of distribution functions are shown in Fig. 3.1, taken from Refs. [56, 62]. Here, Ref. [56] has used DIS and semi-inclusive DIS (SIDIS) [63–67] data and data from proton-proton collisions available at the BNL Relativistic Heavy Ion Collider (RHIC) [68, 69], while Ref. [62] uses additionally new data from the RHIC's 2009 run

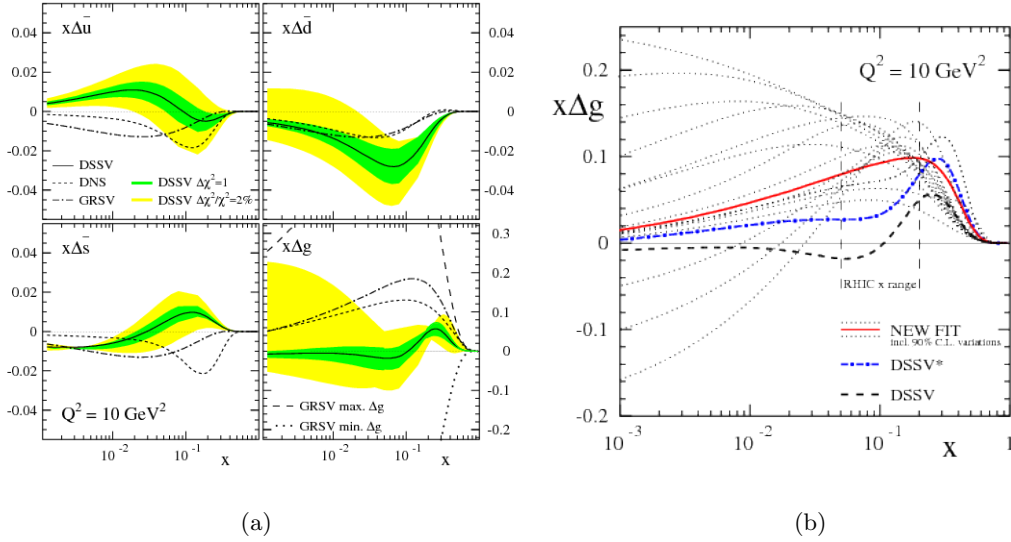


Fig. 3.1.: Parton distribution functions $xf(x)$ for \bar{u} , \bar{d} , and \bar{s} quarks and gluons for $Q^2 = 10 \text{ GeV}^2$ from (a) the DSSV2008 set [56] and (b) the updated gluon helicity distributions $\Delta g(x)$ of DSSV2014 [62]. The plots are taken from Refs. [56, 62].

[70, 71]. The figure shows the DSSV2008 [56] set in (a) and the updated gluon helicity distribution $\Delta g(x)$ of DSSV2014 [62] in (b). As the distributions show a sharp peak for very small x , the plots present $xf(x)$ for all flavors.

Furthermore, we mention that since the proton is a bound state of uud quarks and additional quark-antiquark pairs, the parton distribution functions have to be normalized probabilities of finding various parton constituents [40]. For that we introduce the following sum rules:

$$\int_0^1 dx [f_u(x) - f_{\bar{u}}(x)] = 2, \quad (3.14)$$

$$\int_0^1 dx [f_d(x) - f_{\bar{d}}(x)] = 1. \quad (3.15)$$

In addition, the momentum has to be conserved, meaning that the total amount of the parton's momenta has to match the total momentum of the hadron, so that

$$\int_0^1 dx x [f_u(x) + f_d(x) + f_s(x) + f_{\bar{u}}(x) + f_{\bar{d}}(x) + f_{\bar{s}}(x) + f_g(x)] = 1. \quad (3.16)$$

As we have seen in Sec. 3.1, for a factorization of a semi-inclusive deep inelastic scattering process we need, beside a hard partonic cross section and the parton distribution functions, a precise knowledge of how quarks and gluons hadronize into identified hadrons. This hadronization is described by the universal parton-to-hadron fragmentation functions

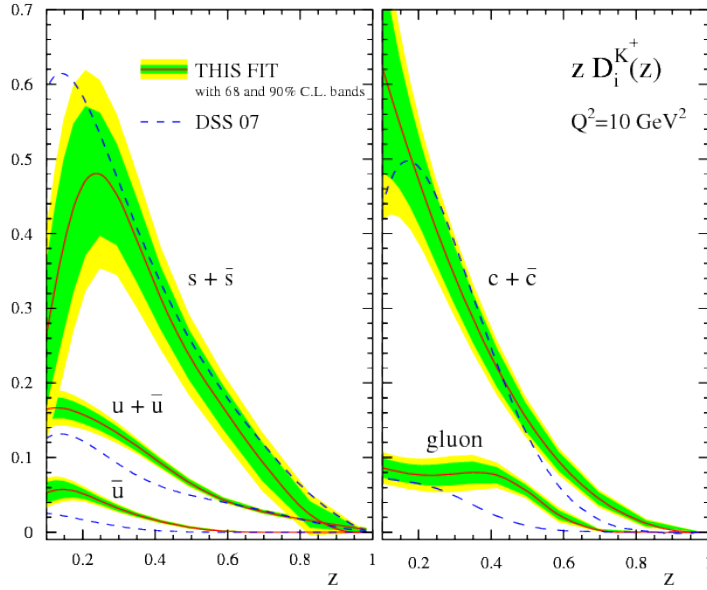


Fig. 3.2.: Updated fragmentation functions $zD_{K^{+}/c}(z, Q^2)$ at $Q^2 = 10 \text{ GeV}^2$ for positively charged kaons [75]. The updated FFs for the individual partons are compared with those of the previous DSS07 sets [76]. The plot is taken from Ref. [75].

(FFs) [72, 73]. A general review over fragmentation functions is given in [74].

The momentum sum rule [73] is an important constraint on FFs and describes the fragmentation of each parton in the final state into a hadron h . Since there are no free partons and each parton in the final state is confined and assumed to fragment into a hadron, summing over all produced hadrons h and integrating over the momentum fraction z gives:

$$\int_0^1 dz z \sum_h D_{h/c}(z, \mu) = 1. \quad (3.17)$$

Analogously to the evolution of parton densities, if once the fragmentation functions are known at a certain initial scale μ_0 , the evolution at other scales is fixed through the DGLAP equations [57–59]:

$$\mu \frac{d}{d\mu} \begin{pmatrix} \Delta D_{h/q}(z, \mu) \\ \Delta D_{h/g}(z, \mu) \end{pmatrix} = \frac{\alpha_s}{2\pi} \int_z^1 \frac{dy}{y} \begin{pmatrix} \Delta P_{qq}(\frac{z}{y}) & \Delta P_{gq}(\frac{z}{y}) \\ \Delta P_{qg}(\frac{z}{y}) & \Delta P_{gg}(\frac{z}{y}) \end{pmatrix} \begin{pmatrix} \Delta D_{h/q}(y, \mu) \\ \Delta D_{h/g}(y, \mu) \end{pmatrix}. \quad (3.18)$$

Note that now the matrix for the time-like splitting function is ΔP_{ji} . It differs from the space-like splitting functions ΔP_{ij} which is relevant for the PDFs in Eq. (3.9). However, the ΔP_{ji} have a perturbative expansion as before in Eq. (3.10). Again, the explicit form of the fragmentation functions has to be fitted to experimental data. In Fig. 3.2 the updated fragmentation functions $zD_{K^{+}/c}(z, Q^2)$ from the DSS17 set of [75] are shown for positively charged kaons. They are compared with the previous kaon fragmentation

functions of [76] (DSS07) at $Q^2 = 10 \text{ GeV}^2$. The main differences between DSS17 and DSS07 are coming from new data from Refs. [77–79]. There exists also an update [80] for the pion fragmentation function of the DSS07 set taking new data from Refs. [81, 82] into account. These are also the sets we will use in Chap. 7 for the calculation of the direct and resolved photon contributions of the photoproduction process $\mu N \rightarrow \mu' h X$ at the COMPASS experiment [18, 19]. Note that besides the extraction of PDFs and FFs from experimental data, remarkable successes have been achieved by lattice calculations [83]. Another ingredient which is still missing are photonic distributions, so that we can handle the parton structure of the photon. We will come to this subject in the next section.

3.3. Parton Structure of the Photon

Photoproduction processes have leptons serving as a source for quasi-real photons which are radiated according to the Weizsäcker-Williams spectrum [84]. The photons can then interact either directly as elementary particles or as resolved-photons through their partonic structure, so that partonic constituents then interact with the partons coming from the scattering target. When the lepton beam is longitudinally polarized, the resulting photon will also carry that polarization and for the resolved case, the spin-dependent parton distributions $\Delta f^\gamma(x, Q^2)$ of the photon enter the theoretical framework. Therefore the focus of this section is on the spin-dependent parton densities $\Delta f^\gamma(x, Q^2)$ of the longitudinally polarized photon according to Refs. [85–91].

Considering the physical cross section, we have to take both photonic contributions into account,

$$d\Delta\sigma = d\Delta\sigma_{dir} + d\Delta\sigma_{res} . \quad (3.19)$$

Keep in mind that the polarized cross section is defined as the difference between the two independent helicity combinations of the initial particles,

$$\Delta\sigma = \frac{1}{2}(\sigma_{++} - \sigma_{+-}) , \quad (3.20)$$

which is used to get directly access to the parton structure of the longitudinally polarized photons. While the parton distribution functions for direct photons are trivial and read

$$\Delta f_{\gamma/\gamma} = \delta(1 - x_\gamma) , \quad (3.21)$$

those for the resolved ones are more complicated. In the following, two models [86] will be reviewed, namely the *maximal* and the *minimal* scenario. However, note that these polarized photonic PDFs are not yet well investigated and are unmeasured so far. They

are defined by

$$\Delta f_\gamma(x, \mu) \equiv f_{\gamma+}^+(x, \mu) - f_{\gamma-}^-(x, \mu), \quad (3.22)$$

where $f_{\gamma+}^+$ ($f_{\gamma+}^-$) denotes the density of a parton with positive (negative) helicity in a photon with helicity '+'. We start with a general investigation of the polarized photonic distributions.

Analogously to the unpolarized ones, the Δf_γ , with $f = q, \bar{q}, g$ satisfy the inhomogeneous evolution equations [85, 87, 92],

$$\begin{aligned} \mu \frac{d\Delta q_\gamma(x, \mu)}{d \ln \mu} &= \frac{\alpha_s}{\pi} \{ \Delta k_q(x, \mu) + [\Delta P_{qq} \otimes \Delta q_\gamma + \Delta P_{qg} \otimes \Delta g_\gamma] \}, \\ \mu \frac{d\Delta g_\gamma(x, \mu)}{d \ln \mu} &= \frac{\alpha_s}{\pi} \{ \Delta k_g(x, \mu) + \Delta P_{gq} \otimes [\Delta q_\gamma + \Delta \bar{q}_\gamma] + \Delta P_{gg} \otimes \Delta g_\gamma \}, \end{aligned} \quad (3.23)$$

with the standard notation for the convolution of the parton-to-parton splitting functions ΔP_{ij} with the parton distributions,

$$\Delta P_{ij} \otimes \Delta f_\gamma = \int_x^1 \frac{dy}{y} \Delta P_{ij}\left(\frac{x}{y}, \mu\right) \Delta f_\gamma(x, \mu). \quad (3.24)$$

Here, Δk_i describe the photon-to-parton splitting functions, and together with the ΔP_{ij} they can be calculated perturbatively and read at NLO [85, 92]:

$$\begin{aligned} \Delta k_i(x, \mu) &= \frac{\alpha_{em}}{2\pi} \Delta k_i(x)^{(0)} + \frac{\alpha_{em}\alpha_s(\mu)}{(2\pi)^2} \Delta k_i(x)^{(1)}, \\ \Delta P_{ij}(x, \mu) &= \frac{\alpha_s(\mu)}{2\pi} \Delta P_{ij}(x)^{(0)} + \left(\frac{\alpha_s(\mu)}{2\pi} \right)^2 \Delta P_{ij}(x)^{(1)}. \end{aligned} \quad (3.25)$$

Taken as a whole, the Δf_γ are of order $\mathcal{O}(\alpha_{em}/\alpha_s)$. Considering the inhomogeneous evolution equations in Eq. (3.23), we find inhomogeneous contributions describing the pointlike photon-to-parton splitting. They determine the perturbative *pointlike* solution $(\Delta)f_\gamma^{\text{pl}}$, vanishing at $Q^2 = \mu^2$. Finally, one finds for the structure of $(\Delta)f_\gamma$ the typical decomposition, namely [87, 93]:

$$\begin{aligned} \Delta f_\gamma(x, Q^2) &= \Delta f_\gamma^{\text{pl}}(x, Q^2) + \Delta f_\gamma^{\text{had}}(x, Q^2), \\ f_\gamma^\gamma(x, Q^2) &= f_\gamma^{\text{pl}}(x, Q^2) + f_\gamma^{\text{had}}(x, Q^2). \end{aligned} \quad (3.26)$$

Additionally to the pointlike part, we have $(\Delta)f_\gamma^{\text{had}}$ denoting the hadronic part, depending on the hadronic input and evolving with the homogeneous evolution equations in Eq. (3.9). The stated distribution has to be obtained non-perturbatively, for example extracted from experimental data. Due to the lack of data we depend on models and assumptions. Hence, the pion parton distribution functions are necessary to describe the unpolarized hadronic components of the photon, since we are using the vector meson dominance (VMD)

model. In that model it is stated that the photon tends to fluctuate into other states with identical quantum numbers, so that the hadronic ansatz is to write $f_\gamma(x, Q^2)$ as a coherent superposition of the lightest vector mesons [90, 91]. Because only the pion PDFs are well known, the ansatz [87]

$$f_\gamma(x, \mu) = \kappa \frac{4\pi\alpha_{em}}{f_\rho^2} f_\pi(x, \mu), \quad (3.27)$$

is usually used, with $f_\pi(x, \mu)$ being the valencelike input, $f_\rho^2/(4\pi) \simeq 2.2$ and $1 \lesssim \kappa \lesssim 2$. The exact value of κ has to be determined from experiment and corresponds to ambiguities appearing when including the ω , ρ and ϕ meson. More details can be found in [87].

When constructing a certain model for the polarized photonic PDFs, we can make use of several theoretical constraints [86]. *Positivity* [60] of the helicity dependent cross sections, see the r.h.s. of Eq. (3.20), yields directly $|\Delta\sigma| \leq \sigma$, so that we have for the photonic density at a given input scale (see, Eq. (3.11)):

$$|\Delta f_\gamma(x, \mu)| \leq f_\gamma(x, \mu). \quad (3.28)$$

Further we have *current conservation*, demanding

$$\Delta q_{\gamma, n=1}^{\text{had}} = 0, \quad (3.29)$$

i.e., the first moment of the photonic quark densities vanishes at the input scale. To deal with the theoretical uncertainties in the polarized photon structure functions due to the unknown hadronic input, we will consider two extreme models to obtain a conservative prediction. For the first case, the *maximal* scenario, we saturate Eq. (3.28) using the unpolarized GRV photon densities,

$$\Delta f_\gamma^{\text{had}}(x, \mu^2) = f_\gamma^{\text{had}}(x, \mu^2), \quad (3.30)$$

opposing to the other extreme input, the *minimal* scenario is used, which reads:

$$\Delta f_\gamma^{\text{had}}(x, \mu^2) = 0. \quad (3.31)$$

The chosen input scale is low. Furthermore, for higher scales the polarized and unpolarized densities evolve in a different way.

Eq. (3.29) is only satisfied by the last scenario for the hadronic input, the minimal one. As we are only interested here in the region of $x > 0.01$, the maximal input could satisfy Eq. (3.29), too, for suitable contributions from smaller x which do not affect the evolutions at larger x . [86]. To summarize, those two extreme hadronic input functions give different sets for the photonic parton distribution functions, see Refs. [88, 89] and [87], and are used in our following resolved calculations. Fig. 3.3 shows the difference between

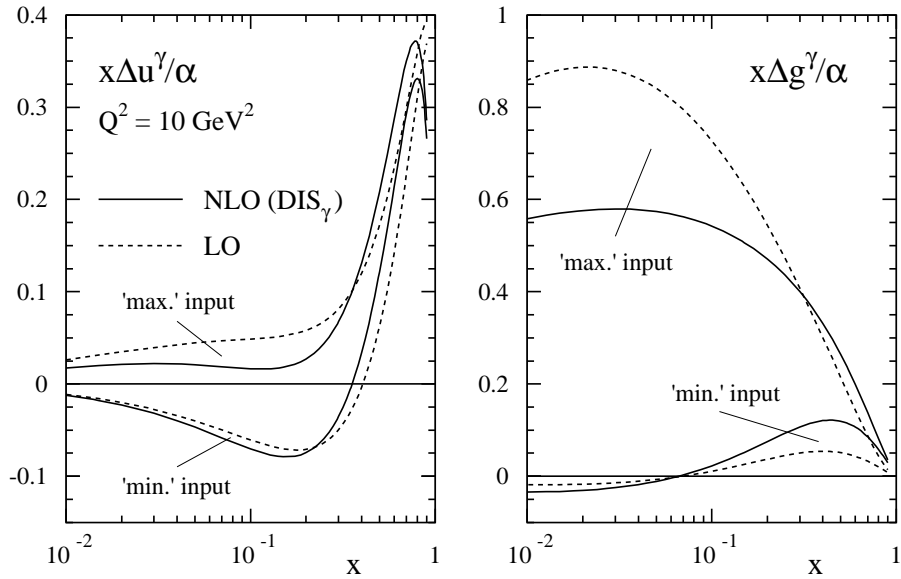


Fig. 3.3.: Comparison of the spin-dependent partonic sets of an u-quark (left) and a gluon (right) in the photon received in [92] for the *maximal* and *minimal* scenario. The figures are taken from Ref. [92].

the maximal and the minimal saturated polarized photon densities for an u-quark and a gluon, by $x\Delta u_\gamma/\alpha_{em}$ and $x\Delta g_\gamma/\alpha_{em}$, at LO and NLO [92]. We will adopt the maximal set of distributions in case of the polarized cross section, however, it was shown in Ref. [25] that the minimal set of [88, 89] will lead to rather similar results. This is so, because the process $\gamma N \rightarrow hX$ mostly probes the high- x region where the inhomogeneous term in the photon evolution equations tends to dominate and the photonic PDFs become relatively insensitive to the boundary condition applied for evolution.

Altogether detailed knowledge of the hadronic structure of the photon can only be obtained from experimental data, however, until there are exact experimental photonic quark and gluon densities available, those models have to satisfy our needs.

In the next chapter we want to apply our detailed knowledge of factorization and partonic distribution functions, as well as fragmentation functions, and consider a single-particle inclusive cross section to derive threshold resummation functions. For that we will start with an exponentiation formula in QED and QCD and proceed with an examination of the Mellin momentum space, before we consider the radiative exponents.

What we find is that if you have a goal that is very, very far out,
and you approach it in little steps, you start to get there faster.
Your mind opens up to the possibilities.

Mae Jemison

4

Foundations of Threshold Resummation

This chapter serves as a pedagogical introduction into threshold resummation. We want to show the foundation for our future calculation, the basic concepts and the underlying ideas for the reorganization of threshold corrections. Soft gluon emission, where the gluons carry a total energy $(1-z)\hat{s}$, with $z \equiv Q^2/\hat{s}$ compared to the mass of the final-state partons Q^2 , yield large logarithmic QCD corrections from the incomplete cancelation of infrared divergences between real and virtual diagrams. In kinematical regions, where nearly all of the available energy is used for the production of the final-state partons, only little phase space is left for additional radiation. In this *threshold* region, hence when the total available center-of-mass energy \hat{s} is only slightly larger than Q^2 , hence $z \rightarrow 1$, logarithmic corrections become large and spoil the perturbative expansion [28]. These logarithms start at next-to-leading order and can be observed at every higher order in perturbation theory [26, 27], so that we have at n -th order contributions up to

$$\alpha_s^n \left[\frac{\ln^{2n-1}(1-z)}{1-z} \right]_+, \quad (4.1)$$

in form of *plus distributions*, to which we will come later. Subleading terms go down by one or more powers of $\ln(1-z)$. Taking the *Mellin moments*, these distributions turn into powers of logarithms in the Mellin variable N up to $\alpha_s^k \ln^{2k} N$, which are taken into account by threshold resummation. Note that the threshold region $z \rightarrow 1$ corresponds to large N . Thus, logarithmic threshold corrections cannot be neglected and require an involved treatment. Threshold resummation to all orders of perturbation theory [29–36] provides an expedient. In the following, we implement threshold resummation at a certain level, called *next-to-leading logarithmic* (NLL) order. In that case, the three leading “towers” are included that means, $\alpha_s^n [\ln^{2n-1}(1-z)/(1-z)]_+$ at leading-logarithmic (LL) accuracy, as well as $\alpha_s^k [\ln^{2n-2}(1-z)/(1-z)]_+$, and $\alpha_s^n [\ln^{2n-3}(1-z)/(1-z)]_+$ at NLL.

The chapter is organized as follows. First we want to investigate an exponentiation formula of soft photons and gluons, leading to the fact that threshold resummation takes place in Mellin space. Then we will investigate the Mellin momentum space in more detail, finding a way, how these threshold terms may be reorganized. Then, we want to derive radiative exponents for single-particle inclusive cross sections explicitly, which gives the starting point for the next chapter. For that we will use a technique based on refactorization.

4.1. Exponentiation for (Non-)Abelian Gauge Theories

In this section we want to demonstrate the exponentiation of soft large logarithms in QCD. In [94] the exponentiation of large logarithmic contributions has been already proven for QED. To make the idea clear, we want to review the main steps and results of the exponentiation in QED briefly, based on [40]. Then, we are ready to generalize the framework for non-abelian gauge theories.

4.1.1. Exponentiation of Soft Photons

We start with a hard scattering process with an outgoing electron line with momentum p' , from which numerous soft photons with momenta k_1, k_2, \dots, k_n are emitted. Not caring whether these are real external photons or virtual photons connecting the electron lines or vertices on other fermion lines, we get in the soft limit for the amplitude:

$$i\mathcal{M} = \bar{u}(p') \left(e \frac{p'^{\mu_1}}{p' \cdot k_1} \right) \left(e \frac{p'^{\mu_2}}{p' \cdot (k_1 + k_2)} \right) \cdots \left(e \frac{p'^{\mu_n}}{p' \cdot (k_1 + k_2 + \dots + k_n)} \right) (i\mathcal{M}_{\text{hard}}). \quad (4.2)$$

While we cannot determine the ordering of the photon momenta k_1, \dots, k_n , we have to sum over all permutations and use the identity

$$\begin{aligned} \sum_{\pi} \frac{1}{p' \cdot k_{\pi(1)}} \frac{1}{p' \cdot (k_{\pi(1)} + k_{\pi(2)})} \cdots \frac{1}{p' \cdot (k_{\pi(1)} + k_{\pi(2)} + \dots + k_{\pi(n)})} \\ = \frac{1}{p' \cdot k_1} \frac{1}{p' \cdot k_2} \cdots \frac{1}{p' \cdot k_n}, \end{aligned} \quad (4.3)$$

so that we obtain

$$\begin{aligned} i\mathcal{M} &= \bar{u}(p') e^n \left(\frac{p'^{\mu_1}}{p' \cdot k_1} \right) \left(\frac{p'^{\mu_2}}{p' \cdot k_2} \right) \cdots \left(\frac{p'^{\mu_n}}{p' \cdot k_n} \right) (i\mathcal{M}_{\text{hard}}) \\ &= \bar{u}(p') e^n \left(\prod_{i=1}^n \frac{p'^{\mu_i}}{p' \cdot k_i} \right) (i\mathcal{M}_{\text{hard}}). \end{aligned} \quad (4.4)$$

For the case of soft photon emission from an incoming electron line we get an additional minus sign for each photon. As we can not distinguish from which electron line the emitted photon comes, we have to sum over all possible diagrams. The amplitude reads

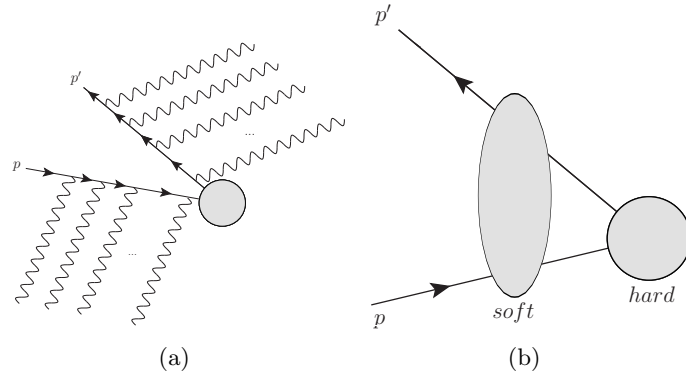


Fig. 4.1.: (a) Soft photons coming from the initial and outgoing fermion. (b) The sum of all diagrams, both real and virtual ones.

for n photons:

$$\bar{u}(p')(i\mathcal{M}_{\text{hard}})u(p)e^n \left(\frac{p'^{\mu_1}}{p' \cdot k_1} - \frac{p^{\mu_1}}{p \cdot k_1} \right) \left(\frac{p'^{\mu_2}}{p' \cdot k_2} - \frac{p^{\mu_2}}{p \cdot k_2} \right) \cdots \left(\frac{p'^{\mu_n}}{p' \cdot k_n} - \frac{p^{\mu_n}}{p \cdot k_n} \right). \quad (4.5)$$

From now on we want to distinguish whether the photons are real or virtual. We count n real and m virtual ones. For virtual photons we connect the two fermion lines through a photon propagator and set the momenta $k_i = -k_j \equiv k$ - with a sign change as k_i is absorbed in the other fermion line - and integrate over k . Including a symmetry factor of $1/2$ to avoid double counting, we have for each virtual photon:

$$\frac{e^2}{2} \int \frac{d^4k}{(2\pi)^4} \frac{-ig_{\mu\nu}}{k^2 + i\epsilon} \left(\frac{p'^{\mu}}{p' \cdot k} - \frac{p^{\mu}}{p \cdot k} \right) \left(\frac{p'^{\nu}}{-p' \cdot k} - \frac{p^{\nu}}{-p \cdot k} \right) \equiv X_{\text{virt}}. \quad (4.6)$$

Summing over m , we need again a symmetry factor of $1/m!$ as interchanging the photons with each other does not change the diagrams. Hence the full virtual matrix element for m soft photon reads:

$$\bar{u}(\vec{p}')(i\mathcal{M}_{\text{hard}})u(p) \sum_{m=0}^{\infty} \frac{X_{\text{virt}}^m}{m!} = \bar{u}(\vec{p}')(i\mathcal{M}_{\text{hard}})u(p) \exp(X_{\text{virt}}). \quad (4.7)$$

Additionally, if we have a real photon, we multiply by its polarization vector $\epsilon_i^{\mu_i}$, sum over polarizations and integrate the squared matrix element over the phase space of the photon:

$$\int \frac{d^3k}{(2\pi)^3} \frac{1}{2k_0} e^2 (-g_{\mu\nu}) \left(\frac{p'^{\mu}}{p' \cdot k} - \frac{p^{\mu}}{p \cdot k} \right) \left(\frac{p'^{\nu}}{p' \cdot k} - \frac{p^{\nu}}{p \cdot k} \right) \equiv Y_{\text{real}}. \quad (4.8)$$

Again, for n radiated photons we include a symmetry factor of $1/n!$ and sum over n . Combining then the real and the virtual contributions of the squared matrix elements, we

then obtain our final result for the cross section with an arbitrary number of emitted and absorbed virtual and real photons, see Fig. (4.1b):

$$\begin{aligned} d\sigma &= \sum_{n,m=0}^{\infty} d\sigma^{(0)} \sum_{n=0}^{\infty} \frac{Y_{\text{real}}}{n!} \left(\sum_{m=0}^{\infty} \frac{X_{\text{virt}}^m}{m!} \right)^2 \\ &= d\sigma^{(0)} \exp(Y_{\text{real}}) \exp(2X_{\text{virt}}) . \end{aligned} \quad (4.9)$$

Our result shows that only the single emission contribution is needed and that it exponentiates completely. Further, the cross section factorizes into a hard-scattering contribution and a soft exponentiated part. While this resummation formula was quite easy to construct for soft photons, the case for soft gluons is more complicated.

4.1.2. Exponentiation of Soft Gluons

The exponentiation formalism for a cross section of soft emissions in a non-abelian gauge theory like QCD is highly non-trivial. This is due to the self-interaction of gluons and with that the three-gluon vertex. However, Gatheral [95] and Frenkel and Taylor [96] have proven an exponentiation theorem for soft gluons in the eikonal approximation of QCD. They stated that a cross section X with two external colored fermion lines can be written as the exponential

$$X = \exp Y, \quad (4.10)$$

where Y fulfills the following properties:

- (i) Y is calculated perturbatively from a series of terms, each corresponding to a single Feynman diagram.
- (ii) These diagrams are a subset of those diagrams contributing to X .
- (iii) Each diagram of Y is connected to a color weight, which is in general different from those color weights of the corresponding terms in X .

To proof this we have to consider the diagrammatic structures and derive the color weights. Therefore we want to introduce some definitions first, all based on [95, 96].

A *web* is a set of gluon lines, crossed or directly connected. A special case is the *c-web*, short for connected web, which is a connected set of gluon lines. The color factor $\tilde{C}(W)$ of a c-web W is in general not equal to the color factor $C(D[W])$ of the corresponding Feynman diagram $D[W]$. Further, one can decompose every color diagram by using the commutation relation of the Lie algebra,

$$[t^a, t^b] = if^{abc}t^c, \quad (4.11)$$

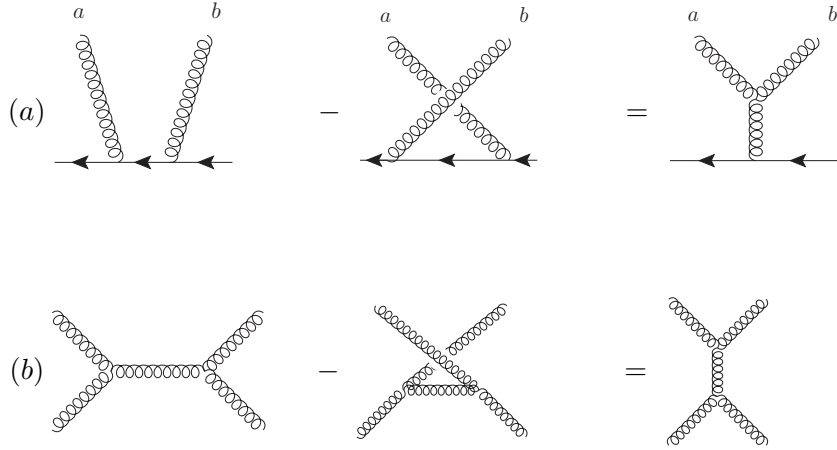


Fig. 4.2.: (a) The commutation relation and (b) the Jacobi identity illustrated through color diagrams [96].

and the Jacobi identity,

$$f^{ade} f^{bcd} + f^{bde} f^{cad} + f^{cde} f^{abd} = 0, \quad (4.12)$$

into a sum of products of c-webs. The color structure of both identities is depicted in Fig. (4.2). Hence,

$$C(D[W]) = \sum_k C^{(k)}, \quad (4.13)$$

where $C^{(k)}$ is also a sum with each term containing exactly k c-webs. Each term $C^{(k)}$ is called a decomposition d . Further, the color factor $C(d)$ of a decomposition into $n(d)$ c-webs W_i is the product of all color factors $\tilde{C}(W_i)$ of the $n(d)$ c-webs:

$$C(d) = \prod_{i=1}^{n(d)} \tilde{C}(W_i). \quad (4.14)$$

The modified color factor of a web W is defined through the normalized color factor of a diagram $D[W]$, minus the sum of the color factors of all non-trivial decompositions Dec' of W into $i \leq n(d)$ webs W_i , where Dec' is a subset of all possible decompositions Dec :

$$\begin{aligned} \tilde{C}(W) &= \frac{1}{\text{Tr } \mathbb{1}} C(D[W]) - \sum_{d \in Dec'} C(d) \\ &= \frac{1}{\text{Tr } \mathbb{1}} C(D[W]) - \sum_{d \in Dec'} \prod_{i=1}^{n(d)} \tilde{C}(W_i). \end{aligned} \quad (4.15)$$

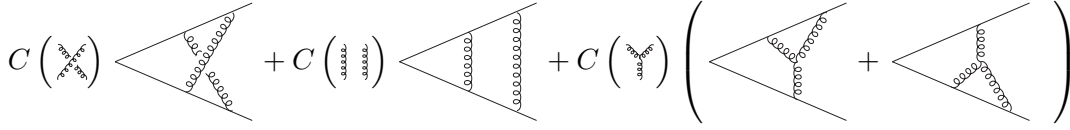


Fig. 4.3.: Diagrams contributing to $\mathcal{O}(\alpha_s^2)$; self-energies are neglected.

Here, we have used the normalization $\text{Tr } \mathbb{1} = N_c$. For instance, if a considered web W is a c-web, then its trivial decomposition is the web itself and its color factor is given by the first term of the sum in Eq. (4.13), $C^{(1)}$. Furthermore, a non-trivial decomposition Dec' contains more than one c-web.

After introducing the color factors or color weights, the next step will be to deduce a generalized eikonal identity, an analogue to the identity in Eq. (4.3) for QED. This identity was stated and proven in [95]. In the following, S_d denotes the set of Feynman diagrams F , whose color diagrams are decomposed into $n(d)$ webs. $\mathcal{F}(W_i)$ is the Feynman integral in the soft limit which corresponds to a web W_i . Then, the generalized eikonal identity is given by

$$\sum_{F \in S_d} F = \prod_{i=1}^{n(d)} \mathcal{F}(W_i). \quad (4.16)$$

What has changed for the non-abelian case compared to QED is that we have no more radiation of numerous independent photons, but bundled gluons due to their self-interaction, collected into a web. Now we have everything together to go on with the proof of the non-abelian exponentiation formula, stated in Eq. (4.10). For that purpose we will follow the formalism of [97] and start with an example. Consider the first non-trivial diagrams in $\mathcal{O}(\alpha_s^2)$ for quark and antiquark eikonal lines, given in Fig. (4.3). Note that the order of a web m corresponds to the order in the strong coupling constant, so that the web is of order $\mathcal{O}(\alpha_s^m)$. Self-energies are excluded as they vanish at one loop level if we work in Feynman gauge. Using Eq. (4.15) we connect ordinary color factors with the corresponding modified color weight of a web. This is crucial for the following exponentiation. We use:

$$\begin{aligned} C \left(\begin{array}{c} \text{---} \\ \diagup \quad \diagdown \\ \text{---} \end{array} \right) &= C \left(\begin{array}{c} \text{---} \\ \text{---} \\ \text{---} \end{array} \right) - C \left(\begin{array}{c} \text{---} \\ \diagdown \quad \diagup \\ \text{---} \end{array} \right) = -C_F \left(C_F - \frac{C_A}{2} \right), \\ C \left(\begin{array}{c} \text{---} \\ \text{---} \\ \text{---} \end{array} \right) &= C \left(\begin{array}{c} \text{---} \\ \text{---} \\ \text{---} \end{array} \right)^2 = C_F^2, \\ C \left(\begin{array}{c} \text{---} \\ \diagup \quad \diagdown \\ \text{---} \end{array} \right) &= C_F \frac{C_A}{2}, \end{aligned} \quad (4.17)$$

and get:

$$\begin{aligned}
\tilde{C}\left(\begin{array}{c} \diagup \\ \diagdown \end{array}\right) &= C\left(\begin{array}{c} \diagup \\ \diagdown \end{array}\right) - \tilde{C}\left(\begin{array}{c} \diagup \\ \diagdown \end{array}\right)^2 = -C\left(\begin{array}{c} \diagup \\ \diagdown \end{array}\right) = -C_F \frac{C_A}{2}, \\
\tilde{C}\left(\begin{array}{c} \diagup \\ \diagup \end{array}\right) &= C\left(\begin{array}{c} \diagup \\ \diagup \end{array}\right) - \tilde{C}\left(\begin{array}{c} \diagup \\ \diagup \end{array}\right)^2 = 0, \\
\tilde{C}\left(\begin{array}{c} \diagup \\ \diagdown \\ \diagup \end{array}\right) &= C\left(\begin{array}{c} \diagup \\ \diagdown \\ \diagup \end{array}\right) = C_F \frac{C_A}{2}.
\end{aligned} \tag{4.18}$$

Further we need the eikonal identity for two gluons,

$$\mathcal{F}\left(\begin{array}{c} \diagup \\ \diagdown \end{array}\right) + \mathcal{F}\left(\begin{array}{c} \diagup \\ \diagdown \end{array}\right) = \mathcal{F}\left(\begin{array}{c} \diagup \\ \diagdown \end{array}\right)\Big|_{k_1} \times \mathcal{F}\left(\begin{array}{c} \diagup \\ \diagdown \end{array}\right)\Big|_{k_2}, \tag{4.19}$$

so that we can now rewrite the considered diagrams in $\mathcal{O}(\alpha_s^2)$ of Fig. (4.3):

$$\begin{aligned}
X^{(2)} &= C\left(\begin{array}{c} \diagup \\ \diagdown \end{array}\right) \mathcal{F}\left(\begin{array}{c} \diagup \\ \diagdown \end{array}\right) + C\left(\begin{array}{c} \diagup \\ \diagdown \end{array}\right) \mathcal{F}\left(\begin{array}{c} \diagup \\ \diagdown \end{array}\right) \\
&\quad + C\left(\begin{array}{c} \diagup \\ \diagdown \end{array}\right) \left[\mathcal{F}\left(\begin{array}{c} \diagup \\ \diagdown \end{array}\right) + \mathcal{F}\left(\begin{array}{c} \diagup \\ \diagdown \end{array}\right) \right] \\
&= \frac{1}{2} \left[\tilde{C}\left(\begin{array}{c} \diagup \\ \diagdown \end{array}\right) \mathcal{F}\left(\begin{array}{c} \diagup \\ \diagdown \end{array}\right) \right]^2 + \tilde{C}\left(\begin{array}{c} \diagup \\ \diagdown \end{array}\right) \mathcal{F}\left(\begin{array}{c} \diagup \\ \diagdown \end{array}\right) \\
&\quad + \tilde{C}\left(\begin{array}{c} \diagup \\ \diagdown \end{array}\right) \left[\mathcal{F}\left(\begin{array}{c} \diagup \\ \diagdown \end{array}\right) + \mathcal{F}\left(\begin{array}{c} \diagup \\ \diagdown \end{array}\right) \right].
\end{aligned} \tag{4.20}$$

We have introduced a symmetry factor of 1/2 to avoid overcounting as we cannot distinguish two webs with the same structure, so for instance we have $\mathcal{F}^{(1)}(k_1)\mathcal{F}^{(2)}(k_2, k_3) = \mathcal{F}^{(1)}(k_2)\mathcal{F}^{(2)}(k_1, k_3)$. Now we want to include further order contributions and introduce therefore an additional index for a web of order m , with $1 \leq i \leq m$:

$$\tilde{C}(W^{(m)}) = \frac{1}{\text{Tr} \mathbb{1}} C(D[W^{(m)}]) - \sum_{d \in \text{Dec}'} \prod_{i=1}^{n(d)} \tilde{C}(W_i). \tag{4.21}$$

Then we obtain the all-order expansion X

$$\begin{aligned}
X &= 1 + \sum_{\substack{\text{all webs} \\ \text{of order 1}}} \tilde{C}(W^{(1)}) \mathcal{F}(W^{(1)}) \\
&\quad + \frac{1}{2!} \left(\sum_{\substack{\text{all webs} \\ \text{of order 1}}} \tilde{C}(W^{(1)}) \mathcal{F}(W^{(1)}) \right)^2 + \sum_{\substack{\text{all webs} \\ \text{of order 2}}} \tilde{C}(W^{(2)}) \mathcal{F}(W^{(2)}) + \dots
\end{aligned} \tag{4.22}$$

With the example above it is now clear that any Feynman diagram with two external eikonal lines can be decomposed into a sum of products of webs by using Eqs. (4.15) and (4.16). According to [97], induction of the lower-order contribution yield for a set of

Feynman diagrams of $\mathcal{O}(\alpha_s^m)$:

$$F^{(m)} = \sum_{\{n_i\} | \sum_i i n_i = m} \prod_i \frac{1}{n_i!} \left(\sum_{\substack{\text{all webs} \\ \text{of order } i}} \tilde{C}(W^{(i)}) \mathcal{F}(W^{(i)}) \right)^{n_i}. \quad (4.23)$$

We sum over all sets n_i such that the condition $\sum_i i n_i = m$ is fulfilled. Again, i labels the order of the webs. As before, we require a factor of $1/n_i!$ to avoid overcounting. Summing over all possible orders in Eq. (4.23) gives us the full perturbative series

$$X = \sum_{m=0}^{\infty} F^{(m)}. \quad (4.24)$$

We rewrite this as an exponential:

$$\begin{aligned} X &= \sum_{m=0}^{\infty} \sum_{\{n_i\}} \delta_{m(\sum_i i n_i)} \prod_i \frac{1}{n_i!} \left(\sum_{\substack{\text{all webs} \\ \text{of order } i}} \tilde{C}(W^{(i)}) \mathcal{F}(W^{(i)}) \right)^{n_i} \\ &= \sum_{\substack{\text{all possible} \\ \{n_i\}}} \prod_i \frac{1}{n_i!} \left(\sum_{\substack{\text{all webs} \\ \text{of order } i}} \tilde{C}(W^{(i)}) \mathcal{F}(W^{(i)}) \right)^{n_i} \\ &= \prod_i \left\{ \sum_{n_i} \frac{1}{n_i!} \left(\sum_{\substack{\text{all webs} \\ \text{of order } i}} \tilde{C}(W^{(i)}) \mathcal{F}(W^{(i)}) \right)^{n_i} \right\} \\ &= \prod_i \exp \left(\sum_{\substack{\text{all webs} \\ \text{of order } i}} \tilde{C}(W^{(i)}) \mathcal{F}(W^{(i)}) \right). \end{aligned} \quad (4.25)$$

Here, we made use of the relation

$$\sum_{\substack{\text{all possible} \\ \{n_i\}}} \prod_i f(n_i, i) = \prod_i \sum_{n_i} f(n_i, i), \quad (4.26)$$

valid for any function $f(n_i, i)$. Hence, we arrive at our desired exponentiation formula and have proven the statement of Eq. (4.10):

$$X = \exp Y = \exp \left(\sum_i \sum_{\substack{\text{all webs} \\ \text{of order } i}} \tilde{C}(W^{(i)}) \mathcal{F}(W^{(i)}) \right). \quad (4.27)$$

This means that only a subset of the full diagrammatic contributions enters the exponent, connected with their color weights. What now is still missing for a complete exponentiation formalism is an examination of the phase space of soft gluon radiation, which also has to be exponentiated. For this we refer to the next section where this demand will be satisfied with help of the Mellin- N momentum space.

4.2. Phase Space Factorization in Mellin Moment Space

In this section we want to introduce the Mellin- N momentum space and investigate the phase space for soft gluon radiation. In the last section the exponentiation for abelian and non-abelian gauge theories was shown and with that, the exponentiation of soft gluons as an ingredient for threshold resummation. Now we want to investigate if also the phase space factorizes. As an introductory example, let us consider the Drell-Yan process, where a quark-antiquark pair, carrying the momenta p_1 and p_2 , annihilate into a photon of momentum q_{γ^*} and into n additional radiated soft gluons, each with a momentum k_i [98]:

$$d\mathcal{P}_{\gamma^*,ng} = (2\pi^4)\delta^{(4)}\left(p_1 + p_2 - q_{\gamma^*} - \sum_{i=1}^n k_i\right) \frac{d^3q}{(2\pi)^3 2q_0} \prod_{i=1}^n \frac{d^3k_i}{(2\pi)^3 2(k_i)_0}. \quad (4.28)$$

The δ -function connects the gluon momenta with the initial partons and the produced photon. Then, the kinematical threshold for $z \rightarrow 1$ allows us to use the soft-gluon approximation. After integrating over the photon's phase space we obtain

$$d\mathcal{P}_{\gamma^*,ng} = \frac{2\pi}{\hat{s}} \delta\left(1 - z - \sum_{i=1}^n \frac{(k_i)_0}{E}\right) \prod_{i=1}^n \frac{d^3k_i}{(2\pi)^3 2(k_i)_0}. \quad (4.29)$$

As several gluon momentum integrals are not independent from each other, an exponentiation cannot be simply performed. The inverse *Mellin* (or Laplace) *transformation* helps us out of this situation: Rewriting the δ -function,

$$\delta\left(1 - z - \sum_{i=1}^n z_{k_i}\right) = \frac{1}{2\pi i} \int_{\mathcal{C}} dN e^{N(1-z-\sum_{i=1}^n z_{k_i})}, \quad (4.30)$$

with the energy fraction of the i -th gluon $z_{k_i} = (k_i)_0/E = 2(k_i)_0/\sqrt{\hat{s}}$, implies that when $z \rightarrow 1$ we get $z_{k_i} \rightarrow 0$. This means, soft gluon momenta give rise to large Mellin N [99]. Utilizing then the limit $z \rightarrow 1$ or $z_{k_i} \rightarrow 0$, and the corresponding large N limit, we can approximate $e^{N(1-z)} \approx e^{-N \ln z} = z^{-N}$, so that we finally identify the delta-function as an inverse Mellin transform:

$$\delta\left(1 - z - \sum_{i=1}^n z_{k_i}\right) = \frac{1}{2\pi i} \int_{\mathcal{C}} dN z^{-N} \prod_{i=1}^n e^{-N z_{k_i}}. \quad (4.31)$$

Combining the rewritten δ -function with the phase space gives

$$\begin{aligned} d\mathcal{P}_{\gamma^*,ng} &= \frac{2\pi}{\hat{s}} \delta\left(1 - z - \sum_{i=1}^n z_{k_i}\right) \prod_{i=1}^n \frac{d^3k_i}{(2\pi)^3 2(k_i)_0} \\ &= \frac{2\pi}{\hat{s}} \frac{1}{2\pi i} \int_{\mathcal{C}} dN z^{-N} \prod_{i=1}^n e^{-N z_{k_i}} \frac{d^3k_i}{(2\pi)^3 2(k_i)_0}. \end{aligned} \quad (4.32)$$

Transformed into Mellin moment space,

$$\int_0^1 dz z^{N-1} d\mathcal{P}_{\gamma^*, ng} = \frac{2\pi}{\hat{s}} \prod_{i=1}^n e^{-Nz_{k_i}} \frac{d^3 k_i}{(2\pi)^{32} (k_i)_0}, \quad (4.33)$$

we have found a factorization formula for the n -gluon phase space [98, 99] through exponentiation. This is the reason, why threshold resummation takes place in Mellin momentum space.

4.3. Threshold Resummation in Mellin Space

As we have introduced the Mellin- N transformation in the last section, we shortly show its formalism: Transforming a function f into Mellin- N space gives

$$f^N = \int_0^1 dx x^{N-1} f(x), \quad (4.34)$$

accompanied by a Mellin inverse transformation of the form

$$f(x) = \frac{1}{2\pi i} \int_{\mathcal{C}} dN x^{-N} f^N, \quad (4.35)$$

if we want to transform the function f^N back into x -space. Note that the contour integration $\mathcal{C} = \int_{c-i\infty}^{c+i\infty}$ takes place in the complex- N space, and that the constant c is chosen such that all singularities lie to the left of the integration contour, except for the Landau poles, which lie to the far right. However, this will be examined later in Sec. 5.6 more detailed.

Note that a Mellin transformation is connected to the Laplace transformation

$$f^N = \int_0^1 dx e^{-Nx} f(x) \quad (4.36)$$

at threshold limit where $x \rightarrow 0$. Mellin techniques are quite useful besides the phase space factorization, as one can simplify convoluted integrals very easily:

$$\begin{aligned} \int_0^1 dx x^{N-1} \int_x^1 \frac{dy}{y} h(y) g\left(\frac{x}{y}\right) &= \int_0^1 dx x^{N-1} \left[\int_0^1 dy \int_0^1 dz h(y) g(z) \delta(x - zy) \right] \\ &= \int_0^1 dy y^{N-1} h(y) \int_0^1 dz z^{N-1} g(z) = h^N \times g^N. \end{aligned} \quad (4.37)$$

Further, large threshold logarithms appearing in Mellin space arise from plus distributions in higher-order calculations [100]:

$$\begin{aligned} \int_0^1 dz z^{N-1} \left(\frac{\ln^m(1-z)}{1-z} \right)_+ &= \int_0^1 dz \frac{z^{N-1} - 1}{1-z} \ln^m(1-z) \\ &= \frac{(-1)^m}{m+1} \ln^{m+1} \bar{N} + \mathcal{O}(\ln^{m-1} N), \end{aligned} \quad (4.38)$$

where $\bar{N} = Ne^{\gamma_E}$ and with the definition of the plus-distribution,

$$\int_0^1 dw f(w) [g(w)]_+ = \int_0^1 dw [f(w) - f(1)] g(w). \quad (4.39)$$

These logarithms appear at every higher order of perturbation theory with larger exponent, so that we get at n -th order in the coupling constant:

$$\alpha_s^n \left[\frac{\ln^m(1-z)}{1-z} \right]_+ \leftrightarrow \alpha_s^n \ln^{m+1} \bar{N}, \quad \text{for } m \leq 2n-1. \quad (4.40)$$

These logarithms shall be reorganized into a typical resummation structure, which we want to introduce in the following. Starting with a perturbative expansion of a cross section at kinematic threshold, summing over each order in α_s , we find that each further order gives us two additional powers in the N -logarithm [28]. With that, at n -th order the upper limit of the sum over the logarithmic exponents reads $m = 2n - 1$:

$$d\sigma^N / \sigma_B^N = 1 + \sum_{n=1}^{\infty} \alpha_s^n \sum_{m=0}^{2n-1} c_{n,m} \ln^{m+1} N, \quad (4.41)$$

where we have normalized the cross section with the Born contribution σ_B^N , so that the LO contribution gives simply unity. Reorganizing the logarithmic contributions such that we obtain an exponential form [101] gives rise to the functions $h^{(i)}$, including the leading-logarithmic contributions of the form $\alpha_s^n \ln^{n+1} N$ into the function $\ln N h^{(1)}$ and all next-to-leading logarithms $\alpha_s^n \ln^n N$ in the function $h^{(2)}$:

$$\begin{aligned} d\sigma^N / \sigma_B^N &= 1 + \sum_{n=1}^{\infty} \alpha_s^n \sum_{m=0}^{2n-1} c_{n,m} \ln^{m+1} N \\ &= \exp \left\{ \sum_{n=1}^{\infty} \alpha_s^n \sum_{m=0}^n \tilde{c}_{n,m} \ln^{m+1} N \right\} C(\alpha_s) \\ &= \exp \left(\underbrace{\ln N h^{(1)}(\alpha_s \ln N)}_{LL} + h^{(2)}(\alpha_s \ln N) + \alpha_s h^{(3)}(\alpha_s \ln N) \right) C(\alpha_s). \end{aligned} \quad (4.42)$$

NLL

	LL	NLL		NNLL		...
LO	1					
NLO	$\alpha_s L^2$	$\alpha_s L$	α_s	1		
NNLO	$\alpha_s^2 L^4$	$\alpha_s^2 L^3$	$\alpha_s^2 L^2$	$\alpha_s^2 L$	α_s^2	...
N ³ LO	$\alpha_s^3 L^6$	$\alpha_s^3 L^5$	$\alpha_s^3 L^4$	$\alpha_s^3 L^3$	$\alpha_s^3 L^2$...
N ⁴ LO	$\alpha_s^4 L^8$	$\alpha_s^4 L^7$	$\alpha_s^4 L^6$	$\alpha_s^4 L^5$	$\alpha_s^4 L^4$...
⋮						
N ^k LO	$\alpha_s^k L^{2k}$	$\alpha_s^k L^{2k-1}$	$\alpha_s^k L^{2k-2}$	$\alpha_s^k L^{2k-3}$	$\alpha_s^k L^{2k-4}$...
	↓		↓		↓	
	$Lh^1(\alpha_s L)$	$h^2(\alpha_s L)$		$\alpha_s h^3(\alpha_s L)$		

Fig. 4.4.: Schematic description of the reorganized perturbative structure in a perturbative cross section up to k -th order in α_s , with $L \equiv \ln N$.

While in the exponentiation procedure the upper limit of the sum \sum_m changes from $2n - 1$ to n , single-logarithmic behaviour takes place. For example, by exponentiation of the lowest-order logarithms $\alpha_s \tilde{c}_{n=1, m=1} \ln^2 N$ we can take all double logarithms $\alpha_s^n c_{n, 2n-1} \ln^{2n} N$ of Eq. (4.41) into account. The leading logarithms collected into $\ln N h^{(1)}$ are the most dominant terms, however, it is obvious that the expansion becomes more accurate, the more lower order logarithms are taken into account. For an illustration of the reorganization of the logarithmic contributions, see Fig. (4.4). Hence we conclude that once one has calculated the functions $h^{(i)}$, we are able to treat soft-gluon radiation in the region of large- N systematically and perturbatively. If one has at least the functions $h^{(1)}$, $h^{(2)}$ and $h^{(3)}$ and the coefficient $C(\alpha_s)$ up to the two-loop order on hand, then one is able to control the first five logarithmic towers [102] shown in Fig. (4.4).

4.4. Threshold Corrections for Single-Particle Inclusive Cross Section

In the following section we construct threshold resummation expressions for hadronic single-inclusive cross sections and introduce a technique called *refactorization*. Following the formalism of Refs. [26, 31, 32], we will derive radiative exponent formulas in moment space for the initial- and final-state partons at next-to-leading logarithmic accuracy. Our starting point will be the usual factorization theorem for di-jet cross sections.

4.4.1. Refactorization

Consider the single-inclusive hadronic scattering,

$$h_A(p_A) + h_B(p_B) \rightarrow c(p) + X(k_S + p_X), \quad (4.43)$$

with the initial-state hadrons h_A and h_B , the final-state particle c which will be observed, and an unobserved part X . In this case, c denotes an observed photon or light jet. At partonic level, the process corresponds to

$$a(p_a) + b(p_b) \rightarrow c(p) + X(k_S + p_X), \quad (4.44)$$

where the parton a (and b) carry the momentum fraction $x_a = p_a/p_A$ (and analogously for x_b) of the incoming hadron h_A (h_B). Then, the factorized cross section can be written as [26]

$$E_p \frac{d\sigma_{h_A h_B \rightarrow c(p)+X}}{d^3p} = \frac{1}{S^2} \sum_{a,b=q,\bar{q},g} \int dx_a dx_b \Phi_{a/h_A}(x_a, \mu) \Phi_{b/h_B}(x_b, \mu) \times w_{ab \rightarrow c+X} \left(\frac{\hat{s}_4}{\mu^2}, \frac{\hat{t}}{\mu^2}, \frac{\hat{u}}{\mu^2}, \alpha_s(\mu^2) \right), \quad (4.45)$$

with Φ_{a/h_A} and Φ_{b/h_B} denoting the non-perturbative parton distribution functions, as introduced in Section 3.1 and 3.2. We have introduced the kinematic invariant s_4 ,

$$\hat{s}_4 \equiv \hat{s} + \hat{t} + \hat{u} = p^2 + M_X^2 \approx M_X^2, \quad (4.46)$$

describing the squared invariant mass of the observed final-state photon or jet, which may be neglected plus the unobserved radiation recoiling against it. It is written in terms of the partonic Mandelstam variables,

$$\hat{s} = (p_a + p_b)^2, \quad \hat{t} = (p_a - p)^2, \quad \hat{u} = (p_b - p)^2, \quad (4.47)$$

with $S = (p_A + p_B)^2$ being the hadronic counterpart to $\hat{s} = x_a x_b S$ describing the overall center of mass energy. Partonic threshold is reached for values of x_a and x_b , where \hat{s}_4 vanishes [26]. As the cross section is organized at n -th order of perturbation theory in terms of

$$\left[\frac{\ln^m(\hat{s}_4/\hat{s})}{\hat{s}_4} \right]_+, \quad m \leq 2n - 1, \quad (4.48)$$

integrals which are going down to $\hat{s}_4 = 0$ lead to logarithmic corrections. Alternatively one can express these logarithmic contributions in terms of the variable z ,

$$\left[\frac{\ln^m(1-z)}{1-z} \right]_+, \quad m \leq 2n-1, \quad (4.49)$$

where we have at kinematic threshold,

$$z \equiv \frac{M_{JJ}^2}{x_a x_b S} = \frac{(p+p_X)^2}{\hat{s}} = 1, \quad (4.50)$$

so that there is just enough energy available to produce the observed final-state and its recoiling counterpart, but no further energy is left for additional radiation. Then, only phase space for soft gluon emission is left, so that the logarithmic corrections of Eq. (4.49) become important and spoil the cross section. Hence, it is inevitable to resum those terms to all orders of perturbation theory using *threshold resummation*.

For that, we want to *refactorize* the cross section at threshold and rely on further factorization properties. We split it up into a *hard scattering* part H_{IL} , some *jet functions*, $\Psi_{i/i}$ and J_i , describing collinear soft-gluon radiation off the initial- and final-state partons, and a *soft function* S_{LI} describing non-collinear, large-angle soft gluons coupling to the incoming and outgoing partons, initiating color exchange. The contribution of the functions to the refactorized cross section have to be weighted, so that we will connect them with dimensionless weights w_i which will vanish at threshold [31, 32]. Implying partonic momentum conservation,

$$x_a p_A + x_b p_B = p + p_X + k_S, \quad (4.51)$$

and neglecting terms of order \hat{s}_4^2 , one finds [31]:

$$\begin{aligned} S_4 &= (1-x_a)2p_A \cdot p_X + (1-x_b)2p_B \cdot p_X + 2k_S \cdot p_X + p_X^2 + p^2 \\ &\equiv \left[w_a \left(\frac{\hat{u}}{\hat{t} + \hat{u}} \right) + w_b \left(\frac{\hat{t}}{\hat{t} + \hat{u}} \right) + w_S + w_X + w_p \right] S \\ &= \left[(1-x_a) \left(\frac{\hat{u}}{\hat{t} + \hat{u}} \right) + (1-x_b) \left(\frac{\hat{t}}{\hat{t} + \hat{u}} \right) + \frac{\hat{s}_4}{S} \right] S. \end{aligned} \quad (4.52)$$

We introduce the momentum vector p_X of the unobserved jet recoiling against the observed particle. At threshold, we get in the center of mass frame $p_X^\mu = (p_0, -\vec{p}) \equiv \sqrt{S}\zeta^\mu$. In the second line of Eq. (4.52) the additive weights are introduced. The last line connects the hadronic S_4 with its partonic counterpart \hat{s}_4 and corresponds to the standard factorized form of Eq. (4.45), while the second line displays the new factorization procedure. Hence, w_i refers to the function $\Psi_{i/i}$, whereas x_i refers to the parton distribution function Φ_i , so that we cannot set w_i and $(1-x_i)$ equal. At partonic threshold, the dynamics of the various functions becomes independent, and the partonic cross section reduces to a

convolution.

Convoluting thus the soft, hard, and jet functions, we receive an expression for the total partonic cross section in $n \cdot A = 0$ gauge [31]:

$$\begin{aligned}
E_p \frac{\hat{\sigma}_{ab \rightarrow c(p)+X}}{d^3p} &= \sum_{IL} H_{IL}^{(f)}(\hat{t}, \hat{u}) \int dw_a dw_b dw_p dw_S dw_X \\
&\times \delta \left(\frac{S_4}{S} - w_a \left(\frac{\hat{u}}{\hat{t} + \hat{u}} \right) - w_b \left(\frac{\hat{t}}{\hat{t} + \hat{u}} \right) - \sum_{i=p,S,X} w_i \right) \\
&\times \Psi_{a/a}(w_a, p_a, \zeta, n) \Psi_{b/b}(w_b, p_b, \zeta, n) \\
&\times J_c(w_p, p, \zeta, n) J_X(w_X, p_X, \zeta, n) S_{LI}^{(f)} \left(\frac{w_S S}{\mu}, \beta_i, \zeta, n \right). \quad (4.53)
\end{aligned}$$

The integration over the δ -function enforces the requirements for threshold. Further, β_i denotes the four-velocity for a parton i , $\beta_i^\mu = \sqrt{2/\hat{s}} p_i^\mu$, and $\Psi_{i/i}$ is the distribution of parton i in parton i with fixed momentum. The indices of the hard scattering function H_{IL} label the color structure for the scattering amplitude and its complex conjugate, so that we have for a given flavor f [32]:

$$H_{IL}^{(f)}(\hat{t}, \hat{u}, \alpha_s(\mu^2)) = h_L^{*(f)}(\hat{t}, \hat{u}, \alpha_s(\mu^2)) h_I^{(f)}(\hat{t}, \hat{u}, \alpha_s(\mu^2)). \quad (4.54)$$

Then, $H_{IL} S_{LI}$ is a matrix in the space of color exchange, except for the case of direct photon production, where H_{IL} and S_{LI} are simply functions. For that case $J_{c=\gamma}$ can be replaced by unity. Note further that S_{LI} is infrared safe due to the universality of collinear singularities, which have been absorbed into the $\Psi_{i/i}$. The next step is the transformation into Mellin moment space, which was introduced in Sec. 4.3. Starting with the hard-scattering function in Eq. (4.45), we get in N -space:

$$w_{ab}^N = \int_0^S d \left(\frac{\hat{s}_4}{S} \right) \left(1 - \frac{\hat{s}_4}{S} \right)^{N-1} w_{ab} \left(\frac{\hat{s}_4}{\mu^2}, \frac{\hat{t}}{\mu^2}, \frac{\hat{u}}{\mu^2}, \alpha_s(\mu^2) \right). \quad (4.55)$$

Comparing now the different structure of the partonic cross sections in Eqs. (4.45) and (4.53), where we have used different types of factorization, we obtain for the Mellin-transformed hard scattering function at threshold:

$$\begin{aligned}
w_{ab}^N &= \left[\frac{\Psi_{a/a}^{N, \frac{\hat{u}}{\hat{t}+\hat{u}}}(p_a \cdot \zeta) \Psi_{b/b}^{N, \frac{\hat{t}}{\hat{t}+\hat{u}}}(p_b \cdot \zeta)}{\Phi_{a/a}^{N, \frac{\hat{u}}{\hat{t}+\hat{u}}}(\mu^2) \Phi_{b/b}^{N, \frac{\hat{t}}{\hat{t}+\hat{u}}}(\mu^2)} \right] J_c^N(p \cdot \zeta) J_X^N(p_X \cdot n) \\
&\times \sum_{IL} H_{IL}^{(f)}(\hat{t}, \hat{u}) S_{LI}^{(f), \frac{S}{N\mu^2}}(\beta_i, \zeta, n) + \mathcal{O} \left(\frac{1}{N} \right). \quad (4.56)
\end{aligned}$$

For that we have set the initial-state partons $A = a$ and $B = b$ and have used Eq. (4.52) to connect S_4 and \hat{s}_4 . The term in the brackets containing the $\Psi_{i/i}$ and the $\Phi_{i/i}$ is universal

and depends only on the involved partons, but not on the process itself. It was first calculated for the Drell-Yan cross section [29]. The jet functions J_c are universal, too, and leading-logarithmic corrections are included in J_c and in $\Psi_{i/i}/\Phi_{i/i}$, while next-to-leading logarithmic corrections can then be found in J_c , $\Psi_{i/i}/\Phi_{i/i}$ and S .

By solving the evolution equations for each of the functions describing soft gluon emission in Eq. (4.56), we arrive at an explicit resummation formula for the hard scattering function w_{ab}^N and find out that N -dependences exponentiate. The explicit forms of the refactorized parton distribution functions $\Psi_{i/i}$ are collected in [29, 32, 103] and read,

$$\begin{aligned}\Psi_{q/q}(x, p, \zeta, \epsilon) &= \frac{1}{2N_c} \frac{p \cdot \zeta}{2\pi p \cdot v} \int_{-\infty}^{\infty} dy e^{-ixyp \cdot \zeta} \langle q(p) | \bar{q}(y\zeta) \frac{1}{2} v \cdot \gamma q(0) | q(p) \rangle, \\ \Psi_{\bar{q}/\bar{q}}(x, p, \zeta, \epsilon) &= \frac{1}{2N_c} \frac{p \cdot \zeta}{2\pi p \cdot v} \int_{-\infty}^{\infty} dy e^{-ixyp \cdot \zeta} \langle \bar{q}(p) | \text{Tr} \left[\frac{1}{2} v \cdot \gamma q(y\zeta) \bar{q}(0) \right] | \bar{q}(p) \rangle, \\ \Psi_{g/g}(x, p, \zeta, \epsilon) &= \frac{1}{2(N_c^2 - 1)} \frac{p \cdot \zeta}{4\pi(p \cdot v)^2} \int_{-\infty}^{\infty} dy e^{-ixyp \cdot \zeta} \langle g(p) | F^{\mu\perp}(y\zeta) [v_\mu v_\nu F^{\nu\perp}(0)] | g(p) \rangle,\end{aligned}\tag{4.57}$$

in terms of matrix elements of composite operators. They are evaluated in the center-of-mass frame using axial $n \cdot A = 0$ gauge and differ from standard light-cone parton distributions as they are defined at fixed energy, instead of at a light-like momentum fraction. The light-like vector v points in the opposite direction from p^μ , yielding $v \cdot \gamma = \gamma^\pm$. The argument ϵ labels a collinear singularity which is absorbed by Ψ in the factorized expression.

How we obtain now from Eq. (4.56) the resummed partonic cross section and how the radiative exponents are constructed is shown in the next subsection.

4.4.2. Radiative Factors

In the last section we found an expression for the threshold resummed hard scattering function in Mellin space in Eq. (4.56). Now we want to use the renormalization properties of the jet and soft functions to find a treatment for the N -dependence in that refactorized cross section. The matrices H and S act in a product, hence the renormalization takes place multiplicatively, with separate renormalization constants for the amplitude and its complex conjugate [32, 33],

$$\begin{aligned}H_{IL}^{(f)(0)} &= \prod_{i=a,b,c,X} Z_i^{-1} \left(Z_S^{(f)-1} \right)_{IC} H_{CD} \left[\left(Z_S^{(f)\dagger} \right)^{-1} \right]_{DL}, \\ S_{LI}^{(f)(0)} &= \left(Z_S^{(f)\dagger} \right)_{LB} S_{BA} Z_{S,AI}^{(f)}.\end{aligned}\tag{4.58}$$

We differ between Z_i , a renormalization constant of an incoming parton i , and $Z_{S,CD}^{(f)}$, being a matrix of renormalization constants connected to the renormalization of the soft

function $S_{IL}^{(f)}$. Then, by introducing $\Gamma_S^{(f)}$ as the soft anomalous dimension matrix, $S_{IL}^{(f)}$ satisfies the renormalization group equation:

$$\left(\mu \frac{\partial}{\partial \mu} + \beta(g) \frac{\partial}{\partial g} \right) S_{LI}^{(f)} = - \left(\Gamma_S^{(f)\dagger} \right)_{LB} S_{BI}^{(f)} - S_{LA}^{(f)} \left(\Gamma_S^{(f)} \right)_{AI}. \quad (4.59)$$

In $\overline{\text{MS}}$, the modified minimal subtraction renormalization scheme, with $\epsilon = 4 - D$ and D the space-time dimension, $\Gamma_S^{(f)}$ reads:

$$\Gamma_S^{(f)}(g) = -\frac{g}{2} \frac{\partial}{\partial g} \text{Res}_{\epsilon \rightarrow 0} Z_S^{(f)}(g, \epsilon). \quad (4.60)$$

The product of the hard scattering amplitude and the soft function is a trace taken in the basis of color space,

$$H_{IL}^{(f)} S_{LI}^{(f),N} = \text{Tr} \left\{ H^{(f)} S^{(f),N} \right\}. \quad (4.61)$$

Then, solving the renormalization group equation in Eq. (4.59) yields:

$$\begin{aligned} & \text{Tr} \left\{ H^{(f)} \left(\frac{M_{JJ}}{\mu}, \alpha_s(\mu^2) \right) S^{(f),N} \left(\frac{M_{JJ}}{N\mu}, \alpha_s(\mu^2) \right) \right\} \\ &= \text{Tr} \left\{ H^{(f)} \left(\frac{M_{JJ}}{\mu}, \alpha_s(\mu^2) \right) \times \overline{\mathcal{P}} \exp \left[\int_{\mu}^{M_{JJ}/N} \frac{d\mu'}{\mu'} \Gamma_S^{(f)\dagger}(\alpha_s(\mu'^2)) \right] \right. \\ & \quad \left. \times S^{(f),N} \left(1, \alpha_s(M_{JJ}^2/N^2) \right) \times \mathcal{P} \exp \left[\int_{\mu}^{M_{JJ}/N} \frac{d\mu'}{\mu'} \Gamma_S^{(f)}(\alpha_s(\mu'^2)) \right] \right\}. \end{aligned} \quad (4.62)$$

Note that the path ordering operator \mathcal{P} orders with respect to μ' such that for instance $\Gamma_S^{(f)}(\alpha_s(\mu^2))$ is to the far right and $\Gamma_S^{(f)}(\alpha_s(M_{JJ}^2/N^2))$ is on the far left. Choosing a basis, where $\Gamma_S^{(f)}$ appears to be diagonal, Eq. (4.62) simplifies and becomes a sum of exponentials [32].

Our next step is to obtain explicit expressions for the radiative exponents of resummation. We follow the formalism presented in [32, 104], but use the notation based on [26] when it comes to the radiative factors. Our starting point is Eq. (4.56), where the fraction of the functions Ψ_f and Φ_f appears. As a composite operator, the center of mass distribution Ψ does not need an overall renormalization [29]. Its renormalization behaviour is multiplicatively, as from its definition can be seen, where it is a matrix element [32] composed of a product of renormalized operators. From that, the renormalization group equation

$$\mu \frac{d\Psi_{f/f}^N(M_{JJ}/\mu, \epsilon)}{d\mu} = 2\gamma_f(\alpha_s(\mu^2)) \Psi_{f/f}^N(M_{JJ}/\mu, \epsilon), \quad (4.63)$$

is satisfied, with γ_f being the N-independent anomalous dimension of a field with flavor f . For the light-cone distribution Φ we have to choose a certain factorization scheme, so that we will choose again $\overline{\text{MS}}$. Then, the renormalization group equation with the anomalous

dimension of the color-diagonal splitting function is solved by

$$\mu \frac{d\Phi_{f/f}^N(\mu^2, \epsilon)}{d\mu} = 2\gamma_{ff}(N, \alpha_s(\mu^2))\Phi_{f/f}^N(\mu^2, \epsilon). \quad (4.64)$$

Only color diagonal splitting functions are singular for $x \rightarrow 1$, so that only flavor-diagonal evolution survives in the large- N region [32]. Up to one loop order, the anomalous dimensions γ_i of the quark- and gluon-fields and the corresponding terms of the diagonal splitting functions γ_{ii} read [26]:

$$\begin{aligned} \gamma_q(\alpha_s) &= \frac{3}{4}C_F \frac{\alpha_s}{\pi}, & \gamma_{qq}(N, \alpha_s) &= -\left(\ln N - \frac{3}{4}\right)C_F \frac{\alpha_s}{\pi}, \\ \gamma_g(\alpha_s) &= b_0\alpha_s, & \gamma_{gg}(N, \alpha_s) &= -(C_A \ln N - \pi b_0) \frac{\alpha_s}{\pi}. \end{aligned} \quad (4.65)$$

Remember, $b_0 = (11C_A - 4T_R N_f)/(12\pi)$ with $T_R = 1/2$ is the one-loop coefficient of the β -function, see Eq. (2.11). Finally we have reached a point, where the factorization scale dependence is determined by the evolution equations in Eqs. (4.63) and (4.64), so that we are ready to obtain the prefactor of Eq. (4.56) in $\overline{\text{MS}}$, describing jets:

$$\begin{aligned} \left[\frac{\Psi_{f/f}^N(M_{JJ}/\nu, \epsilon)}{\Phi_{f/f}^N(\nu^2, \epsilon)} \right] &= R_{(f)}(\alpha_s(M_{JJ}^2)) \exp[E_{(f)}(N, M_{JJ})] \\ &\times \exp\left\{-2 \int_{\mu}^{M_{JJ}} \frac{d\mu'}{\mu'} [\gamma_f(\alpha_s(\mu'^2)) - \gamma_{ff}(N, \alpha_s(\mu'^2))]\right\}. \end{aligned} \quad (4.66)$$

The radiative exponent is given in $\overline{\text{MS}}$ by:

$$\begin{aligned} E_{(f)}(N, M) &= -\int_0^1 dz \frac{z^{N-1} - 1}{1-z} \left\{ \int_{(1-z)^2}^1 \frac{dt}{t} A_f[\alpha_s(tM^2)] \right. \\ &\quad \left. + \bar{B}_f\left(\nu_i, \frac{M^2}{\hat{s}}, \alpha_s((1-z)^2 M^2)\right) \right\}. \end{aligned} \quad (4.67)$$

At zeroth-order we can normalize the N -independent function of the coupling $R_{(f)}(\alpha_s)$ to unity. In here, we use the following perturbative expansions,

$$\begin{aligned} A_f(\alpha_s) &= \frac{\alpha_s}{\pi} A_f^{(1)} + \left(\frac{\alpha_s}{\pi}\right)^2 A_f^{(2)} + \mathcal{O}(\alpha_s^3) = C_f \left(\frac{\alpha_s}{\pi} + \frac{1}{2}K \left(\frac{\alpha_s}{\pi}\right)^2\right) + \mathcal{O}(\alpha_s^3), \\ \bar{B}_f(\alpha_s) &= \frac{\alpha_s}{\pi} \bar{B}_f^{(1)} + \mathcal{O}(\alpha_s^2) = C_f \frac{\alpha_s}{\pi} \left[1 - \ln(2\nu_f) + \ln\left(\frac{M_f^2}{\hat{s}}\right)\right] + \mathcal{O}(\alpha_s^2), \end{aligned} \quad (4.68)$$

where N_f denotes the number of flavors, $C_f = C_F$ labels an incoming quark and $C_f = C_A$ an incoming gluon. Further,

$$K = C_A \left(\frac{67}{18} - \frac{\pi^2}{6}\right) - \frac{5}{9}N_f, \quad (4.69)$$

and $\nu_f \equiv (\beta_f \cdot n)^2 / (|n^2|)$ is the parton velocity. Finally, we are able to present the definition of the radiative soft-gluon exponent for initial-state partons [22] in $\overline{\text{MS}}$ scheme. In Mellin moment space we have,

$$\ln \Delta_f^{N_i}(M_f^2, \mu) = E_{(f)}(N_i, M_f) - 2 \int_{\mu}^{M_f} \frac{d\mu'}{\mu'} [\gamma_f(\alpha_s(\mu'^2)) - \gamma_{ff}(N, \alpha_s(\mu'^2))]. \quad (4.70)$$

with N_i defined for parton a as $N_a = (-\hat{u}/\hat{s})N$, and for parton b as $N_b = (-\hat{t}/\hat{s})N$.

The last step is to find some expressions for the still missing final-state jet function J_f^N in Eq. (4.56). For that we want to skip the derivation and refer to Ref. [32], as the calculation is shown very detailed there and follows in an analogous way to the initial-state contributions. It reads at NLL accuracy:

$$\begin{aligned} \ln J_f^N(M_{JJ}^2) = & \int_0^1 dz \frac{z^{N-1} - 1}{1-z} \left\{ \int_{(1-z)^2}^{(1-z)} \frac{dt}{t} A_f[\alpha_s(tM_{JJ}^2)] - \gamma_f[\alpha_s((1-z)M_{JJ}^2)] \right. \\ & \left. - \bar{B}_f[\nu_f, 1, \alpha_s((1-z)^2M_{JJ}^2)] \right\} + 2 \int_{\mu}^{M_{JJ}} \frac{d\mu'}{\mu'} \gamma_f(\alpha_s(\mu'^2)). \quad (4.71) \end{aligned}$$

Comparing the exponents for incoming and outgoing partons, see Eqs. (4.70) and (4.71), we find that leading logarithmic contributions, which emerge from the functions A_f of Eq. (4.68), are connected with opposite overall sign for the both soft gluon exponents. This results into an enhancement of the cross section from the LL contributions of the initial-state partons, and a suppression from the LL contributions of the final-state radiation. The amount of an overall suppression or enhancement depends on the partonic subprocess [32, 105].

Let us now put all terms together, the soft function, as well as the initial- and final-state jet functions, to arrive at the resummed partonic cross section in $\overline{\text{MS}}$:

$$\begin{aligned} w_{ab \rightarrow cX}^N = & \Delta_a^{N_a}(\hat{s}, \mu_{fi}) \Delta_b^{N_b}(\hat{s}, \mu_{fi}) J_c^N(\hat{s}) J_X^N(\hat{s}) \\ & \times \text{Tr} \left\{ H^{(f)} \left(\frac{\sqrt{\hat{s}}}{\mu}, \alpha_s(\mu^2) \right) \times \bar{\mathcal{P}} \exp \left[\int_{\mu}^{\sqrt{\hat{s}}/N} \frac{d\mu'}{\mu'} \Gamma_S^{(f)\dagger}(\alpha_s(\mu'^2)) \right] \right. \\ & \left. \times S^{(f),N}(1, \alpha_s(\hat{s}/N^2)) \times \mathcal{P} \exp \left[\int_{\mu}^{\sqrt{\hat{s}}/N} \frac{d\mu'}{\mu'} \Gamma_S^{(f)}(\alpha_s(\mu'^2)) \right] \right\}, \quad (4.72) \end{aligned}$$

where we have $N_a = (-\hat{u}/\hat{s})N$ and $N_b = (-\hat{t}/\hat{s})N$. As we will distinguish in the following between direct and resolved subprocesses, we have to modify the resummed cross section slightly. If one of the incoming or outgoing particles is a photon, the exponent is simply replaced by unity. Moreover, if we consider a final-state parton c , which fragments into the observed hadron h rather than a photon or a jet as final-state c , we get collinear singularities, which are absorbed into the fragmentation functions. Analogously to the initial-state partons we get thus an exponent Δ_c^N as in Eq. (4.70) [22], depending on the

final-state factorization scale μ_{ff} . However, the details of the construction of a resummed cross section for hadron-inclusive high- p_T lepton-nucleon scattering are shown in the next chapter. This case then pictures exactly the needed framework for COMPASS.

I am among those who think that science has great beauty.

Marie Curie

5

Threshold Resummation for Single-Inclusive Hadron Production

In the following chapter we want to address soft-gluon resummation to lepton-nucleon scattering as it takes place at COMPASS. This process is chosen due to different reasons. The question, how the nucleon spin of $1/2$ is composed of the gluon and quark spins and orbital angular momenta, is still much debated. Improved experimental results from high-energy scattering including longitudinally polarized nucleons were claimed, and the COMPASS experiment at CERN provides such data, namely for semi-inclusive hadron photoproduction $\gamma N \rightarrow hX$. Corresponding to the spin-averaged cross sections [18], COMPASS has presented results for the double-longitudinal spin asymmetry A_{LL} [19, 20]. This asymmetry is directly sensitive to the spin-dependent gluon distribution Δg , which in turn yields information on the gluon spin contribution to the proton spin.

This requires, however, high precision, implying the demand that the theoretical uncertainty of the analyses has to be much smaller than the experimental uncertainties. On the other hand, the kinematics at COMPASS for the chosen process is relatively close to the kinematic threshold, what means that nearly all available energy of the incoming partons is used to produce the high- p_T final-state parton and its recoiling counterpart. Then, the phase space for radiation of additional partons becomes small, and the cancelation of infrared singularities between real and virtual diagrams leave behind large logarithmic corrections to the cross section. These logarithms start at NLO and show up at every higher order in perturbation theory. In the threshold region, these logarithmic corrections may be resummed to all perturbative orders [29–36]. Threshold resummation to all orders is therefore an essential ingredient for the calculation of the cross sections and double-longitudinal spin asymmetries of lepton-nucleon scattering in these kinematic regions. Here, we complement the calculation of Ref. [22], where the spin-averaged resummed cross section has been investigated. Now we consider the polarized cross section, threshold resummed and

compare the NLO one, and afterwards use the polarized and unpolarized cross sections to obtain theoretical predictions for the double-longitudinal spin asymmetry. Besides direct contributions, for which the photon interacts in the usual point-like manner in the hard scattering, we also include resolved-photon contributions, where the photon reveals its partonic structure and interacts like a hadron. Note that the resolved subprocesses of $\gamma N \rightarrow hX$ are structurally equivalent to $pp \rightarrow hX$ scattering, for which relevant techniques have been presented in Refs. [31–35]. In these investigations spin-averaged cross sections were considered. Spin-polarized hadronic scattering $pp \rightarrow hX$, was considered in the framework of threshold resummation in Ref. [27], however, only integrated over all rapidities of the produced hadron. In the following, we perform resummation at *arbitrary fixed* rapidity, using the techniques developed in Refs. [22, 26, 37, 106].

The chapter starts with the general theoretical framework in Sec. 5.1, followed by a discussion of the transformation into Mellin momentum space in Sec. 5.2, so that we can then come to the resummed hard-scattering function in Sec. 5.3. For that we will need hard- and soft-matrices, which will be examined in Sec. 5.3.2. We follow then with an investigation of the NLO calculation in Sec. 5.4 and how the fixed-order calculation can be used to extract matching-coefficients in Sec. 5.5. Finally we apply an inverse Mellin transformation in Sec. 5.6 to the resummed cross section and match it to the NLO one. We conclude the chapter with a sketchy introduction of the double-longitudinal spin asymmetry in Sec. 5.7. Parts of this chapter are already published in Refs. [38, 39].

5.1. Theoretical Framework

We consider the hadron production process (see Fig. 5.1)

$$\ell N \rightarrow \ell' hX, \quad (5.1)$$

in which an initial lepton ℓ scatters off a nucleon N , both with longitudinal polarization. A (semi-inclusively) produced parton c hadronizes then into the charged hadron h with high transverse momentum p_T , ensuring the demanded large momentum transfer. As the scattered lepton ℓ' is required to have a small scattering angle with respect to the initial one, the underlying process can be treated as *photoproduction* process $\gamma N \rightarrow hX$, for which the main contributions come from almost on-shell photons exchanged between the lepton and the nucleon. Then, if the transverse momentum p_T of the observed hadron is sufficiently large, perturbative-QCD techniques can be applied.

We use factorization to write the differential spin-dependent cross section $d\Delta\sigma$ as func-

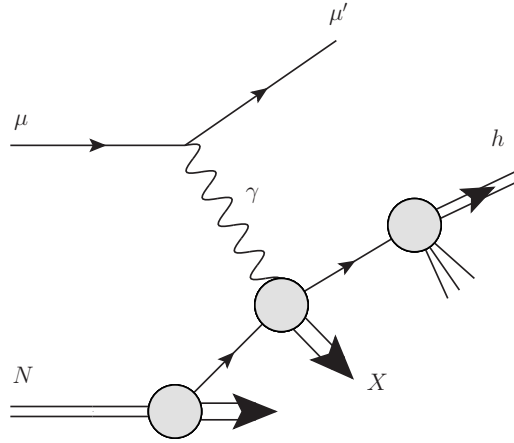


Fig. 5.1.: Single-inclusive high- p_T hadron production in lepton scattering (direct contribution).

tion of p_T and the hadron's pseudorapidity η as [24, 25]:

$$\frac{p_T^3 d\Delta\sigma}{dp_T d\eta} = \sum_{abc} \int_{x_\ell^{\min}}^1 dx_\ell \int_{x_n^{\min}}^1 dx_n \int_x^1 dz \frac{\hat{x}_T^4 z^2 \hat{s} d\Delta\hat{\sigma}_{ab \rightarrow cX}(v, w, \hat{s}, \mu_r, \mu_{fi}, \mu_{ff})}{8v} \times \Delta f_{a/\ell}(x_\ell, \mu_{fi}) \Delta f_{b/N}(x_n, \mu_{fi}) D_{h/c}(z, \mu_{ff}), \quad (5.2)$$

where the sum runs over all possible partonic channels $ab \rightarrow cX$. $\Delta f_{a/\ell}(x_\ell, \mu_{fi})$ and $\Delta f_{b/N}(x_n, \mu_{fi})$ label the polarized parton distribution functions for the lepton and the nucleon, respectively, depending on the momentum fractions x_ℓ and x_n , carried by the partons a and b , and on the initial-state factorization scale μ_{fi} . They can be written as differences of distributions for positive and negative helicity in a parent nucleon of positive helicity,

$$\Delta f_{b/N}(x, \mu) \equiv f_{b/N}^+(x, \mu) - f_{b/N}^-(x, \mu). \quad (5.3)$$

The $D_{h/c}(z, \mu_{ff})$ are the parton-to-hadron fragmentation functions describing the hadronization of parton c into the observed hadron h , with z being the fraction of the parton's momentum taken by the hadron. Further they depend on the final-state factorization scale μ_{ff} . Finally, the $d\Delta\hat{\sigma}_{ab \rightarrow cX}$ are the differential spin-dependent partonic hard-scattering cross sections, and can be obtained as well as the spin-averaged cross sections as difference and sum of helicity cross sections, analogously to Eq. (5.3),

$$\begin{aligned} d\Delta\hat{\sigma}_{ab \rightarrow cX} &\equiv \frac{1}{2} [(d\hat{\sigma}_{ab \rightarrow cX})^{++} - (d\hat{\sigma}_{ab \rightarrow cX})^{+-}], \\ d\hat{\sigma}_{ab \rightarrow cX} &\equiv \frac{1}{2} [(d\hat{\sigma}_{ab \rightarrow cX})^{++} + (d\hat{\sigma}_{ab \rightarrow cX})^{+-}], \end{aligned} \quad (5.4)$$

where the superscripts denote the helicities of the initial states. We have implied parity conservation, i.e. $d\sigma^{+-} \equiv d\sigma^{-+}$ and $d\sigma^{++} \equiv d\sigma^{--}$. In the case of spin-averaged hadronic

cross sections, we also need spin-averaged distribution functions. Both cross sections are at high energies and thus can be expanded in terms of the coupling constant α_s :

$$d\Delta\hat{\sigma}_{ab\rightarrow cX} = d\Delta\hat{\sigma}_{ab\rightarrow cX}^{(0)} + \frac{\alpha_s}{\pi}d\Delta\hat{\sigma}_{ab\rightarrow cX}^{(1)} + \dots \quad (5.5)$$

Besides their dependence on the factorization scales μ_{fi} and μ_{ff} , a renormalization scale μ_r is introduced, where one chooses them all to be equal, typically $\mu_{fi} = \mu_{ff} = \mu_r = p_T$. Further the cross section varies with the kinematic variables introduced in Eq. (5.2):

$$v \equiv 1 + \frac{\hat{t}}{\hat{s}} = 1 - \frac{\hat{x}_T}{2}e^{-\hat{\eta}}, \quad \text{and} \quad w \equiv \frac{-\hat{u}}{\hat{s} + \hat{t}} = \frac{1}{v} \frac{\hat{x}_T}{2}e^{\hat{\eta}}, \quad (5.6)$$

with the partonic Mandelstam variables

$$\begin{aligned} \hat{s} &= (p_a + p_b)^2 = x_\ell x_n S, \\ \hat{t} &= (p_a - p_c)^2 = -\frac{\hat{s}\hat{x}_T}{2}e^{-\hat{\eta}}, \\ \hat{u} &= (p_b - p_c)^2 = -\frac{\hat{s}\hat{x}_T}{2}e^{\hat{\eta}}, \end{aligned} \quad (5.7)$$

and where p_a, p_b, p_c are the four-momenta of the participating partons. Furthermore, $S = (p_\ell + p_n)^2$, with the lepton (nucleon) momentum p_ℓ (p_n). Moreover, we have

$$\hat{x}_T \equiv \frac{x_T}{z\sqrt{x_\ell x_n}}, \quad \text{and} \quad \hat{\eta} \equiv \eta - \frac{1}{2} \ln \frac{x_\ell}{x_n}, \quad (5.8)$$

where $x_T \equiv 2p_T/\sqrt{S}$, with \sqrt{S} and η being the hadronic center-of-mass energy and rapidity, respectively, the latter counted positive in the lepton forward direction. The lower integration bounds in Eq. (5.2) are given by

$$\begin{aligned} x_\ell^{\min} &= \frac{x_T e^\eta}{2 - x_T e^{-\eta}}, \\ x_n^{\min} &= \frac{x_\ell x_T e^{-\eta}}{2x_\ell - x_T e^\eta}, \\ x &= \frac{x_T \cosh \hat{\eta}}{\sqrt{x_n x_\ell}}. \end{aligned} \quad (5.9)$$

An important aspect of photoproduction is that the quasi-real photons can interact in two different ways. On the one hand, it participates as a pointlike photon *directly* (see Fig. 5.1), i.e. electromagnetically, coupling to the parton b in the nucleon. This contribution is called the direct part of the cross section $\Delta\sigma_{\text{dir}}$. On the other hand, the photon reveals its own partonic structure: Photons couple to quantum fluctuations containing quarks, antiquarks and gluons. For a quasi-real photon these contributions are not suppressed by additional, strongly virtual propagators and the physical photon eigenstate contains an appreciable

QCD part. This behaviour is described by photonic parton distribution functions just as for normal hadrons, see Fig. 5.2. The resulting contribution is called *resolved* photon contribution. The physical cross section is the sum of both parts together:

$$d\Delta\sigma = d\Delta\sigma_{\text{dir}} + d\Delta\sigma_{\text{res}}. \quad (5.10)$$

The corresponding parton density can thus be written by introducing a suitable “parton-in-lepton” distribution [24, 25]:

$$\Delta f_{a/\ell}(x_\ell, \mu_{fi}) = \int_{x_\ell}^1 \frac{dy}{y} \Delta P_{\gamma\ell}(y) \Delta f_{a/\gamma}\left(x_\gamma = \frac{x_\ell}{y}, \mu_{fi}\right). \quad (5.11)$$

It is a convolution of the probability density $\Delta P_{\gamma\ell}(y)$ of having a polarized “Weizsäcker-Williams” photon with lepton momentum fraction y accompanying the initial-state lepton, with the probability density $\Delta f_{a/\gamma}(x_\gamma, \mu_{fi})$ of finding a polarized parton a with momentum fraction x_γ in this photon. One can write the direct photon case, see Fig. 5.1, in the same manner as the resolved one by setting

$$\Delta f_{\gamma/\gamma} = \delta(1 - x_\gamma). \quad (5.12)$$

$\Delta f_{a/\gamma}$ is dominated at high x_γ by the perturbative “pointlike” contribution and at low-to-mid x_γ by the non-perturbative “hadronic” piece. The hadronic contribution has the same quantum numbers as the photon, i.e. it is of vector meson type. In a popular approximation it is assumed to have a hadronic structure similar to the ρ meson. The probability density $\Delta P_{\gamma\ell}(y)$ is given by [107]

$$\Delta P_{\gamma\ell}(y) = \frac{\alpha}{2\pi} \left[\frac{1 - (1 - y)^2}{y} \ln \left(\frac{Q_{\text{max}}^2(1 - y)}{m_\ell^2 y^2} \right) + 2m_\ell^2 y^2 \left(\frac{1}{Q_{\text{max}}^2} - \frac{1 - y}{m_\ell^2 y^2} \right) \right]. \quad (5.13)$$

Here α is the fine structure constant, m_ℓ the lepton mass, and the virtuality Q^2 is restricted by an upper limit Q_{max}^2 determined by experimental conditions on the small-angle scattered lepton. At leading order there are three different direct subprocesses,

$$\gamma q \rightarrow g(q), \quad \gamma q \rightarrow q(g), \quad \gamma g \rightarrow q(\bar{q}), \quad (5.14)$$

where the final-state particle in brackets is understood to be unobserved and is fully phase-space integrated, while the other fragments into the detected high- p_T hadron. The first and second subprocesses describe Compton scattering, the third one describes photon-gluon-fusion, which is symmetric under exchange of q and \bar{q} . The direct cross sections start at lowest order (LO) at $\mathcal{O}(\alpha\alpha_s)$ [23] and read:

$$\frac{\hat{s} d\Delta\hat{\sigma}_{\gamma q \rightarrow g(q)}^{(0)}(v, w)}{dv dw} = 2\pi\alpha\alpha_s e_q^2 C_F \frac{1 - v^2}{v} \delta(1 - w),$$

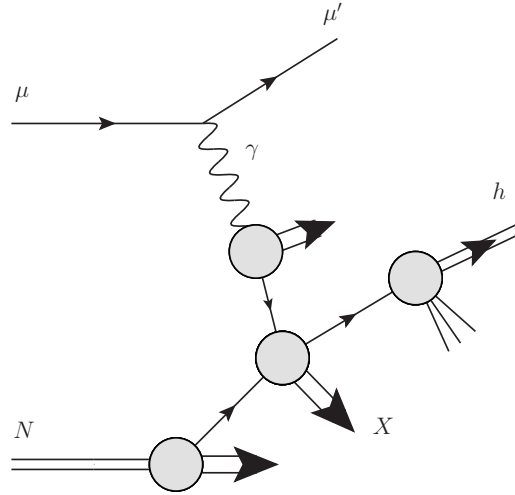


Fig. 5.2.: Resolved-photon contribution to high- p_T hadron production in lepton scattering.

$$\begin{aligned} \frac{\hat{s}d\Delta\hat{\sigma}_{\gamma q \rightarrow q(g)}^{(0)}(v, w)}{dv dw} &= 2\pi\alpha\alpha_s e_q^2 C_F \frac{1 - (1-v)^2}{1-v} \delta(1-w), \\ \frac{\hat{s}d\Delta\hat{\sigma}_{\gamma g \rightarrow q(\bar{q})}^{(0)}(v, w)}{dv dw} &= -2\pi\alpha\alpha_s e_q^2 T_R \frac{v^2 + (1-v)^2}{v(1-v)} \delta(1-w), \end{aligned} \quad (5.15)$$

with $C_F = 4/3$, $T_R = 1/2$ and the fractional electromagnetic charge of the quark e_q .

For the resolved contributions, all $2 \rightarrow 2$ QCD partonic processes contribute to LO:

$$\begin{aligned} q q' \rightarrow q q', \quad q \bar{q}' \rightarrow q \bar{q}', \quad q \bar{q} \rightarrow q' \bar{q}', \quad q q \rightarrow q q, \quad q \bar{q} \rightarrow q \bar{q}, \\ q \bar{q} \rightarrow g g, \quad g q \rightarrow q g, \quad g g \rightarrow g q, \quad g g \rightarrow g g, \quad g g \rightarrow q \bar{q}, \end{aligned} \quad (5.16)$$

where one of the final-state partons fragments into the observed hadron. The cross section is of order $\mathcal{O}(\alpha_s^2)$. Since, however, the photon's parton distributions $\Delta f_{a/\gamma}$ are of order α/α_s [21], the resolved contribution is of the same perturbative order as the direct one. For the ℓN cross section they are of order $\alpha^2\alpha_s$ and for the γN one they are of order $\alpha\alpha_s$. This is true to all orders. As one can see in Eq. (5.15), the LO partonic cross section is proportional to $\delta(1-w)$ [28],

$$\frac{\hat{s}d\Delta\hat{\sigma}_{\gamma b \rightarrow cd}^{(0)}(v, w)}{dv dw} = \frac{\hat{s}d\Delta\hat{\sigma}_{\gamma b \rightarrow cd}^{(0)}(v)}{dv} \delta(1-w), \quad (5.17)$$

accounting for the fact that one has $2 \rightarrow 2$ kinematics, hence $w \equiv 1$ and therefore $x_T \cosh \hat{\eta} \equiv 1$. The reason for this is that $(1-w)$ measures the invariant mass of the partonic recoil. Hence, from (5.6) follows that the invariant mass squared of the final state that recoils against the fragmenting parton is given by

$$\hat{s}_4 = \hat{s} + \hat{t} + \hat{u} = \hat{s}v(1-w) = \hat{s}(1 - \hat{x}_T \cosh \hat{\eta}). \quad (5.18)$$

The structure of the NLO cross section is more complicated. NLO ($\mathcal{O}(\alpha_s^2)$) QCD corrections to polarized high- p_T photoproduction of hadrons can be found in [23–25]. Now various types of distributions in $(1-w)$ arise, and analytical expressions are presented in Refs. [23, 24, 108–111]. They can be cast into the form

$$\frac{\hat{s}d\Delta\hat{\sigma}_{ab\rightarrow cX}^{(1)}}{dv dw} = A(v)\delta(1-w) + B(v)\left(\frac{\ln(1-w)}{1-w}\right)_+ + C(v)\left(\frac{1}{1-w}\right)_+ + F(v,w), \quad (5.19)$$

with the plus-distributions defined as

$$\int_0^1 dw f(w) [g(w)]_+ \equiv \int_0^1 dw [f(w) - f(1)]g(w). \quad (5.20)$$

$A(v), B(v), C(v), F(v, w)$ in (5.19) are well-known functions and depend on the partonic process under consideration. $F(v, w)$ collects all terms without distributions in $(1-w)$. Then, the terms with plus-distributions give rise to the large double-logarithmic threshold corrections which recur with higher logarithmic power at every higher order of α_s . They arise from soft-gluon radiation and will be addressed by threshold resummation. At k -th order we have leading corrections proportional to $\alpha_s^k [\ln^{2k-1}(1-w)/(1-w)]_+$ (not counting the overall power of the partonic process in α_s), and subleading terms down by one or more powers of $\ln(1-w)$. We resum these logarithmic corrections on next-to-leading logarithmic (NLL) level, so that we take the three “towers” $\alpha_s^k [\ln^{2k-1}(1-w)/(1-w)]_+$, $\alpha_s^k [\ln^{2k-2}(1-w)/(1-w)]_+$ and $\alpha_s^k [\ln^{2k-3}(1-w)/(1-w)]_+$ into account to all orders in α_s . The framework for that will be described in the following.

5.2. Transformation to Mellin Moment Space

As we have seen in Sec. 4.2, a transformation into Mellin moment space is suitable due to different reasons, so that we will perform our calculations in Mellin space. We need an exponentiation and hence factorization of the phase space factor, which is only provided in Mellin space. This has the advantage that a convolution of distribution functions and the partonic cross section turn then into an ordinary product of moments. However, we will not transform the complete expression, i.e. the partonic cross section is convoluted with parton distribution functions and fragmentation function. Only a part of it will be transformed yielding to rapidity dependence in the resummed cross section. Afterwards we take the Mellin inverse of the corresponding products of Mellin moments, see [22, 37]. We transform only the fragmentation functions convoluted with the partonic hard scattering cross section, in the following the scaling variable x^2 :

$$\int_0^1 dx^2 (x^2)^{N-1} \int_x^1 dz \frac{\hat{x}_T^4 z^2}{8v} D_{h/c}(z, \mu_{ff}) \frac{\hat{s}d\Delta\hat{\sigma}_{ab\rightarrow cX}}{dv dw} \equiv D_{h/c}^{2N+3}(\mu_{ff}) \Delta\tilde{w}_{ab\rightarrow cX}^{2N}(\hat{\eta}). \quad (5.21)$$

$\Delta\tilde{w}(N, \hat{\eta})$ is the hard scattering function in Mellin- N moment space

$$\Delta\tilde{w}_{ab\rightarrow cX}^N(\hat{\eta}) = 2 \int_0^1 d\left(\frac{\hat{s}_4}{\hat{s}}\right) \left(1 - \frac{\hat{s}_4}{\hat{s}}\right)^{N-1} \frac{\hat{x}_T^4 z^2}{8v} \frac{\hat{s} d\Delta\hat{\sigma}_{ab\rightarrow cX}}{dv dw}, \quad (5.22)$$

written as an integration over $\hat{s}_4/\hat{s} = v(1-w)$ and depending further without additional listing on \hat{s} , μ_r , μ_{fi} and μ_{ff} by having its origin in $d\Delta\hat{\sigma}_{ab\rightarrow cX}$. $D_{h/c}^N$ are the fragmentation functions transformed in z

$$D_{h/c}^N(\mu_{ff}) = \int_0^1 dz z^{N-1} D_{h/c}(z, \mu_{ff}). \quad (5.23)$$

Their presence is important for making the Mellin-inverse well-behaved yielding good numerical convergence, as they fall off rapidly at large N , typically as $1/N^4$ or faster, and thus tame the logarithms in N . The integration contour \mathcal{C} of the Mellin inverse goes in a tilted line from $C - i\infty$ to $C + i\infty$, with C being a positive real number and chosen in such a way that all singularities of the integrand lie to the left of the contour \mathcal{C} , except the Landau pole. We will come later to this point. After performing the inverse Mellin transform we are ready to receive the cross section in Eq. (5.2):

$$\begin{aligned} \frac{p_T^3 d\Delta\hat{\sigma}}{dp_T d\eta} &= \sum_{a,b,c} \int_0^1 dx_l \int_0^1 dx_n \Delta f_{a/l}(x_l, \mu_{fi}) \Delta f_{b/N}(x_n, \mu_{fi}) \\ &\times \int_{\mathcal{C}} \frac{dN}{2\pi i} (x^2)^{-N} D_{h/c}^{2N+3}(\mu_{ff}) \Delta\tilde{w}_{ab\rightarrow cX}^{2N}(\hat{\eta}). \end{aligned} \quad (5.24)$$

At all times we keep the parton distribution functions in x -space. Now the threshold region $w \rightarrow 1$ comes along with large Mellin moments in N and soft-gluon corrections appearing through plus-distributions, see Eq. (5.19), are transferred into powers of $\ln N$. In more detail, the ‘‘towers’’ $\alpha_s^k [\ln^{2k-1}(1-w)/(1-w)]_+$, $\alpha_s^k [\ln^{2k-2}(1-w)/(1-w)]_+$ and $\alpha_s^k [\ln^{2k-3}(1-w)/(1-w)]_+$ mentioned before, turn into the NLL terms $\alpha_s^k \ln^{2k} N$, $\alpha_s^k \ln^{2k-1} N$, and $\alpha_s^k \ln^{2k-2} N$ in Mellin space.

5.3. NLL-Resummed Hard-Scattering Function

In the previous section we have seen that resummation has to take place in Mellin momentum space. Let us now consider the resummed hard-scattering function at NLL accuracy and the functions it is composed of in more detail. We found out in Chap. 4 that the resummed cross section in Mellin space factorizes into functions describing soft gluon emission off each parton, a function describing the hard scattering process, and a soft function. However, we have investigated in that chapter single-inclusive resummed cross sections for a final observed photon or jet. Now our final state is a parton fragmenting into an observed hadron with high transverse momentum p_T . We get final-state collinear singularities, which are absorbed into the fragmentation functions and yield analogously to the

initial-state partons an exponent of the form Δ_c^N as in Eq. (4.70). Thus, the resummed hard-scattering function reads [22, 26, 31, 32]:

$$\begin{aligned} \Delta \tilde{w}_{ab \rightarrow cd}^{\text{resum}, N}(\hat{\eta}) = & \Delta_a^{N_a}(\hat{s}, \mu_{fi}, \mu_r) \Delta_b^{N_b}(\hat{s}, \mu_{fi}, \mu_r) \Delta_c^N(\hat{s}, \mu_{ff}, \mu_r) J_d^N(\hat{s}, \mu_r) \\ & \times \text{Tr} \left\{ \Delta H S_N^\dagger S S_N \right\}_{ab \rightarrow cd}, \end{aligned} \quad (5.25)$$

with $N_a = (-\hat{u}/\hat{s})N$ and $N_b = (-\hat{t}/\hat{s})N$. The dynamics of soft radiated gluons is described for each interacting initial- and final-state parton by a specific function, namely the functions $\Delta_a^{(-\hat{u}/\hat{s})N}$, $\Delta_b^{(-\hat{t}/\hat{s})N}$ and Δ_c^N in (5.25), which describe soft radiation collinear to the initial-state parton a , b and the final and fragmenting parton c , respectively. They are spin-independent exponentials and given in the $\overline{\text{MS}}$ scheme by [31]

$$\begin{aligned} \ln \Delta_i^N(\hat{s}, \mu_f, \mu_r) = & - \int_0^1 dz \frac{z^{N-1} - 1}{1-z} \int_{(1-z)^2}^1 \frac{dt}{t} A_i(\alpha_s(t\hat{s})) \\ & - 2 \int_{\mu_r}^{\sqrt{\hat{s}}} \frac{d\mu'}{\mu'} \gamma_i(\alpha_s(\mu'^2)) + 2 \int_{\mu_f}^{\sqrt{\hat{s}}} \frac{d\mu'}{\mu'} \gamma_{ii}(N, \alpha_s(\mu'^2)), \end{aligned} \quad (5.26)$$

where the functions A_i , γ_i and γ_{ii} , for $i = q, g$ describing a quark or a gluon, are perturbative series in the strong coupling. The function J_d^N describes soft and hard collinear emission off the unobserved recoiling parton d . We have [31]

$$\begin{aligned} \ln J_d^N(\hat{s}, \mu_r) = & \int_0^1 dz \frac{z^{N-1} - 1}{1-z} \left\{ \int_{(1-z)^2}^{(1-z)} \frac{dt}{t} A_d(\alpha_s(t\hat{s})) - \gamma_d(\alpha_s((1-z)\hat{s})) \right\} \\ & + 2 \int_{\mu_r}^{\sqrt{\hat{s}}} \frac{d\mu'}{\mu'} \gamma_d(\alpha_s(\mu'^2)). \end{aligned} \quad (5.27)$$

The first terms of the perturbative function A_i are given by

$$A_i(\alpha_s) = \frac{\alpha_s}{\pi} A_i^{(1)} + \left(\frac{\alpha_s}{\pi} \right)^2 A_i^{(2)} + \mathcal{O}(\alpha_s^3) = C_f \left(\frac{\alpha_s}{\pi} + \frac{1}{2} K \left(\frac{\alpha_s}{\pi} \right)^2 \right), \quad (5.28)$$

with

$$K = C_A \left(\frac{67}{18} - \frac{\pi^2}{6} \right) - \frac{5}{9} N_f, \quad (5.29)$$

N_f being the number of flavors,

$$C_{f=q} = C_F = \frac{N_c^2 - 1}{2N_c} = 4/3 \quad (5.30)$$

for a quark and $C_{f=g} = C_A = N_c = 3$ for a gluon. The quark and gluon field anomalous dimensions are γ_i and the γ_{ii} correspond to the constant and logarithmic terms of the

moments of the diagonal splitting functions, reading to one-loop order [26, 31]:

$$\begin{aligned}\gamma_q(\alpha_s) &= \frac{3}{4}C_F\frac{\alpha_s}{\pi}, & \gamma_{qq}(N, \alpha_s) &= -\left(\ln N - \frac{3}{4}\right)C_F\frac{\alpha_s}{\pi}, \\ \gamma_g(\alpha_s) &= b_0\alpha_s, & \gamma_{gg}(N, \alpha_s) &= -(C_A \ln N - \pi b_0)\frac{\alpha_s}{\pi},\end{aligned}\quad (5.31)$$

where b_0 is the one-loop coefficient of the β -function, $b_0 = (11C_A - 4T_R N_f)/(12\pi)$, with $T_R = 1/2$. Generally, γ_{ii} can be expressed through the anomalous dimension at lowest order:

$$\gamma_{ii} = -\ln N A_i^{(1)}\frac{\alpha_s}{\pi} + \gamma_i(\alpha_s). \quad (5.32)$$

Next, we consider the trace in Eq. (5.25), being comprised of functions which are matrices in the space of color exchange operators. The trace has to be taken also in this space [32, 33, 37] and is the only part of the hard-scattering function which carries an $\hat{\eta}$ -dependence. Spin-dependence is taken explicitly into account through the hard-scattering function $\Delta H_{ab\rightarrow cd}$ and $S_{ab\rightarrow cd}$ is a soft function. One can expand each of the functions perturbatively [37], so that the hard-scattering function reads,

$$\Delta H_{ab\rightarrow cd}(\hat{\eta}, \alpha_s) = \Delta H_{ab\rightarrow cd}^{(0)}(\hat{\eta}) + \frac{\alpha_s}{\pi}\Delta H_{ab\rightarrow cd}^{(1)}(\hat{\eta}) + \mathcal{O}(\alpha_s^2), \quad (5.33)$$

and analogously the soft function describing large-angle gluons,

$$S_{ab\rightarrow cd}(\hat{\eta}, \alpha_s) = S_{ab\rightarrow cd}^{(0)} + \frac{\alpha_s}{\pi}S_{ab\rightarrow cd}^{(1)}\left(\hat{\eta}, \alpha_s, \frac{\sqrt{\hat{s}}}{N}\right) + \mathcal{O}(\alpha_s^2), \quad (5.34)$$

both approximated by their lower order contributions. In the latter the N dependence of the NLO term enters the hard-scattering function only at next-to-next-to-leading logarithmic level (NNLL). At LO, the soft terms $S_{ab\rightarrow cd}^{(0)}$ are independent of $\hat{\eta}$. Wide-angle soft gluons interchanged between the partons are taken into account by the functions $\mathcal{S}_{N,ab\rightarrow cd}$ and $\mathcal{S}_{N,ab\rightarrow cd}^\dagger$. These functions are path- and antipath-ordered exponentials in terms of the soft anomalous dimension matrices $\Gamma_{ab\rightarrow cd}$ [32, 33, 37]:

$$\mathcal{S}_{N,ab\rightarrow cd}(\hat{\eta}, \alpha_s) = \mathcal{P} \exp \left[\int_{\mu_r}^{\sqrt{\hat{s}}/N} \frac{d\mu'}{\mu'} \Gamma_{ab\rightarrow cd}(\hat{\eta}, \alpha_s(\mu')) \right]. \quad (5.35)$$

Starting at $\mathcal{O}(\alpha_s)$, the soft anomalous dimension matrices read:

$$\Gamma_{ab\rightarrow cd}(\hat{\eta}, \alpha_s) = \frac{\alpha_s}{\pi}\Gamma_{ab\rightarrow cd}^{(1)}(\hat{\eta}) + \mathcal{O}(\alpha_s^2). \quad (5.36)$$

We will consider later in Sec. 5.3.2 the hard, soft and Γ -matrices in more detail and will distinguish between the direct- and the resolved-photon contributions. We will summarize them in Appendix B.

5.3.1. Exponents at NLL

Before we have introduced the hard-scattering function. It consists of hard and soft matrices and various functions, all exponentials, describing the dynamics of soft radiated gluons collinear to the initial- or final-state partons. Their structure is shown in Eq. (5.26) and (5.27), where we have several integrations to solve. In this part of the work we will show how to receive the exponents in Mellin space at next-to-leading logarithmic accuracy. The calculation will take place at threshold limit implying large N .

Let us start with the function describing radiation off the observed partons a , b or c . We start with the first part of the expression in Eq. (5.26). The t -integration can be solved by using the NLO solution of the renormalization group equation to express the running coupling $\alpha_s(k^2) \equiv \alpha_s(t\hat{s})$ in terms of $\alpha_s(\mu^2)$ [44, 45]:

$$\begin{aligned} \alpha_s(k^2) = & \frac{\alpha_s(\mu^2)}{1 + b_0\alpha_s(\mu^2) \ln\left(\frac{k^2}{\mu^2}\right)} \left[1 - \frac{b_1}{b_0} \frac{\alpha_s(\mu^2)}{1 + b_0\alpha_s(\mu^2) \ln\left(\frac{k^2}{\mu^2}\right)} \ln\left(1 + b_0\alpha_s(\mu^2) \ln\left(\frac{k^2}{\mu^2}\right)\right) \right. \\ & \left. + \mathcal{O}\left(\alpha_s^2(\mu^2) \left(\alpha_s(\mu^2) \ln\left(\frac{k^2}{\mu^2}\right)\right)^n\right) \right]. \end{aligned} \quad (5.37)$$

Using the approximation [30],

$$z^{N-1} - 1 \simeq -\Theta\left(1 - \frac{1}{N} - z\right), \quad (5.38)$$

where $\bar{N} \equiv Ne^{\gamma_E}$, we get for the first NLL expanded integral,

$$\begin{aligned} & - \int_0^1 dz \frac{z^{N-1} - 1}{1 - z} \int_{(1-z)^2}^1 \frac{dt}{t} A_i[\alpha_s(t\hat{s})] \\ & = \int_0^1 dz \frac{1}{1 - z} \Theta\left(1 - z - \frac{1}{\bar{N}}\right) \int_{(1-z)^2}^1 \frac{dt}{t} A_i[\alpha_s(t\hat{s})] \\ & = - \frac{A_i^{(2)}}{2\pi^2 b_0^2} [2\lambda + \ln(1 - 2\lambda)] + \frac{A_i^{(1)}}{2\pi b_0^2 \alpha_s} [2\lambda + (1 - 2\lambda) \ln(1 - 2\lambda)] \\ & \quad + \frac{A_i^{(1)} b_1}{2\pi b_0^3} \left[2\lambda + \ln(1 - 2\lambda) + \frac{1}{2} \ln^2(1 - 2\lambda) \right] + \frac{A_i^{(1)}}{2\pi b_0} [2\lambda + \ln(1 - 2\lambda)] \ln\left(\frac{\hat{s}}{\mu_r^2}\right) \\ & \quad - \frac{A_i^{(1)} \gamma_E}{\pi b_0} \ln(1 - 2\lambda), \end{aligned} \quad (5.39)$$

depending on λ ,

$$\lambda \equiv b_0 \alpha_s \ln N. \quad (5.40)$$

As was pointed out in Eq. (5.24) for a NLL resummed cross section, we need the hard scattering function shifted in its Mellin moments, this means in dependence of $2N$. Further we have seen the various Mellin-dependences in Eq. (5.25). This means, instead of the

usual exponent $\ln \Delta_i^N$ we need the one depending on $2N_i$ to calculate the appropriate hard scattering function. Therefore, we have to shift $N \rightarrow 2N_i \equiv a_i N$, with $N_a = (-\hat{u}/\hat{s})N$, $N_b = (-\hat{t}/\hat{s})N$ for the initial-state partons a and b , and with $N_c = N$ for the final-state parton c . This gives us an additional term in the exponent,

$$-\frac{A_i^{(1)} \ln(a_i)}{b_0 \pi} \ln(1 - 2\lambda). \quad (5.41)$$

The integration of the anomalous dimensions γ_i in form of the second integral gives no contribution at all to a NLL-expanded exponent. However, the third integration in Eq. (5.26) does:

$$2 \int_{\mu_{fi}}^{\sqrt{\hat{s}}} \frac{d\mu'}{\mu'} \gamma_{ii}(N, \alpha_s(\mu'^2)) = -\frac{A_i^{(1)} \lambda}{\pi b_0} \ln \frac{\hat{s}}{\mu_{fi}^2}. \quad (5.42)$$

Here, a shift $N \rightarrow 2N_i$ does not change the NLL contribution. Remember, in a NLL expanded exponent at k -th order only the leading terms of order $\alpha_s^k \ln^{k+1} N$ and the next-to-leading logarithmic terms of order $\alpha_s^k \ln^k N$ contribute. We have used expansions like

$$\begin{aligned} \ln(1 - 2\alpha_s b_0 \ln(a_i N)) &= \ln(1 - 2\lambda - 2\alpha_s b_0 \ln a_i) \\ &= \ln(1 - 2\lambda) - \sum_{k=1}^{\infty} \frac{(2\alpha_s b_0 \ln a_i)^k}{k(1 - 2\lambda)^k} \approx \ln(1 - 2\lambda) - \frac{2\alpha_s b_0 \ln a_i}{1 - 2\lambda}, \end{aligned} \quad (5.43)$$

and we sort by the final contributions towards their logarithmic order. Analogously we solve the integration in Eq. (5.27) and cut all terms beyond NLL accuracy. Hence, we get for the universal next-to-leading logarithmic expansions, which coincide with those in [22, 26, 101] and which were recalculated here:

$$\ln \Delta_i^N(\hat{s}, \mu_f, \mu_r) = \ln N h_i^{(1)}(\lambda) + h_i^{(2)} \left(\lambda, \frac{\hat{s}}{\mu_r^2}, \frac{\hat{s}}{\mu_f^2} \right) - \frac{A_i^{(1)} \gamma_E}{\pi b_0} \ln(1 - 2\lambda), \quad (5.44)$$

and

$$\ln J_i^N(\hat{s}, \mu_r) = \ln N f_i^{(1)}(\lambda) + f_i^{(2)} \left(\lambda, \frac{\hat{s}}{\mu_r^2} \right) - \frac{A_i^{(1)} \gamma_E}{\pi b_0} [\ln(1 - \lambda) - \ln(1 - 2\lambda)], \quad (5.45)$$

where the factorization scale μ_f stands either for μ_{fi} for an initial parton, or for μ_{ff} for an outgoing parton. The functions $h_i^{(1)}$ and $f_i^{(1)}$ collect all leading logarithmic terms $\alpha_s^k \ln^{k+1} N$ in the exponent, while the $h_i^{(2)}$ and $f_i^{(2)}$ produce next-to-leading logarithms

$\alpha_s^k \ln^k N$. They read

$$h_i^{(1)}(\lambda) = \frac{A_i^{(1)}}{2\pi b_0 \lambda} [2\lambda + (1 - 2\lambda) \ln(1 - 2\lambda)], \quad (5.46)$$

$$\begin{aligned} h_i^{(2)}\left(\lambda, \frac{Q^2}{\mu_r^2}, \frac{Q^2}{\mu_f^2}\right) &= -\frac{A_i^{(2)}}{2\pi^2 b_0^2} [2\lambda + \ln(1 - 2\lambda)] \\ &\quad + \frac{A_i^{(1)} b_1}{2\pi b_0^3} \left[2\lambda + \ln(1 - 2\lambda) + \frac{1}{2} \ln^2(1 - 2\lambda)\right] \\ &\quad - \frac{A_i^{(1)}}{\pi b_0} \lambda \ln \frac{Q^2}{\mu_f^2} + \frac{A_i^{(1)}}{2\pi b_0} [2\lambda + \ln(1 - 2\lambda)] \ln \frac{Q^2}{\mu_r^2}, \end{aligned} \quad (5.47)$$

with $b_1 = (17C_A^2 - 5C_A N_f - 3C_F N_f)/(24\pi^2)$. Furthermore,

$$\begin{aligned} f_i^{(1)}(\lambda) &= h_i^{(1)}(\lambda/2) - h_i^{(1)}(\lambda), \\ f_i^{(2)}\left(\lambda, \frac{Q^2}{\mu_r^2}\right) &= 2h_i^{(2)}\left(\frac{\lambda}{2}, \frac{Q^2}{\mu_r^2}, 1\right) - h_i^{(2)}\left(\lambda, \frac{Q^2}{\mu_r^2}, 1\right) \\ &\quad + \frac{B_i^{(1)}}{2\pi b_0} \ln(1 - \lambda), \end{aligned} \quad (5.48)$$

where $B_i^{(1)} = -2\gamma_i^{(1)}$. In more detail, the functions for the unobserved final parton reads:

$$\begin{aligned} f_i^{(1)}(\lambda) &= -\frac{A_i^{(1)}}{2\pi b_0 \lambda} [(1 - 2\lambda) \ln(1 - 2\lambda) - 2(1 - \lambda) \ln(1 - \lambda)], \quad (5.49) \\ f_i^{(2)}\left(\lambda, \frac{Q^2}{\mu_r^2}\right) &= -\frac{A_i^{(1)} b_1}{2\pi b_0^3} \left[\ln(1 - 2\lambda) - 2\ln(1 - \lambda) + \frac{1}{2} \ln^2(1 - 2\lambda) - \ln^2(1 - \lambda)\right] \\ &\quad + \frac{B_i^{(1)}}{2\pi b_0} \ln(1 - \lambda) - \frac{A_i^{(2)}}{2\pi^2 b_0^2} [2\ln(1 - \lambda) - \ln(1 - 2\lambda)] \\ &\quad + \frac{A_i^{(1)}}{2\pi b_0} [2\ln(1 - \lambda) - \ln(1 - 2\lambda)] \ln \frac{Q^2}{\mu_r^2}. \end{aligned} \quad (5.50)$$

Again, we need to calculate the shift $N \rightarrow 2N$ for the hard scattering function, which leads to an additional contribution in the exponent:

$$-\frac{A_i^{(1)}}{\pi b_0} \ln 2 \left[\ln(1 - \lambda) - \ln(1 - 2\lambda) \right]. \quad (5.51)$$

5.3.2. Hard- and Soft-Matrices

Let us consider now the soft and hard matrices in the trace of Eq. (5.25) in more detail. We have to distinguish between the direct- and the resolved-photon case. We identify the Born cross sections with $\text{Tr} \{H^{(0)} S^{(0)}\}_{ab \rightarrow cd}$. Following [37] we expand the trace up to

first order of α_s and find:

$$\begin{aligned} \text{Tr} \left\{ H \mathcal{S}_N^\dagger S \mathcal{S}_N \right\}_{ab \rightarrow cd} &= \text{Tr} \left\{ H^{(0)} S^{(0)} \right\}_{ab \rightarrow cd} \\ &+ \frac{\alpha_s}{\pi} \text{Tr} \left\{ - \left[H^{(0)} (\Gamma^{(1)})^\dagger S^{(0)} + H^{(0)} S^{(0)} \Gamma^{(1)} \right] \ln \bar{N} \right. \\ &\quad \left. + H^{(1)} S^{(0)} + H^{(0)} S^{(1)} \right\}_{ab \rightarrow cd} + \mathcal{O}(\alpha_s^2). \end{aligned} \quad (5.52)$$

Taking the trace above would require higher-order contributions from the hard and soft functions, $H^{(1)}$ and $S^{(1)}$, which can be obtained by performing the NLO calculation near threshold in terms of a color decomposition. However, we can make use of the simplified formalism using the approximation at NLL [28, 37]

$$\text{Tr} \left\{ H \mathcal{S}_N^\dagger S \mathcal{S}_N \right\}_{ab \rightarrow cd} \approx \left(1 + \frac{\alpha_s}{\pi} \Delta C_{ab \rightarrow cd}^{(1)} \right) \text{Tr} \left\{ H^{(0)} \mathcal{S}_N^\dagger S^{(0)} \mathcal{S}_N \right\}_{ab \rightarrow cd}, \quad (5.53)$$

which becomes exact for the direct photon case, where only one color configuration contributes. The spin-dependent coefficient $\Delta C^{(1)}$ is given by

$$\Delta C_{ab \rightarrow cd}^{(1)}(\hat{\eta}) = \frac{\text{Tr} \left\{ H^{(1)} S^{(0)} + H^{(0)} S^{(1)} \right\}_{ab \rightarrow cd}}{\text{Tr} \left\{ H^{(0)} S^{(0)} \right\}_{ab \rightarrow cd}}. \quad (5.54)$$

and is in general part of the N -independent perturbative expansion [27],

$$\Delta C_{ab \rightarrow cd}(\hat{\eta}) = 1 + \frac{\alpha_s}{\pi} \Delta C_{ab \rightarrow cd}^{(1)}(\hat{\eta}) + \mathcal{O}(\alpha_s^2). \quad (5.55)$$

Their origin lies in virtual corrections at NLO and match the resummed cross section to the NLO one, so that they can be calculated through a comparison of the exact NLO calculation with the first-order expanded resummed cross section. Considering the direct partonic subprocess $\gamma b \rightarrow cd$, we are dealing with a special case among the multiparton configurations where only one color-singlet state appears [101], constructed by combining the interacting partons. Due to color conservation soft gluonic radiation cannot induce further color transitions. Then, the hard-scattering function $H_{\gamma b \rightarrow cd}$, the soft function $S_{\gamma b \rightarrow cd}$, and the anomalous dimensions $\Gamma_{\gamma b \rightarrow cd}$ are no longer matrices but scalars in color space. The trace in Eq. (5.53) simplifies by using Eq. (5.35) and gives

$$\text{Tr} \left\{ H^{(0)} \mathcal{S}_N^\dagger S^{(0)} \mathcal{S}_N \right\}_{ab \rightarrow cd} = \Delta \hat{\sigma}_{\gamma b \rightarrow cd}^{(0)}(N, \hat{\eta}) \exp \left[\int_{\mu_r}^{\sqrt{\hat{s}}/(N)} \frac{d\mu'}{\mu'} 2\text{Re} \Gamma_{\gamma b \rightarrow cd}(\hat{\eta}, \alpha_s(\mu')) \right], \quad (5.56)$$

leading to the direct resummed hard-scattering function

$$\begin{aligned} \Delta \tilde{w}_{\gamma b \rightarrow cd}^{\text{resum}, 2N}(\hat{\eta}) &= \left(1 + \frac{\alpha_s}{\pi} \Delta C_{\gamma b \rightarrow cd}^{(1)}\right) \Delta_b^{2N_b}(\hat{s}, \mu_{fi}) \Delta_c^{2N}(\hat{s}, \mu_{ff}) J_d^{2N}(\hat{s}) \\ &\times \Delta \hat{\sigma}_{\gamma b \rightarrow cd}^{(0)}(2N, \hat{\eta}) \exp \left[\int_{\mu_r}^{\sqrt{\hat{s}}/(2N)} \frac{d\mu'}{\mu'} 2\text{Re}\Gamma_{\gamma b \rightarrow cd}(\hat{\eta}, \alpha_s(\mu')) \right]. \end{aligned} \quad (5.57)$$

Also the Born cross section has to be transformed into Mellin space

$$\Delta \hat{\sigma}_{\gamma b \rightarrow cd}^{(0)}(2N, \hat{\eta}) \equiv 2 \int_0^1 d\left(\frac{\hat{s}_4}{\hat{s}}\right) \left(1 - \frac{\hat{s}_4}{\hat{s}}\right)^{2N-1} \frac{\hat{x}_T^4 z^2}{8v} \frac{\hat{s} d\Delta \hat{\sigma}_{\gamma b \rightarrow cd}^{(0)}}{dv dw}, \quad (5.58)$$

which then can be simplified by using Eq. (5.17) and Eq. (5.18), so that

$$\begin{aligned} \Delta \hat{\sigma}_{\gamma b \rightarrow cd}^{(0)}(2N, \hat{\eta}) &= 2 \int_{w_{\min}}^1 dw (1 - v(1 - w))^{2N-1} \frac{\hat{x}_T^4 z^2}{8} \frac{\hat{s} d\Delta \hat{\sigma}_{\gamma b \rightarrow cd}^{(0)}}{dv} \delta(1 - w) \\ &= \frac{\hat{x}_T^4 z^2}{4} \frac{\hat{s} d\Delta \hat{\sigma}_{\gamma b \rightarrow cd}^{(0)}}{dv}. \end{aligned} \quad (5.59)$$

Performing the integral in Eq. (5.57) and expanding the solution to NLL gives then

$$\begin{aligned} 2 \ln \mathcal{S}_{N, ab \rightarrow cd}(\hat{\eta}, \alpha_s) &= \int_{\mu_r}^{\sqrt{\hat{s}}/(2N)} \frac{d\mu'}{\mu'} 2\text{Re}\Gamma_{\gamma b \rightarrow cd}(\hat{\eta}, \alpha_s(\mu')) \\ &= \frac{\ln(1 - 2\lambda)}{\pi b_0} \Gamma_{ab \rightarrow cd}^{(1)}(\hat{\eta}). \end{aligned} \quad (5.60)$$

The first order contributions of the anomalous dimensions

$$\Gamma_{\gamma q \rightarrow qg}^{(1)}(\hat{\eta}) = C_F \ln\left(\frac{-\hat{u}}{\hat{s}}\right) + \frac{C_A}{2} \left[\ln\left(\frac{\hat{t}}{\hat{u}}\right) - i\pi \right], \quad (5.61)$$

$$\Gamma_{\gamma q \rightarrow gq}^{(1)}(\hat{\eta}) = \Gamma_{\gamma q \rightarrow qg}^{(1)}(\hat{\eta})|_{\hat{t} \leftrightarrow \hat{u}}, \quad (5.62)$$

$$\Gamma_{\gamma g \rightarrow q\bar{q}}^{(1)}(\hat{\eta}) = C_F i\pi + \frac{C_A}{2} \left[\ln\left(\frac{\hat{t}\hat{u}}{\hat{s}^2}\right) + i\pi \right], \quad (5.63)$$

are given by those contributions for the prompt-photon production processes, $q\bar{q} \rightarrow \gamma g$ and $qg \rightarrow \gamma q$ [26, 31, 101, 112].

Going now on with the resolved calculation, the formalism is rather different. The anomalous dimensions $\Gamma_{ab \rightarrow cd}$, see Eq. (5.36), are now matrices and are listed at lowest-order in [32, 33, 105, 113]. Consider again the hard functions in Eq. (5.33). Polarized expressions are presented in [27], and unpolarized ones are give in [32, 105, 114], as well as the LO terms of the soft matrices in Eq. (5.34). For completeness these lowest-order matrices, $\Delta H_{ab \rightarrow cd}^{(0)}$, $S_{ab \rightarrow cd}^{(0)}$ and $\Gamma_{ab \rightarrow cd}^{(0)}$, which are needed for the polarized calculation, are listed in

Appendix B. The hard-scattering function reads then:

$$\begin{aligned} \Delta \tilde{w}_{ab \rightarrow cd}^{\text{resum}, 2N}(\hat{\eta}) &= \Delta_a^{2N_a}(\hat{s}, \mu_{fi}, \mu_r) \Delta_b^{2N_b}(\hat{s}, \mu_{fi}, \mu_r) \Delta_c^{2N}(\hat{s}, \mu_{ff}, \mu_r) J_d^{2N}(\hat{s}, \mu_r) \\ &\times \left(1 + \frac{\alpha_s}{\pi} \Delta C_{ab \rightarrow cd}^{(1)}\right) \text{Tr} \left\{ \Delta H^{(0)} \mathcal{S}_N^\dagger \mathcal{S}^{(0)} \mathcal{S}_N \right\}_{ab \rightarrow cd}. \end{aligned} \quad (5.64)$$

5.4. NLO Calculation

In the last sections we have seen the general structure of the hadron production process at hadronic level and also at partonic level, taking place in Mellin space. In case of threshold resummation, we found out how the hard scattering function appears and is composed of. In this section we want to consider the NLO cross section and its transformation into Mellin space. This enables us to compare the first-order expanded threshold resummed result with the fixed-order contribution, what gives us the coefficients $\Delta C_{ab \rightarrow cd}^{(1)}$ of Eq. (5.64). Recall Eq. (5.19), where the analytical NLO expressions [23, 24, 108–111] were cast into the form

$$\frac{\hat{s} d \Delta \hat{\sigma}_{ab \rightarrow cX}^{(1)}(v, w)}{dv dw} = A(v) \delta(1-w) + B(v) \left(\frac{\ln(1-w)}{1-w} \right)_+ + C(v) \left(\frac{1}{1-w} \right)_+ + F(v, w). \quad (5.65)$$

We transform the expression in Mellin space according to the hard scattering function in Eq. (5.22),

$$\begin{aligned} \Delta \tilde{w}(2N, \hat{\eta}) &= 2 \int_0^1 d \left(\frac{\hat{s}_4}{\hat{s}} \right) \left(1 - \frac{\hat{s}_4}{\hat{s}} \right)^{2N-1} \frac{\hat{x}_T^4 z^2}{8v} \frac{\hat{s} d \Delta \hat{\sigma}_{ab \rightarrow cX}}{dv dw} \\ &= 2 \int_0^1 dm m^{2N-1} \frac{\hat{x}_T^4 z^2}{8v} \frac{\hat{s} d \Delta \hat{\sigma}_{ab \rightarrow cX}}{dv dw} \\ &= \frac{1}{4 \cosh^4 \hat{\eta}} \int_0^1 dm m^{2N+3} \frac{\hat{z}^2}{v} \frac{\hat{s} d \Delta \hat{\sigma}_{ab \rightarrow cX}}{dv dw}. \end{aligned} \quad (5.66)$$

rewriting the NLO expression in terms of the variable m

$$m := 1 - \frac{\hat{s}_4}{\hat{s}} = 1 - v(1-w). \quad (5.67)$$

In this case we are interested in terms with distributions in threshold limit only and as we are neglecting $F(v, w)$ in the extractions of the coefficients $\Delta C_{ab \rightarrow cd}^{(1)}$, we can simplify the whole investigation and fix v according to w and $\hat{\eta}$. Note that the hard scattering function is normally also a function with respect to w or m . Hence, if we are interested in the functions $F(v, w)$ in Mellin space, or if we want to calculate the whole expression without threshold-approach, we have to proceed slightly differently. However, for now it is sufficient to transform functions in w into functions with respect to m and v independently and integrate over m .

We start with the plus distributions, which can be rewritten by using the expansion

$$(1-x)^{-1-\varepsilon} = -\frac{1}{\varepsilon}\delta(1-x) + \left(\frac{1}{1-x}\right)_+ - \varepsilon \left(\frac{\ln(1-x)}{1-x}\right)_+ + \mathcal{O}(\varepsilon^2), \quad (5.68)$$

so that we can compute:

$$\begin{aligned} (v(1-w))^{-1-\varepsilon} &= -\frac{1}{\varepsilon}\delta(v(1-w)) + \left(\frac{1}{v(1-w)}\right)_+ - \varepsilon \left(\frac{\ln(v(1-w))}{v(1-w)}\right)_+ + \mathcal{O}(\varepsilon^2) \\ &\stackrel{!}{=} v^{-1-\varepsilon} \left[-\frac{1}{\varepsilon}\delta(1-w) + \left(\frac{1}{1-w}\right)_+ - \varepsilon \left(\frac{\ln(1-w)}{1-w}\right)_+ + \mathcal{O}(\varepsilon^2) \right] \\ &= \left\{ \frac{1}{v} \left(1 - \varepsilon \ln v + \frac{\varepsilon^2}{2} \ln^2 v - \frac{\varepsilon^3}{3} \ln^3 v + \dots \right) \right\} \\ &\quad \times \left[-\frac{1}{\varepsilon}\delta(1-w) + \left(\frac{1}{1-w}\right)_+ - \varepsilon \left(\frac{\ln(1-w)}{1-w}\right)_+ + \mathcal{O}(\varepsilon^2) \right] \\ &= \frac{1}{v} \left[-\frac{1}{\varepsilon}\delta(1-w) + \left(\frac{1}{1-w}\right)_+ + \ln v \times \delta(1-w) \right. \\ &\quad \left. - \varepsilon \left\{ \left(\frac{\ln(1-w)}{1-w}\right)_+ + \ln v \left(\frac{1}{1-w}\right)_+ + \frac{1}{2} \ln^2 v \times \delta(1-w) \right\} + \mathcal{O}(\varepsilon^2) \right]. \end{aligned} \quad (5.69)$$

First, we apply the expansion on the whole expression, and then we consider only the inner term of the brackets, $(1-w)$. Expanding $v^{-1-\varepsilon}$ and collecting terms according to their ε -dependence, we compare now at $\mathcal{O}(\varepsilon)$ the corresponding contributions proportional to $\frac{1}{\varepsilon}$ or ε and find:

$$\begin{aligned} \delta(1-w) &= v \delta(v(1-w)) = v \delta(1-m), \\ \left(\frac{\ln(1-w)}{1-w}\right)_+ &= v \left\{ \left(\frac{\ln(v(1-w))}{v(1-w)}\right)_+ - \ln v \left(\frac{1}{v(1-w)}\right)_+ + \frac{1}{2} \ln^2 v \delta(v(1-w)) \right\} \\ &= v \left\{ \left(\frac{\ln(1-m)}{1-m}\right)_+ - \ln v \left(\frac{1}{1-m}\right)_+ + \frac{1}{2} \ln^2 v \delta(1-m) \right\}, \\ \left(\frac{1}{1-w}\right)_+ &= v \left\{ \left(\frac{1}{v(1-w)}\right)_+ - \ln v \delta(v(1-w)) \right\} \\ &= v \left\{ \left(\frac{1}{1-m}\right)_+ - \ln v \delta(1-m) \right\}. \end{aligned} \quad (5.70)$$

Therefore, the integrations of the plus- and δ -distributions of Eq. (5.65) can be rewritten in terms of m with the following leading solutions:

$$\begin{aligned} \int_0^1 dm m^{2N+3} \left(\frac{\ln(1-m)}{1-m} \right)_+ &= \frac{1}{12} \pi^2 + \frac{1}{2} (H_{2N+3})^2 - \frac{1}{2} \psi^{(1)}(2N+4), \\ &= \frac{1}{12} \pi^2 + \frac{1}{2} \ln^2(2\bar{N}) + \mathcal{O}\left(\frac{1}{\bar{N}}\right), \\ \int_0^1 dm m^{2N+3} \left(\frac{1}{1-m} \right)_+ &= -H_{2N+3} = -\ln(2\bar{N}) + \mathcal{O}\left(\frac{1}{\bar{N}}\right) \\ \int_0^1 dm m^{2N+3} \delta(1-m) &= 1. \end{aligned} \quad (5.71)$$

To extract the coefficients $\Delta C_{ab \rightarrow cd}^{(1)}$ in Eq. (5.25), we neglect terms proportional to $\mathcal{O}\left(\frac{1}{\bar{N}}\right)$ and consider only N -logarithmic contributions and N -independent terms. Moreover, in Eq. (5.71), where $\bar{N} = Ne^{\gamma_E}$, the harmonic number H_n appears, which simplifies for large n according to

$$H_n = \sum_{k=1}^n \frac{1}{k} = \ln n + \gamma_E + \frac{1}{2n} + \mathcal{O}\left(\frac{1}{n^2}\right). \quad (5.72)$$

Further,

$$H_{n+1} = H_n + \frac{1}{n+1}. \quad (5.73)$$

The polygamma function of order n is defined as

$$\begin{aligned} \psi^{(n)}(z) &= \frac{d^n}{dz^n} \psi(z) = \frac{d^{n+1}}{dz^{n+1}} \ln(\Gamma(z)), \\ \psi^{(0)}(z) &= \psi(z) = \frac{\Gamma'(z)}{\Gamma(z)}, \end{aligned} \quad (5.74)$$

with the gamma function $\Gamma(z) = (z-1)!$. Its first order is given by:

$$\psi^{(1)}(z) = \frac{1}{z^2} + \sum_{k=1}^{\infty} \frac{1}{(k+z)^2}, \quad (5.75)$$

and it is linked to the $(n-1)$ -th harmonic number H_n through

$$\psi^{(0)}(n) = \sum_{k=1}^{n-1} \frac{1}{k} - \gamma_E. \quad (5.76)$$

5.5. Extraction of the Coefficients

Let us now come back to Eq. (5.54), where we have seen the first-order contribution of the coefficients $\Delta C_{ab \rightarrow cd}^{(1)}$, expressed through hard and soft matrices. They are N -independent, spin-dependent hard-scattering coefficients and originate from virtual corrections at NLO. As they match the resummed cross section to the next-to-leading order one, we can extract them by comparing the first-order expanded threshold resummed partonic cross section with the exact NLO one, which can be found in Ref. [108].

Using then the formalism presented in Sec. 5.4 to transform the partonic NLO cross section, see Eq. (5.65), into Mellin moment space following Eq. (5.66), we are able to compare the fixed-order result with the resummed one. The final missing step is then the expansion of the soft-gluon resummed partonic cross section to first order. We have checked that all single- and double-logarithmic terms of the exact NLO partonic cross sections are reproduced, in both cases, direct and resolved. Then, the terms constant in N also match provided we use the coefficients, which we have extracted. Those for the direct subprocesses, $\Delta C_{\gamma b \rightarrow cd}^{(1)}$, are given in Appendix C. As our results for the resolved coefficients $\Delta C_{ab \rightarrow cd}^{(1)}$ are rather lengthy, one can obtain them upon request.

5.6. Inverse Mellin Transform and Matching Procedure

After the calculation of the resummed hard scattering function, we need to perform an inverse Mellin transform of the result convoluted with the fragmentation functions in Mellin space, see Eq. (5.24). In the course of that we have to deal with singularities appearing in the soft-gluon exponents at NLL accuracy, at $\lambda = 1/2$ and $\lambda = 1$, see Eqs. (5.44) and (5.45), where $\lambda = \alpha_s b_0 N$. These singularities are a consequence of the Landau pole in the perturbative strong coupling due to the sensitivity of the resummed expression to it. They correspond to the Mellin moments $N_L = \exp(1/(2\alpha_s b_0))$ and $N'_L = \exp(1/(\alpha_s b_0))$ and lie on the positive real axis in the complex- N plane, see Fig. 5.3. They signal the onset of non-perturbative phenomena in the kinematic region close to threshold [26]. Therefore we will follow the *Minimal Prescription* formula introduced in [115], which is based on several requirements. On the one hand we have to use the NLL expanded exponents, which is already fulfilled. On the other hand we have to choose a reasonable contour in the complex- N plane for the inverse Mellin transformation, see Fig. 5.3. More precisely, it has to be chosen such that all singularities, originating e.g. from the fragmentation function or the LO cross section, have to lie to the left of the integration contour, except the Landau poles N_L , which lie to the far right. Hence, the contour intersects the real axis at a value C_{MP} that lies to the left of N_L , satisfying $b_0 \alpha_s \ln C_{MP} < 1/2$, with C_{MP} being real and positive. The Mellin integral, defined in Eq.

(5.24) as

$$\int_{C_{MP-i\infty}}^{C_{MP+i\infty}} \frac{dN}{2\pi i} (x^2)^{-N} D_{h/c}^{2N+3}(\mu_{ff}) \Delta \tilde{w}^{\text{resum}, 2N}(\hat{\eta}), \quad (5.77)$$

has support for both $x^2 < 1$ and $x^2 \geq 1$. Note that the latter range arises only because of the way the Landau poles are treated in the Minimal Prescription. It is unphysical in the sense that the cross section at any finite order of perturbation theory must not receive any contributions from $x^2 \geq 1$. Mathematically, however, those unphysical contributions are needed to make sure that the expansions of the resummed cross section to higher orders in α_s converge to the fully resummed result. Contributions for $x^2 \geq 1$ decrease, however, exponentially with x^2 , so that its numerical impact is suppressed. As one can see in Fig. 5.3, we tilt the contour with respect to the real axis into the negative real half-plane by using the parametrization

$$N = C_{MP} + ze^{i\phi}, \quad (5.78)$$

with $0 \leq z \leq \infty$, as described in [22, 38]. This helps to improve the numerical convergence of the Mellin integral. The restriction for the angle ϕ valid at $x^2 < 1$ reads $\pi/2 < \phi < \pi$, and for $x^2 \geq 1$ the angle fulfills $\phi_2 < \pi/2$, such that the factor $(x^2)^{-z \exp(i\phi)}$ dampens the integral. For numerics, we have chosen the angles explicitly to be $\phi_1 = \frac{3}{4}\pi$ and $\phi_2 = \frac{7}{16}\pi$. To make sure that the exact NLO calculation is fully included in the theoretical predictions, as well as all soft-gluon contributions beyond NLO to NLL accuracy, we match our resummed cross section to the NLO one. This is done by subtracting all NLO contributions that are present in the resummed result, adding instead the full NLO cross section:

$$\begin{aligned} \frac{p_T^3 \Delta d\hat{\sigma}^{\text{matched}}}{dp_T d\eta} &= \frac{p_T^3 d\Delta\sigma^{\text{NLO}}}{dp_T d\eta} + \sum_{bc} \int_0^1 dx_\ell \int_0^1 dx_n \times \Delta f_{\gamma/\ell}(x_\ell, \mu_{fi}) \Delta f_{b/N}(x_n, \mu_{fi}) \\ &\times \int_{\mathcal{C}} \frac{dN}{2\pi i} (x^2)^{-N} D_{h/c}^{2N+3}(\mu_{ff}) \left[\Delta \tilde{w}_{\gamma b \rightarrow cd}^{2N, \text{resum}}(\hat{\eta}) - \Delta \tilde{w}_{\gamma b \rightarrow cd}^{2N, \text{resum}}(\hat{\eta}) \Big|_{\text{NLO}} \right], \end{aligned} \quad (5.79)$$

Double-counting of perturbative terms can be avoided through this procedure, as well as we can guarantee the highest available precision of our theoretical results.

5.7. Double-Spin Asymmetry

As our theoretical framework for the spin-dependent and spin-averaged cross sections is now complete, we are ready to come to the double-longitudinal spin asymmetry. It is given by the ratio of the polarized and the unpolarized cross sections,

$$A_{\text{LL}} = \frac{d\Delta\sigma}{d\sigma}, \quad (5.80)$$

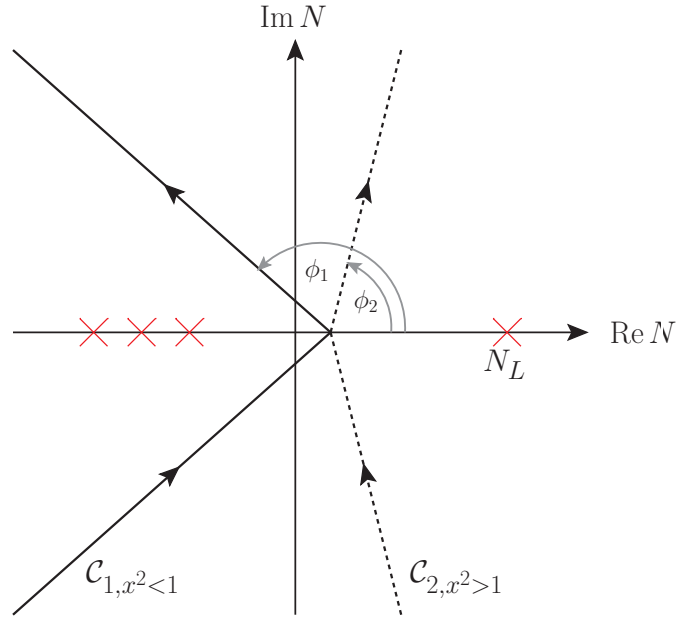


Fig. 5.3.: Our choices for the contours of the inverse Mellin transform: \mathcal{C}_1 with $\phi_1 > \pi/2$ for $x^2 < 1$ and \mathcal{C}_2 with $\phi_2 < \pi/2$ for $x^2 \geq 1$.

where these cross sections are defined through

$$d\sigma_{\ell N} \equiv \frac{1}{2} [d\sigma_{\ell N}^{++} + d\sigma_{\ell N}^{+-}] , \quad (5.81)$$

$$d\Delta\sigma_{\ell N} \equiv \frac{1}{2} [d\sigma_{\ell N}^{++} - d\sigma_{\ell N}^{+-}] . \quad (5.82)$$

Here, the superscripts $(++)$, $(+-)$ label the helicities of the incoming lepton and nucleon. As the cross sections under consideration are hadronic, we can rewrite the asymmetries in a factorized form as

$$A_{LL} = \frac{d\Delta\sigma}{d\sigma} = \frac{\sum_{a,b,c} \Delta f_{a,\ell} \otimes \Delta f_{b/N} \otimes \Delta \hat{\sigma}_{ab \rightarrow cX} \otimes D_{h/c}}{\sum_{a,b,c} f_{a,\ell} \otimes f_{b/N} \otimes \hat{\sigma}_{ab \rightarrow cX} \otimes D_{h/c}} . \quad (5.83)$$

As it was often claimed that higher perturbative order corrections and with that threshold logarithms may cancel when considering the ratio of the cross sections, we will investigate this situation in Chap. 7 in more detail. However, we want to mention already at this point that these assumptions do not remain valid within further examination of the threshold corrections.

Understand well as I may, my comprehension can only be an infinitesimal fraction of all I want to understand.

Ada Lovelace

6

Subleading Contributions

As discussed in Chap. 4 and Chap. 5 we want to resum large logarithmic corrections appearing at threshold limit. Besides the leading logarithmic contributions we also have considered next-to-leading logarithms. However, as we will see, an even higher level of theoretical precision will be needed for example for an upcoming EIC. Therefore, we want to investigate some basic ideas for certain subleading effects, however, for our phenomenological examination we will restrict ourselves to threshold resummation at NLL without subleading contributions. This chapter is intended to give a short overview only on how a subleading framework could work.

In Fig. 6.1 various subleading contributions for large N are compared and it shows that $\ln N/N$ contributes the most compared with other subleading contributions. Therefore we will focus on these terms only.

We will calculate explicitly $\ln N/N$ -contributions for the NLO cross section and provide these terms, supposing that these terms should be included in a future resummation calculation. This could be for example when investigating the matching-coefficients $\Delta C_{\gamma b \rightarrow cd}^{(1)}$ of Sec. 5.5. Furthermore, a future project could be to extend the radiative exponents for resummation with the $\ln N/N$ contributions. In the following, we will sketch how these contributions may be generated.

6.1. Formalism to Calculate Subleading Mellin-Contributions

The first step is to rewrite the integrand weight $(z^{N-1} - 1)$ in Eqs. (5.26) and (5.27) into a new form, where subleading contributions can be included. The formalism we are using is based on Refs. [116] and [30]. Calculating soft gluon functions in the large- N limit, it

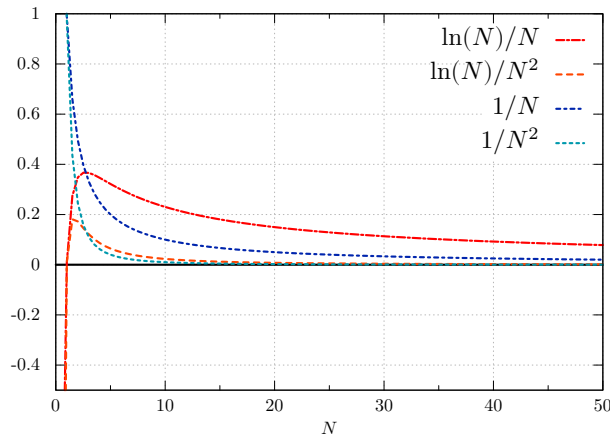


Fig. 6.1.: Comparison of different subleading contributions for large N .

is sufficient to use the approximation [30]

$$z^{N-1} - 1 \simeq -\Theta \left(1 - \frac{1}{N e^{\gamma_E}} - z \right). \quad (6.1)$$

This prescription can be generalized, so that we get any logarithmic order including subleading contributions. In the following we want to extend this formalism up to $1/N$ suppressed NLL logarithms, starting with the Mellin transformation of the plus distribution,

$$\begin{aligned} I_n(N) &= \int_0^1 dz z^{N-1} \left(\frac{\ln^n(1-z)}{1-z} \right)_+ = \int_0^1 dz (z^{N-1} - 1) \frac{\ln^n(1-z)}{1-z} \\ &= \lim_{\epsilon \rightarrow 0} \left(\frac{\partial}{\partial \epsilon} \right)^n \int_0^1 dz (z^{N-1} - 1) \frac{(1-z)^\epsilon}{1-z} \\ &= \lim_{\epsilon \rightarrow 0} \left(\frac{\partial}{\partial \epsilon} \right)^n \frac{1}{\epsilon} \left[\frac{\Gamma(N)\Gamma(\epsilon+1)}{\Gamma(\epsilon+N)} - 1 \right], \end{aligned} \quad (6.2)$$

where we have used the definition $\int_0^1 dz f(z) [g(z)]_+ \equiv \int_0^1 dz [f(z) - f(1)] g(z)$ for plus distributions, as well as the identity

$$\ln^n(1-z) = \lim_{\epsilon \rightarrow 0} \left(\frac{\partial}{\partial \epsilon} \right)^n (1-z)^\epsilon. \quad (6.3)$$

With

$$\frac{\Gamma(N)}{\Gamma(\epsilon+N)} = N^{-\epsilon} \left(1 + \frac{1}{2N} (\epsilon - \epsilon^2) + \mathcal{O}\left(\frac{1}{N^2}\right) \right), \quad (6.4)$$

and

$$e^{-\epsilon \ln N} \Gamma(1 + \epsilon) = \Gamma\left(1 - \frac{\partial}{\partial \ln N}\right) e^{-\epsilon \ln N}, \quad (6.5)$$

where the function $\Gamma\left(1 - \frac{\partial}{\partial \ln N}\right)$ can be expanded as

$$\Gamma\left(1 - \frac{\partial}{\partial \ln N}\right) = 1 + \gamma_E \frac{\partial}{\partial \ln N} + \frac{1}{2} (\gamma_E^2 + \zeta(2)) \left(\frac{\partial}{\partial \ln N}\right)^2 + \mathcal{O}\left(\frac{\partial}{\partial \ln N}\right)^3, \quad (6.6)$$

and where $e^{-\epsilon \ln N}$ can be rewritten as a series, follows:

$$\begin{aligned} I_n(N) &= \lim_{\epsilon \rightarrow 0} \left(\frac{\partial}{\partial \epsilon}\right)^n \frac{1}{\epsilon} \left[e^{-\epsilon \ln N} \left(1 + \frac{1}{2N} (\epsilon - \epsilon^2) + \mathcal{O}\left(\frac{1}{N^2}\right)\right) \Gamma(\epsilon + 1) - 1 \right] \\ &= \lim_{\epsilon \rightarrow 0} \left(\frac{\partial}{\partial \epsilon}\right)^n \left[\left(\frac{1}{\epsilon} + \frac{1}{2N} (1 - \epsilon) + \mathcal{O}\left(\frac{1}{N^2}\right)\right) \Gamma\left(1 - \frac{\partial}{\partial \ln N}\right) \sum_{i=0}^{\infty} \frac{(-\ln N)^i \epsilon^i}{i!} \right. \\ &\quad \left. - \frac{1}{\epsilon} \Gamma\left(1 - \frac{\partial}{\partial \ln N}\right) \right] \\ &= \lim_{\epsilon \rightarrow 0} \left(\frac{\partial}{\partial \epsilon}\right)^n \left[\Gamma\left(1 - \frac{\partial}{\partial \ln N}\right) \sum_{i=1}^{\infty} \frac{(-\ln N)^i \epsilon^{i-1}}{i!} \right. \\ &\quad \left. + \frac{1}{2N} \Gamma\left(1 - \frac{\partial}{\partial \ln N}\right) \sum_{i=0}^{\infty} \frac{(-\ln N)^i (\epsilon^i - \epsilon^{i+1})}{i!} \right] + \mathcal{O}\left(\frac{1}{N^2}\right). \quad (6.7) \end{aligned}$$

Now we perform the n -th derivative in ϵ and get

$$\begin{aligned} I_n(N) &= \lim_{\epsilon \rightarrow 0} \Gamma\left(1 - \frac{\partial}{\partial \ln N}\right) \left[\sum_{i=n+1}^{\infty} \frac{(-\ln N)^i \epsilon^{i-1-n} (i-1)!}{i! (i-1-n)!} + \sum_{i=n}^{\infty} \frac{(-\ln N)^i \epsilon^{i-n} i!}{i! (i-n)! 2N} \right. \\ &\quad \left. - \sum_{i=n-1}^{\infty} \frac{(-\ln N)^i \epsilon^{i+1-n} (i+1)!}{i! (i+1-n)! 2N} \right] + \mathcal{O}\left(\frac{1}{N^2}\right) \\ &= \Gamma\left(1 - \frac{\partial}{\partial \ln N}\right) \left[\frac{(-\ln N)^{n+1}}{n+1} + \frac{(-\ln N)^n}{2N} - \frac{n(-\ln N)^{n-1}}{2N} \right] + \mathcal{O}\left(\frac{1}{N^2}\right). \quad (6.8) \end{aligned}$$

Note that

$$\frac{(-\ln N)^{n+1}}{n+1} = - \int_0^{1-\frac{1}{N}} dz \frac{\ln^n(1-z)}{1-z}. \quad (6.9)$$

This yields, neglecting $\mathcal{O}(\frac{1}{N^2})$:

$$\begin{aligned}
I_n(N) &= \\
&= -\Gamma\left(1 - \frac{\partial}{\partial \ln N}\right) \int_0^{1-\frac{1}{N}} dz \left[\frac{\ln^n(1-z)}{1-z} + \frac{n}{2N} \frac{\ln^{n-1}(1-z)}{1-z} - \frac{n(n-1)}{2N} \frac{\ln^{n-2}(1-z)}{1-z} \right] \\
&= -\Gamma\left(1 - \frac{\partial}{\partial \ln N}\right) \int_0^1 dz \Theta\left(1 - z - \frac{1}{N}\right) \\
&\quad \times \left[\frac{\ln^n(1-z)}{1-z} + \frac{n}{2N} \frac{\ln^{n-1}(1-z)}{1-z} - \frac{n(n-1)}{2N} \frac{\ln^{n-2}(1-z)}{1-z} \right]. \tag{6.10}
\end{aligned}$$

We have arrived at our all-order generalization including subleading logarithms up to $\mathcal{O}(\frac{1}{N})$, again neglecting terms of order $\mathcal{O}(\frac{1}{N^2})$,

$$\begin{aligned}
z^{N-1} - 1 &= \\
&= -\Gamma\left(1 - \frac{\partial}{\partial \ln N}\right) \Theta\left(1 - z - \frac{1}{N}\right) \left[1 + \frac{n}{2N} \ln^{-1}(1-z) - \frac{n(n-1)}{2N} \ln^{-2}(1-z) \right]. \tag{6.11}
\end{aligned}$$

This generalization has to be applied on any logarithmic term of the form $\ln^n(1-z)$ with $n = 0, 1, 2, \dots$. Moreover, adopted on contributions without logarithms in z , we have $n = 0$ and with that the second and third contributions in the squared brackets in Eq. (6.11) vanish. For $n = 1$ the third term vanishes and the second yields a $1/N$ -suppressed contribution, and so on. Note further that lower-order contributions are additionally represented with the help of the derivatives in the Γ -function:

$$\begin{aligned}
\Gamma\left(1 - \frac{\partial}{\partial \ln N}\right) \ln^{n+1} N &= \\
&= \ln^{n+1} N + \gamma_E(n+1) \ln^n N + \frac{1}{2} (\gamma_E^2 + \zeta(2)) n(n+1) \ln^{n-1} N + \dots \tag{6.12}
\end{aligned}$$

Adopted for leading logs, the first term in Eq. (6.12) reproduces the very same, the second the next-to-leading logs, then we get the next-to-next-to-leading logs and so on. Depending on when we cut the series, we have to dismantle our result after using Eq. (6.11). In the

following example we are using Eq. (6.12) at NNLL order, so that the solution reads:

$$\begin{aligned}
& \int_0^1 dz (z^{N-1} - 1) \frac{\ln^n(1-z)}{1-z} \\
&= \Gamma \left(1 - \frac{\partial}{\partial \ln N} \right) \left[\underbrace{\frac{(-\ln N)^{n+1}}{n+1}}_{LL} + \underbrace{\frac{(-\ln N)^n}{2N}}_{NLL} - \underbrace{\frac{n(-\ln N)^{n-1}}{2N}}_{NNLL} \right] \\
&= \frac{(-\ln N)^{n+1}}{n+1} + (-\ln N)^n \left[\frac{1}{2N} - \gamma_E \right] + (-\ln N)^{n-1} \left[-\frac{n}{2N} - \frac{n\gamma_E}{2N} + \frac{n}{2} (\gamma_E^2 + \zeta(2)) \right] \\
&\quad + \mathcal{O}(N^3\text{LL}) .
\end{aligned} \tag{6.13}$$

6.2. Subleading Logarithms for NLO Cross Sections

Now we proceed with the partonic NLO cross section. In this section we want to focus on subleading $1/N$ -suppressed logarithms for the next-to-leading order result in Mellin moment space, since we have neglected those terms before. For that we consider each Mellin transformation again. We have seen that the analytical expression for the cross section can be brought into the structure of Eq. (5.19),

$$\frac{\hat{s} d\Delta \hat{\sigma}_{ab \rightarrow cX}^{(1)}(v, w)}{dv dw} = A(v) \delta(1-w) + B(v) \left(\frac{\ln(1-w)}{1-w} \right)_+ + C(v) \left(\frac{1}{1-w} \right)_+ + F(v, w), \tag{6.14}$$

which will be Mellin transformed in the following with the help of the Mellin transformation for the hard scattering function in Eq. (5.66). Contrary to the calculation before, we will not neglect the function describing terms without distributions, $F(v, w)$. In that case we cannot fix v according to w and $\hat{\eta}$, hence v is also a function of m and has to be taken into account in the Mellin transformation, using the relation $m = 1 - v(1-w)$. Bear in mind that now also v is a function of m , as we have

$$v = 1 - \frac{\hat{x}_T}{2} e^{-\hat{\eta}}, \quad w = \frac{1}{v} \frac{\hat{x}_T}{2} e^{\hat{\eta}}. \tag{6.15}$$

Hence, when performing the integration of $F(v, w)$, we cannot fix v as before in the calculation of the coefficients in Chap. 5. This is only allowed in the threshold region. However, as we are interested in the subleading contributions and consider particularly also the terms without any distributions in w , i.e. $F(v, w)$, we will calculate the whole NLO contribution without the threshold-approximation as before. Therefore we rewrite $F(v, w) = F(v(m), w(m))$ and so on. We find for the δ -function and plus-distributions, see Eq. (5.70),

$$\delta(1-w) = v \delta(v(1-w)) = v \delta(1-m),$$

$$\begin{aligned}
\left(\frac{\ln(1-w)}{1-w}\right)_+ &= v \left\{ \left(\frac{\ln(1-m)}{1-m}\right)_+ - \ln\left(1 - \frac{m}{2}(1 + \tanh \hat{\eta})\right) \left(\frac{1}{1-m}\right)_+ \right. \\
&\quad \left. + \frac{1}{2} \ln^2\left(1 - \frac{m}{2}(1 + \tanh \hat{\eta})\right) \delta(1-m) \right\}, \\
\left(\frac{1}{1-w}\right)_+ &= v \left\{ \left(\frac{1}{1-m}\right)_+ - \ln\left(1 - \frac{m}{2}(1 + \tanh \hat{\eta})\right) \delta(1-m) \right\}. \tag{6.16}
\end{aligned}$$

Let us now come to the corresponding integration. We want to use the replacement from the section before and bring therefore the Mellin integral into the suitable structure by splitting it up into two contributions:

$$\begin{aligned}
&\int_0^1 dm m^{2N+3} B(m) \left(\frac{\ln(1-m)}{1-m}\right)_+ = \\
&= \int_0^1 dm m^{2N+3} [B(m) - B(1)] \left(\frac{\ln(1-m)}{1-m}\right)_+ + \int_0^1 dm m^{2N+3} B(1) \left(\frac{\ln(1-m)}{1-m}\right)_+ \\
&= \int_0^1 dm \sum_{k=1}^{\infty} \sum_{\ell=1}^{\infty} m^{2N+3+k+\ell} \frac{(-1)^\ell}{\ell} [B(m) - B(1)] + \int_0^1 dm [m^{2N+3} - 1] B(1) \frac{\ln(1-m)}{1-m} \\
&= \sum_{k=1}^{\infty} \sum_{\ell=1}^{\infty} \frac{(-1)^\ell}{\ell} \left\{ \left[\frac{m^{2N+4+k+\ell}}{2N+4+k+\ell} B(m) \right]_0^1 - \int_0^1 dm \frac{m^{2N+4+k+\ell}}{2N+4+k+\ell} B'(m) \right. \\
&\quad \left. - B(1) \left[\frac{m^{2N+4+k+\ell}}{2N+4+k+\ell} \right]_0^1 \right\} + \int_0^1 dm [m^{2N+3} - 1] B(1) \frac{\ln(1-m)}{1-m} \\
&= \int_0^1 dm [m^{2N+3} - 1] B(1) \frac{\ln(1-m)}{1-m} - \sum_{k=1}^{\infty} \sum_{\ell=1}^{\infty} \frac{(-1)^\ell}{\ell} \int_0^1 dm \frac{m^{2N+4+k+\ell}}{2N+4+k+\ell} B'(m). \tag{6.17}
\end{aligned}$$

We have used that the Mellin moments N are large and that $m \in [0, 1]$. Using then the replacement of Eq. (6.11) for $n = 1$ yields:

$$\begin{aligned}
&\int_0^1 dm m^{2N+3} B(m) \left(\frac{\ln(1-m)}{1-m}\right)_+ = \\
&= - \int_0^1 dm \Gamma\left(1 - \frac{\partial}{\partial \ln(2N+4)}\right) \Theta\left(1 - m - \frac{1}{2N+4}\right) \left[1 + \frac{1}{2(2N+4)} \ln^{-1}(1-m)\right] \times \\
&\quad \times B(1) \frac{\ln(1-m)}{1-m} \\
&= B(1) \left[\frac{1}{2} \ln^2 N + \ln N \left(\frac{7}{4N} + \ln 2 + \gamma_E\right) + \frac{7}{4N} (\ln 2 + \gamma_E) \right. \\
&\quad \left. + \frac{1}{2} \ln^2 2 + \gamma_E \ln 2 + \frac{\gamma_E^2 + \zeta(2)}{2} + \mathcal{O}\left(\frac{1}{N^2}\right) \right] \\
&\quad - \sum_{k=1}^{\infty} \sum_{\ell=1}^{\infty} \frac{(-1)^\ell}{\ell} \int_0^1 dm \frac{m^{2N+4+k+\ell}}{2N+4+k+\ell} B'(m). \tag{6.18}
\end{aligned}$$

For $F(m)$ the Mellin integral is trivial as long as $F(1)$ is well defined. While this is not always the case, and as we will also have terms proportional to $\ln(1-m)$, we define $\tilde{F}(m)$ regarding to

$$F(m) \equiv \ln(1-m)\tilde{F}(m). \quad (6.19)$$

We define further

$$\begin{aligned} H(m) &\equiv \int dm m^{2N+3} \ln(1-m) = \frac{m^{2N+4}}{2N+4} \tilde{H}(m), \\ &\int_0^1 dm m^{2N+3} \ln(1-m) = -\frac{H_{2N+4}}{2N+4}, \\ \text{with } \lim_{m \rightarrow 0} \tilde{H}(m) &= 0, \quad \lim_{m \rightarrow 1} \tilde{H}(m) = -H_{2N+4}. \end{aligned} \quad (6.20)$$

Then, the Mellin transform gives:

$$\begin{aligned} \int_0^1 dm m^{2N+3} \ln(1-m)\tilde{F}(m) &= \left[H(m)\tilde{F}(m) \right]_0^1 - \int_0^1 dm H(m)\tilde{F}'(m) \\ &= -\frac{H_{2N+4}}{2N+4}\tilde{F}(1) - \int_0^1 dm \frac{m^{2N+4}}{2N+4}\tilde{F}'(m) = -\frac{H_{2N+4}}{2N+4}\tilde{F}(1) \\ &= -\frac{\tilde{F}(1)}{2N} (\ln(2N) + \gamma_E) + \mathcal{O}\left(\frac{1}{N^2}\right). \end{aligned} \quad (6.21)$$

Finally, we conclude for all integrations with distributions and without, and find the following contributions with respect to large N and of order $\mathcal{O}\left(\frac{1}{N}\right)$ neglecting higher order terms, which are suppressed:

$$\begin{aligned} \int_0^1 dm m^{2N+3} A(m) \delta(1-m) &= A(1), \\ \int_0^1 dm m^{2N+3} B(m) \left(\frac{\ln(1-m)}{1-m}\right)_+ &= \\ &= B(1) \left[\frac{1}{2} \ln^2 N + \ln N \left(\frac{7}{4N} + \ln 2 + \gamma_E \right) + \frac{7}{4N} (\ln 2 + \gamma_E) \right. \\ &\quad \left. + \frac{1}{2} \ln^2 2 + \gamma_E \ln 2 + \frac{\gamma_E^2 + \zeta(2)}{2} + \mathcal{O}\left(\frac{1}{N^2}\right) \right] \\ &\quad - \sum_{k=1}^{\infty} \sum_{\ell=1}^{\infty} \frac{(-1)^\ell}{\ell} \int_0^1 dm \frac{m^{2N+4+k+\ell}}{2N+4+k+\ell} B'(m), \\ \int_0^1 dm m^{2N+3} C(m) \left(\frac{1}{1-m}\right)_+ &= -C(1) \left[\ln N + \frac{2}{N} + \gamma_E + \ln 2 \right] + \mathcal{O}\left(\frac{1}{N^2}\right), \\ \int_0^1 dm m^{2N+3} F(m) &= \frac{F(1)}{2N} + \mathcal{O}\left(\frac{1}{N^2}\right), \quad \text{if } F(1) \text{ is well defined,} \\ \int_0^1 dm m^{2N+3} \ln(1-m)\tilde{F}(m) &= -\frac{\tilde{F}(1)}{2N} (\ln(2N) + \gamma_E) + \mathcal{O}\left(\frac{1}{N^2}\right), \end{aligned} \quad (6.22)$$

with $\zeta(2) = \pi^2/6$. Calculating the exact NLO cross sections in Mellin moment space gives the following subleading $\ln N/N$ -contributions named $\tilde{w}_{ab \rightarrow cd}^{\text{NLO}}|_{\ln N/N}$ for the various subprocesses. As we have transformed their v - and w -dependence into a dependence with respect to m and $\hat{\eta}$, the latter dependence will be preserved. We start with the direct ones. For $\gamma q \rightarrow q(g)$ we have

$$\begin{aligned} \tilde{w}_{\gamma q \rightarrow q(g)}^{\text{NLO}} \Big|_{\ln N/N} (2N, \hat{\eta}) &= \frac{e_q^2 \alpha \alpha_s^2 \ln N}{\cosh^4 \hat{\eta} N} \frac{2 + e^{2\hat{\eta}}}{16C_A^2 (e^{4\hat{\eta}} + e^{6\hat{\eta}})} \\ &\quad \times [14e^{6\hat{\eta}} + 7C_A^4 e^{6\hat{\eta}} + 2C_A^3 C_F e^{4\hat{\eta}} (2 + 2e^{2\hat{\eta}} + e^{4\hat{\eta}}) \\ &\quad - 2C_A C_F (-2 - 4e^{2\hat{\eta}} + e^{4\hat{\eta}} + 3e^{6\hat{\eta}} + 2e^{8\hat{\eta}}) \\ &\quad + C_A^2 (-21e^{6\hat{\eta}} + C_F (-2 - 4e^{2\hat{\eta}} - 6e^{4\hat{\eta}} + e^{8\hat{\eta}}))] \\ &\quad - \sum_{k=1}^{\infty} \sum_{\ell=1}^{\infty} \frac{(-1)^\ell}{\ell} \int_0^1 dm \frac{m^{2N+4+k+\ell}}{2N+4+k+\ell} B'_{\gamma q \rightarrow q(g)}(m), \end{aligned} \quad (6.23)$$

further for $\gamma q \rightarrow g(q)$ we obtain

$$\begin{aligned} \tilde{w}_{\gamma q \rightarrow g(q)}^{\text{NLO}} \Big|_{\ln N/N} (2N, \hat{\eta}) &= \frac{e_q^2 \alpha \alpha_s^2 \ln N}{\cosh^4 \hat{\eta} N} \frac{1}{64C_A^2 e^{2\hat{\eta}}} \\ &\quad \times [21 + 2C_A C_F + C_A^2 (-126 + 105C_A^2 - 58C_A C_F) \\ &\quad + 4C_A C_F \cosh(2\hat{\eta}) (5 - 19C_A^2) - 4C_A C_F \sinh(2\hat{\eta}) (C_A^2 - 3) \\ &\quad + \tanh \hat{\eta} (C_A^2 - 1) (-7 + 35C_A^2 + 2C_A C_F)] \\ &\quad - \sum_{k=1}^{\infty} \sum_{\ell=1}^{\infty} \frac{(-1)^\ell}{\ell} \int_0^1 dm \frac{m^{2N+4+k+\ell}}{2N+4+k+\ell} B'_{\gamma q \rightarrow g(q)}(m), \end{aligned} \quad (6.24)$$

and finally for γg -fusion we receive:

$$\begin{aligned} \tilde{w}_{\gamma g \rightarrow q(\bar{q})}^{\text{NLO}} \Big|_{\ln N/N} (2N, \hat{\eta}) &= \frac{e_q^2 \alpha \alpha_s^2 \ln N}{\cosh^4 \hat{\eta} N} \frac{1}{16C_A} \\ &\quad \times \left[-1 - 6C_A^2 + \cosh(2\hat{\eta}) (7 - 42C_A^2) - \sinh(2\hat{\eta}) (2 - 19C_A^2) \right. \\ &\quad \left. + \sinh(4\hat{\eta}) (1 - 9C_A^2) \right] \\ &\quad - \sum_{k=1}^{\infty} \sum_{\ell=1}^{\infty} \frac{(-1)^\ell}{\ell} \int_0^1 dm \frac{m^{2N+4+k+\ell}}{2N+4+k+\ell} B'_{\gamma g \rightarrow q(\bar{q})}(m). \end{aligned} \quad (6.25)$$

We proceed with the resolved contributions, where the last parton in $ab \rightarrow cd$ stays unobserved. Further we note that the unobserved part only consists of a single parton

recoiling against the observed one. We have ten such partonic channels. $q\bar{q} \rightarrow q\bar{q}$ gives

$$\begin{aligned} \tilde{w}_{q\bar{q} \rightarrow q\bar{q}}^{\text{NLO}} \Big|_{\ln N/N} (2N, \hat{\eta}) &= \frac{\alpha_s^3 \ln N}{\cosh^4 \hat{\eta} N} \frac{C_F}{32C_A^3(1+e^{2\hat{\eta}})^2} \\ &\times \left[6C_A(-1+3C_A^2) + e^{8\hat{\eta}}(4C_A-2)(-2-2C_A+C_A^2) \right. \\ &\quad + e^{2\hat{\eta}}(18-9C_A+23C_A^3+C_A^2(-34+280C_F)) \\ &\quad + 4e^{4\hat{\eta}}(9+C_A(-6-35C_F+C_A[-17+9C_A+70C_F])) \\ &\quad \left. + e^{6\hat{\eta}}(22+23C_A^3+4C_A^2[-11+35C_F]-C_A[17+140C_F]) \right] \\ &- \sum_{k=1}^{\infty} \sum_{\ell=1}^{\infty} \frac{(-1)^\ell}{\ell} \int_0^1 dm \frac{m^{2N+4+k+\ell}}{2N+4+k+\ell} B'_{q\bar{q} \rightarrow q\bar{q}}(m), \end{aligned} \quad (6.26)$$

for $q\bar{q} \rightarrow q'\bar{q}'$ we have

$$\begin{aligned} \tilde{w}_{q\bar{q} \rightarrow q'\bar{q}'}^{\text{NLO}} \Big|_{\ln N/N} (2N, \hat{\eta}) &= -\frac{\alpha_s^3 \ln N}{\cosh^4 \hat{\eta} N} \frac{C_F e^{2\hat{\eta}}}{16C_A^2(1+e^{2\hat{\eta}})^2} \\ &\times \left[-1+3C_A^2 + \cosh(2\hat{\eta})(-4-4C_A^2+70C_A C_F) \right. \\ &\quad \left. + \cosh(4\hat{\eta})(1-C_A^2) + 2\sinh(2\hat{\eta})(-1+4C_A^2) \right] \\ &- \sum_{k=1}^{\infty} \sum_{\ell=1}^{\infty} \frac{(-1)^\ell}{\ell} \int_0^1 dm \frac{m^{2N+4+k+\ell}}{2N+4+k+\ell} B'_{q\bar{q} \rightarrow q'\bar{q}'}(m), \end{aligned} \quad (6.27)$$

and for $q\bar{q}' \rightarrow q\bar{q}'$ we find:

$$\begin{aligned} \tilde{w}_{q\bar{q}' \rightarrow q\bar{q}'}^{\text{NLO}} \Big|_{\ln N/N} (2N, \hat{\eta}) &= \frac{\alpha_s^3 \ln N}{\cosh^4 \hat{\eta} N} \frac{C_F}{32C_A^2 e^{2\hat{\eta}}} \\ &\times \left[1-C_A^2 + 2e^{2\hat{\eta}}(-1+4C_A^2+35C_A C_F) \right. \\ &\quad \left. + 2e^{4\hat{\eta}}(-4+7C_A^2+70C_A C_F) + 4e^{6\hat{\eta}}(C_A^2-1) \right] \\ &- \sum_{k=1}^{\infty} \sum_{\ell=1}^{\infty} \frac{(-1)^\ell}{\ell} \int_0^1 dm \frac{m^{2N+4+k+\ell}}{2N+4+k+\ell} B'_{q\bar{q}' \rightarrow q\bar{q}'}(m). \end{aligned} \quad (6.28)$$

Moreover, $qq \rightarrow qq$ gives

$$\begin{aligned}
\tilde{w}_{qq \rightarrow qq}^{\text{NLO}} \Big|_{\ln N/N} (2N, \hat{\eta}) &= \frac{\alpha_s^3 \ln N}{\cosh^4 \hat{\eta} N} \frac{C_F}{32C_A^2 e^{4\hat{\eta}}} \\
&\times \left[2(1 + e^{2\hat{\eta}})^2 \left(-8 + 5e^{2\hat{\eta}} + 2e^{4\hat{\eta}} \right) \right. \\
&\quad + C_A^3 \left(-16 - 23e^{2\hat{\eta}} + 4e^{4\hat{\eta}} + 17e^{6\hat{\eta}} + 4e^{8\hat{\eta}} \right) \\
&\quad - C_A \left(-16 + e^{2\hat{\eta}}[-17 + 140C_F] + 8e^{4\hat{\eta}}[2 + 35C_F] \right. \\
&\quad \quad \left. + e^{6\hat{\eta}}[23 + 140C_F] + 4e^{8\hat{\eta}} \right) \\
&\quad \left. - 2C_A^2 \left(-5 - 7e^{2\hat{\eta}}[1 + 10C_F] + e^{4\hat{\eta}}[6 - 70C_F] \right. \right. \\
&\quad \quad \left. \left. + e^{6\hat{\eta}}[13 - 70C_F] + 5e^{8\hat{\eta}} \right) \right] \\
&- \sum_{k=1}^{\infty} \sum_{\ell=1}^{\infty} \frac{(-1)^\ell}{\ell} \int_0^1 dm \frac{m^{2N+4+k+\ell}}{2N+4+k+\ell} B'_{qq \rightarrow qq}(m), \quad (6.29)
\end{aligned}$$

and $qq' \rightarrow qq'$ yields

$$\begin{aligned}
\tilde{w}_{qq' \rightarrow qq'}^{\text{NLO}} \Big|_{\ln N/N} (2N, \hat{\eta}) &= \frac{\alpha_s^3 \ln N}{\cosh^4 \hat{\eta} N} \frac{C_F}{32C_A^2 e^{2\hat{\eta}}} \\
&\times \left[1 - C_A^2 + 2e^{2\hat{\eta}}(-9 + 6C_A^2 + 35C_A C_F) \right. \\
&\quad \left. + 2e^{4\hat{\eta}}(-12 + 9C_A^2 + 70C_A C_F) + 4e^{6\hat{\eta}}(C_A^2 - 1) \right] \\
&- \sum_{k=1}^{\infty} \sum_{\ell=1}^{\infty} \frac{(-1)^\ell}{\ell} \int_0^1 dm \frac{m^{2N+4+k+\ell}}{2N+4+k+\ell} B'_{qq' \rightarrow qq'}(m). \quad (6.30)
\end{aligned}$$

We proceed with those subprocesses, where also gluons are involved. Starting with $q\bar{q} \rightarrow gg$, we receive

$$\begin{aligned}
\tilde{w}_{q\bar{q} \rightarrow gg}^{\text{NLO}} \Big|_{\ln N/N} (2N, \hat{\eta}) &= \frac{\alpha_s^3 \ln N}{\cosh^6 \hat{\eta} N} \frac{C_F}{16C_A^2} 7(3C_A^2 - 2) \cosh(2\hat{\eta}) [C_A - 2C_F - 2C_F \cosh(2\hat{\eta})] \\
&- \sum_{k=1}^{\infty} \sum_{\ell=1}^{\infty} \frac{(-1)^\ell}{\ell} \int_0^1 dm \frac{m^{2N+4+k+\ell}}{2N+4+k+\ell} B'_{q\bar{q} \rightarrow gg}(m), \quad (6.31)
\end{aligned}$$

and for $gg \rightarrow q\bar{q}$ we get:

$$\begin{aligned}
\tilde{w}_{gg \rightarrow q\bar{q}}^{\text{NLO}} \Big|_{\ln N/N} (2N, \hat{\eta}) &= \frac{\alpha_s^3 \ln N}{\cosh^4 \hat{\eta} N} \frac{C_F e^{2\hat{\eta}}}{16C_A(1 - C_A^2)^2(1 + e^{2\hat{\eta}})^2} \\
&\times \left[-2 - 40C_A^2 + 90C_A^4 - 14C_A C_F + 126C_A^3 C_F \right. \\
&\quad + 2 \cosh(2\hat{\eta})(-1 - 25C_A^2 + 9C_A^4 - 14C_A C_F + 126C_A^3 C_F) \\
&\quad + 2C_A \cosh(4\hat{\eta})(-8C_A + 21C_A^3 - 7C_F + 63C_A^2 C_F) \\
&\quad + 5 \sinh(2\hat{\eta}) - 46C_A^2 \sinh(2\hat{\eta}) + 9C_A^4 \sinh(2\hat{\eta}) + 4 \sinh(4\hat{\eta}) \\
&\quad - 40C_A^2 \sinh(4\hat{\eta}) + 36C_A^4 \sinh(4\hat{\eta}) + \sinh(6\hat{\eta}) \\
&\quad \left. - 10C_A^2 \sinh(6\hat{\eta}) + 9C_A^4 \sinh(6\hat{\eta}) \right] \\
&- \sum_{k=1}^{\infty} \sum_{\ell=1}^{\infty} \frac{(-1)^\ell}{\ell} \int_0^1 dm \frac{m^{2N+4+k+\ell}}{2N+4+k+\ell} B'_{gg \rightarrow q\bar{q}}(m). \tag{6.32}
\end{aligned}$$

For quark-gluon scattering $qg \rightarrow qg$ we have

$$\begin{aligned}
\tilde{w}_{qg \rightarrow qg}^{\text{NLO}} \Big|_{\ln N/N} (2N, \hat{\eta}) &= \frac{\alpha_s^3 \ln N}{\cosh^5 \hat{\eta} N} \frac{C_F}{64C_A^2(C_A^2 - 1)e^{5\hat{\eta}}} \\
&\times \left[-4 - C_A + 14C_A^2 + C_A^3 - 10C_A^4 \right. \\
&\quad - 2e^{2\hat{\eta}}(5 - 20C_A^2 + 13C_A^4 + C_A^3(5 - 42C_F) + C_A(2 + 28C_F)) \\
&\quad + 4e^{10\hat{\eta}}(-2 + 6C_A^4 + C_A^2[1 - 2C_F N_f]) \\
&\quad + 2e^{8\hat{\eta}}(-38 + 84C_A^4 - 56C_A C_F + 84C_A^3 C_F + C_A^2[11 - 10C_F N_f]) \\
&\quad + 2e^{6\hat{\eta}}(-80 + 63C_A^4 + C_A[6 - 140C_F] + C_A^3[-8 + 210C_F] + C_A^2[91 - 8C_F N_f]) \\
&\quad \left. + 2e^{4\hat{\eta}}(-37 + 3C_A^4 + C_A[3 - 112C_F] + 8C_A^3[21C_F - 1] + C_A^2[63 - 2C_F N_f]) \right] \\
&- \sum_{k=1}^{\infty} \sum_{\ell=1}^{\infty} \frac{(-1)^\ell}{\ell} \int_0^1 dm \frac{m^{2N+4+k+\ell}}{2N+4+k+\ell} B'_{qg \rightarrow qg}(m), \tag{6.33}
\end{aligned}$$

and when the gluon is observed, $qg \rightarrow gq$, we receive

$$\begin{aligned}
\tilde{w}_{qg \rightarrow gq}^{\text{NLO}} \Big|_{\ln N/N} (2N, \hat{\eta}) &= \frac{\alpha_s^3 \ln N}{\cosh^4 \hat{\eta} N} \frac{C_F}{32C_A^2(C_A^2 - 1)e^{4\hat{\eta}}(1 + e^{2\hat{\eta}})} \\
&\times \left[-76C_A^4 + 2C_A^2 e^{2\hat{\eta}} (-14 + 31C_A^2) + 2C_A^2 e^{4\hat{\eta}} (-31 + 105C_A^2) \right. \\
&\quad + 2e^{6\hat{\eta}} (9 - 95C_A^2 + 100C_A^4) + e^{8\hat{\eta}} (11 - 94C_A^2 + 57C_A^4) \\
&\quad \left. + e^{10\hat{\eta}} (1 - 10C_A^2 + 9C_A^4) \right] \\
&- \sum_{k=1}^{\infty} \sum_{\ell=1}^{\infty} \frac{(-1)^\ell}{\ell} \int_0^1 dm \frac{m^{2N+4+k+\ell}}{2N+4+k+\ell} B'_{qg \rightarrow gq}(m). \quad (6.34)
\end{aligned}$$

Finally, $gg \rightarrow gg$ yields

$$\begin{aligned}
\tilde{w}_{gg \rightarrow gg}^{\text{NLO}} \Big|_{\ln N/N} (2N, \hat{\eta}) &= - \frac{\alpha_s^3 \ln N}{\cosh^4 \hat{\eta} N} \frac{C_A^3 e^{2\hat{\eta}}}{243(-1 + C_A^2)^2(1 + e^{2\hat{\eta}})^2} \\
&\times \left[-122958 + 562N_f + \cosh(2\hat{\eta})(-172044 + 1039N_f) \right. \\
&\quad + 81 \cosh(4\hat{\eta})(-732 + 7N_f) + 162 \cosh(6\hat{\eta})(24 + N_f) \\
&\quad \left. - 43740 \sinh(2\hat{\eta}) - 38880 \sinh(4\hat{\eta}) - 9720 \sinh(6\hat{\eta}) \right] \\
&- \sum_{k=1}^{\infty} \sum_{\ell=1}^{\infty} \frac{(-1)^\ell}{\ell} \int_0^1 dm \frac{m^{2N+4+k+\ell}}{2N+4+k+\ell} B'_{gg \rightarrow gg}(m). \quad (6.35)
\end{aligned}$$

Beyond these ten partonic resolved subprocesses, we receive additional subleading $\ln N/N$ -contributions by including virtual corrections, hence they appear for the first time at next-to-leading order. These channels have three partons in the final state, giving rise to six reactions reading

$$\begin{aligned}
qq' \rightarrow gX, \quad q\bar{q}' \rightarrow gX, \quad qq \rightarrow gX, \\
qg \rightarrow q'X, \quad qg \rightarrow \bar{q}'X, \quad qg \rightarrow \bar{q}X. \quad (6.36)
\end{aligned}$$

They initiate the following subleading contributions for gluon production:

$$\begin{aligned}
\tilde{w}_{qq' \rightarrow gX}^{\text{NLO}} \Big|_{\ln N/N} (2N, \hat{\eta}) &= -\frac{\alpha_s^3 \ln N}{\cosh^4 \hat{\eta} N} \frac{C_F}{16C_A^2} \\
&\times \left[-9 + 13C_A^2 + 8 \cosh(2\hat{\eta})(2C_A^2 - 1) + \cosh(4\hat{\eta})(C_A^2 - 1) \right] \\
&- \sum_{k=1}^{\infty} \sum_{\ell=1}^{\infty} \frac{(-1)^\ell}{\ell} \int_0^1 dm \frac{m^{2N+4+k+\ell}}{2N+4+k+\ell} B'_{qq' \rightarrow gX}(m), \\
\tilde{w}_{q\bar{q}' \rightarrow gX}^{\text{NLO}} \Big|_{\ln N/N} (2N, \hat{\eta}) &= -\frac{\alpha_s^3 \ln N}{\cosh^4 \hat{\eta} N} \frac{C_F}{16C_A^2} \\
&\times \left[7 + 9C_A^2 + 14C_A^2 \cosh(2\hat{\eta}) + (C_A^2 - 1) \cosh(4\hat{\eta}) \right] \\
&- \sum_{k=1}^{\infty} \sum_{\ell=1}^{\infty} \frac{(-1)^\ell}{\ell} \int_0^1 dm \frac{m^{2N+4+k+\ell}}{2N+4+k+\ell} B'_{q\bar{q}' \rightarrow gX}(m), \\
\tilde{w}_{qq \rightarrow gX}^{\text{NLO}} \Big|_{\ln N/N} (2N, \hat{\eta}) &= \frac{\alpha_s^3 \ln N}{\cosh^4 \hat{\eta} N} \frac{C_F}{16C_A^3} \\
&\times \left[-4 \cosh(2\hat{\eta})(1 - 2C_A - 3C_A^2 + 4C_A^3) - 2 + 9C_A \right. \\
&\quad \left. + 10C_A^2 - 13C_A^3 + \cosh(4\hat{\eta})(-2 + C_A + 2C_A^2 - C_A^3) \right] \\
&- \sum_{k=1}^{\infty} \sum_{\ell=1}^{\infty} \frac{(-1)^\ell}{\ell} \int_0^1 dm \frac{m^{2N+4+k+\ell}}{2N+4+k+\ell} B'_{qq \rightarrow gX}(m). \tag{6.37}
\end{aligned}$$

Finally, considering quark or antiquark production, we get:

$$\begin{aligned}
\tilde{w}_{qg \rightarrow q'X}^{\text{NLO}} \Big|_{\ln N/N} (2N, \hat{\eta}) &= -\frac{\alpha_s^3 \ln N}{\cosh^4 \hat{\eta} N} \frac{C_F}{32C_A(C_A^2 - 1)e^{4\hat{\eta}}(1 + e^{2\hat{\eta}})} \\
&\times \left[1 - C_A^2 + 2e^{2\hat{\eta}}(2 + 5C_A)^2 + 2e^{4\hat{\eta}}(8C_A^2 - 3) + 4e^{6\hat{\eta}}(4C_A^2 - 3) \right] \\
&- \sum_{k=1}^{\infty} \sum_{\ell=1}^{\infty} \frac{(-1)^\ell}{\ell} \int_0^1 dm \frac{m^{2N+4+k+\ell}}{2N+4+k+\ell} B'_{qg \rightarrow q'X}(m), \\
\tilde{w}_{qg \rightarrow \bar{q}'X}^{\text{NLO}} \Big|_{\ln N/N} (2N, \hat{\eta}) &= \frac{\alpha_s^3 \ln N}{\cosh^4 \hat{\eta} N} \frac{C_F}{32C_A(C_A^2 - 1)e^{4\hat{\eta}}(1 + e^{2\hat{\eta}})} \\
&\times \left[C_A^2 - 1 - 2e^{4\hat{\eta}}(1 + 7C_A^2 + 12C_A^2 \cosh(4\hat{\eta}) + 4 \sinh(4\hat{\eta})) \right] \\
&- \sum_{k=1}^{\infty} \sum_{\ell=1}^{\infty} \frac{(-1)^\ell}{\ell} \int_0^1 dm \frac{m^{2N+4+k+\ell}}{2N+4+k+\ell} B'_{qg \rightarrow \bar{q}'X}(m),
\end{aligned}$$

$$\begin{aligned}
\tilde{w}_{qg \rightarrow \bar{q}X}^{\text{NLO}} \Big|_{\ln N/N} (2N, \hat{\eta}) &= \frac{\alpha_s^3 \ln N}{\cosh^4 \hat{\eta} N} \frac{C_F}{32C_A^2(C_A^2 - 1)e^{4\hat{\eta}}(1 + e^{2\hat{\eta}})} \\
&\times \left[2 - C_A - 2C_A^2 + C_A^3 + 8e^{3\hat{\eta}} \cosh \hat{\eta}(1 + C_A^2) \right. \\
&\quad \left. - 2C_A e^{4\hat{\eta}}(1 + 7C_A^2 + 12C_A^2 \cosh(2\hat{\eta}) + 4 \sinh(2\hat{\eta})) \right] \\
&- \sum_{k=1}^{\infty} \sum_{\ell=1}^{\infty} \frac{(-1)^\ell}{\ell} \int_0^1 dm \frac{m^{2N+4+k+\ell}}{2N+4+k+\ell} B'_{qg \rightarrow \bar{q}X}(m). \quad (6.38)
\end{aligned}$$

6.3. Subleading Logarithms for Threshold Resummation

It is not yet clear how to construct resummation exponents with subleading $\ln N/N$ contributions. As resummation exponents were derived, there was no focus on subleading logarithms. Therefore it is not yet clear in what extent a procedure yields the right exponents, when extending these exponents afterwards to $\mathcal{O}(\ln N/N)$. However, in the following we want to collect various possible roots of those contributions, and allude that these parts may not be complete nor sufficient. We explicitly encourage to investigate this in greater detail in a future work.

Hence, in the following section we want to set our focus on subleading contributions for the radiative resummation exponents. Our consideration will contain three parts: First, we will adopt the generalized integrand weight on integrations within the exponents, then we will consider subleading contributions coming from the splitting functions and finally we will investigate the shift of the Mellin moments $N \rightarrow a_i N + b_i$ in a convolution of the hard-scattering function with the fragmentation function.

Introduced in Sec. 5.1, we start with the functions for soft radiation collinear to the initial-state parton i , with factorization scale μ_{fi} , (or final-state parton with factorization scale μ_{ff}), see Eq. (5.26),

$$\begin{aligned}
\ln \Delta_i^N(\hat{s}, \mu_{fi}) &= - \int_0^1 dz \frac{z^{N-1} - 1}{1-z} \int_{(1-z)^2}^1 \frac{dt}{t} A_i[\alpha_s(t\hat{s})] \\
&\quad - 2 \int_{\mu_r}^{\sqrt{\hat{s}}} \frac{d\mu'}{\mu'} \gamma_i(\alpha_s(\mu'^2)) + 2 \int_{\mu_{fi}}^{\sqrt{\hat{s}}} \frac{d\mu'}{\mu'} \gamma_{ii}(N, \alpha_s(\mu'^2)), \quad (6.39)
\end{aligned}$$

and further, the function J_d^N , describing soft and hard collinear emission, off the unobserved recoiling parton d , reads, see Eq. (5.27):

$$\begin{aligned}
\ln J_d^N(\hat{s}, \mu_r) &= \int_0^1 dz \frac{z^{N-1} - 1}{1-z} \left\{ \int_{(1-z)^2}^{(1-z)} \frac{dt}{t} A_d(\alpha_s(t\hat{s})) - \gamma_d(\alpha_s((1-z)\hat{s})) \right\} \\
&\quad + 2 \int_{\mu_r}^{\sqrt{\hat{s}}} \frac{d\mu'}{\mu'} \gamma_d(\alpha_s(\mu'^2)). \quad (6.40)
\end{aligned}$$

The perturbative function A_i was given before in Eq. (5.28) and the anomalous dimensions γ_i and the constant and logarithmic terms of the moments of the diagonal splitting functions, γ_{ii} , can be found in Eq. (5.31). We have used for the integration over t in Eq. (6.38) and (6.39) the NLO solution of the RGE to rewrite $\alpha_s(t\hat{s})$ in dependence of $\alpha_s(\mu^2)$, see Eq. (5.37). Adopting now the generalized formalism of Sec. 6.1 on the first double-integral of Eq. (6.38) leads to:

$$\begin{aligned}
& - \int_0^1 dz \frac{z^{N-1} - 1}{1-z} \int_{(1-z)^2}^1 \frac{dt}{t} A_i[\alpha_s(t\hat{s})] \\
&= \int_0^{1-\frac{1}{N}} dz \frac{1}{1-z} \Gamma\left(1 - \frac{\partial}{\partial \ln N}\right) \left(1 + \frac{n}{2N} \ln^{-1}(1-z) - \frac{n(n-1)}{2N} \ln^{-2}(1-z)\right) \\
&\quad \times \int_{(1-z)^2}^1 \frac{dt}{t} A_i[\alpha_s(t\hat{s})] \\
&= \Gamma\left(1 - \frac{\partial}{\partial \ln N}\right) \left[\frac{1}{N} \frac{A_i^{(1)} \ln(1-2\lambda)}{2\pi b_0} - \frac{A_i^{(2)}}{2\pi^2 b_0^2} [2\lambda + \ln(1-2\lambda)] \right. \\
&\quad + \frac{A_i^{(1)}}{2\pi b_0^2 \alpha_s} [2\lambda + (1-2\lambda) \ln(1-2\lambda)] \\
&\quad \left. + \frac{A_i^{(1)} b_1}{2\pi b_0^3} \left[2\lambda + \ln(1-2\lambda) + \frac{1}{2} \ln^2(1-2\lambda)\right] + \frac{A_i^{(1)}}{2\pi b_0} [2\lambda + \ln(1-2\lambda)] \ln\left(\frac{\hat{s}}{\mu_r^2}\right) \right]. \tag{6.41}
\end{aligned}$$

Together with the further integrations and the contribution coming from Eq. (5.42), for which nothing changes when including subleading Mellin moments, we get:

$$\begin{aligned}
\ln \Delta_i^N(\hat{s}, \mu_{fi})|_{\text{sublead.}} &= \Gamma\left(1 - \frac{\partial}{\partial \ln N}\right) \left[\ln N h_i^{(1)} + h_i^{(2)} + \frac{1}{N} \frac{A_i^{(1)} \ln(1-2\lambda)}{2\pi b_0} + \frac{A_i^{(1)} \lambda}{\pi b_0} \ln \frac{\hat{s}}{\mu_{fi}^2} \right] \\
&\quad - \frac{A_i^{(1)} \lambda}{\pi b_0} \ln \frac{\hat{s}}{\mu_{fi}^2}. \tag{6.42}
\end{aligned}$$

Adopting the first derivative of the power series expansion of $\Gamma\left(1 - \frac{\partial}{\partial \ln N}\right)$ on leading logs gives a contribution to NLL, adopting the second derivative gives a contribution to NNLL and so on. Adopting derivatives on next-to-leading logs give terms that do not contribute anymore on our NLL expanded calculation. Therefore it is sufficient to examine the

following derivation, noting that $\lambda = b_0 \alpha_s \ln N$:

$$\begin{aligned}
& \Gamma\left(1 - \frac{\partial}{\partial \ln N}\right) \ln N h_i^{(1)} = \Gamma\left(1 - \frac{\partial}{\partial \ln N}\right) \frac{A_i^{(1)}}{2\pi b_0^2 \alpha_s} [2\lambda + (1 - 2\lambda) \ln(1 - 2\lambda)] \\
&= \frac{A_i^{(1)}}{2\pi b_0^2 \alpha_s} \left(1 + \gamma_E \alpha_s b_0 \frac{\partial}{\partial \lambda} + \frac{1}{2} (\gamma_E^2 + \zeta(2)) (\alpha_s b_0)^2 \left(\frac{\partial}{\partial \lambda}\right)^2 + \dots\right) \left[2\lambda - (1 - 2\lambda) \sum_{k=1}^{\infty} \frac{(2\lambda)^k}{k}\right] \\
&= \ln N h_i^{(1)} + \frac{A_i^{(1)} \gamma_E}{2\pi b_0} \left[2 - \sum_{k=1}^{\infty} 2(2\lambda)^{k-1} + \sum_{k=1}^{\infty} 2(k+1) \frac{(2\lambda)^k}{k}\right] \\
&\quad + \frac{A_i^{(1)} (\gamma_E^2 + \zeta(2))}{4\pi} \alpha_s \left[-\sum_{k=1}^{\infty} 4(k-1)(2\lambda)^{k-2} + \sum_{k=1}^{\infty} 4(k+1)(2\lambda)^{k-1}\right] + \mathcal{O}(\alpha_s^2 \lambda^k) \\
&= \ln N h_i^{(1)} - \frac{A_i^{(1)} \gamma_E}{\pi b_0} \ln(1 - 2\lambda) + \mathcal{O}(\alpha_s \lambda^k). \tag{6.43}
\end{aligned}$$

Note that the γ_E -contribution, which is at next-to-leading order and was missing before, is reproduced again through adopting the second order in the power series expansion of $\Gamma\left(1 - \frac{\partial}{\partial \ln N}\right)$ on a leading-logarithmic contribution. Finally we note that besides the normal contributions of the exponent, see Eq. (5.44) and (5.47), which could be reproduced fully, an additional subleading term appears:

$$\frac{1}{N} \frac{A_i^{(1)} \ln(1 - 2\lambda)}{2\pi b_0}. \tag{6.44}$$

Analogously we get for the outgoing parton d , starting with Eq. (6.39), the new subleading contribution

$$\frac{1}{N} \frac{A_d^{(1)} (\ln(1 - \lambda) - \ln(1 - 2\lambda))}{2\pi b_0}. \tag{6.45}$$

Another root of subleading contributions lies in the splitting functions, which also take place in the calculation of the exponents. The diagonal splitting functions read in x -space [59]:

$$\begin{aligned}
P_{qq} &= C_F \left[\frac{1+x^2}{(1-x)_+} + \frac{3}{2} \delta(1-x) \right] + \mathcal{O}(\alpha_s) \\
P_{gg} &= 2C_A \left[\frac{1-x}{x} + x(1-x) + \frac{x}{(1-x)_+} \right] + 2\pi b_0 \delta(1-x) + \mathcal{O}(\alpha_s). \tag{6.46}
\end{aligned}$$

Transforming into Mellin moment space gives for the quark-quark splitting function

$$\begin{aligned}
P_{qq}^N &= \int_0^1 x^{N-1} P_{qq}(x, \alpha_s) = C_F \left[\frac{-2N-1}{N(N+1)} - 2H_{N-1} + \frac{3}{2} \right] \\
&= -2C_F \left[\ln \bar{N} + \frac{1}{2N} - \frac{3}{4} \right] + \mathcal{O}\left(\frac{1}{N^2}\right), \tag{6.47}
\end{aligned}$$

and for the gluon-gluon case:

$$\begin{aligned} P_{gg}^N &= \int_0^1 x^{N-1} P_{gg}(x, \alpha_s) = 2C_A \left[\frac{1}{N-1} - \frac{1}{N} + \frac{1}{N+1} - \frac{1}{N+2} - H_N \right] + 2\pi b_0 \\ &= -2C_A \left[\ln \bar{N} + \frac{1}{2N} \right] + 2\pi b_0 + \mathcal{O}\left(\frac{1}{N^2}\right). \end{aligned} \quad (6.48)$$

The $1/N$ contributions have been neglected in the usual calculations for the resummation exponents, therefore we want to incorporate these terms now to calculate their subleading contributions. We realize that in both cases, see Eq. (6.46) and (6.47), the logarithmic contribution $\ln \bar{N}$ inherits subleading terms $1/(2N)$. To calculate $1/N$ -suppressed logarithms coming from the splitting functions, we consider a slightly different form for the resummed exponents [117], where logarithms generated by the splitting functions can be isolated from the rest,

$$\begin{aligned} \ln \Delta_i^{N_i} &= \int_{\sqrt{\hat{s}}/\bar{N}_i}^{\sqrt{\hat{s}}} \frac{d\mu}{\mu} A_i(\alpha_s(\mu^2)) \ln \frac{\mu^2 \bar{N}_i^2}{\hat{s}} + \ln(\bar{N}_i) \int_{\sqrt{\hat{s}}}^{\mu_{f_i}^2} \frac{d\mu^2}{\mu^2} A_i(\alpha_s(\mu^2)), \\ J_d^{N_i} &= - \int_{\sqrt{\hat{s}}/\bar{N}_i}^{\sqrt{\hat{s}}/\bar{N}_i} \frac{d\mu}{\mu} A_d(\alpha_s(\mu^2)) \ln \frac{\mu^2 \bar{N}_i^2}{\hat{s}} + \int_{\sqrt{\hat{s}}/\bar{N}_i}^{\sqrt{\hat{s}}} \frac{d\mu}{\mu} \left[A_d(\alpha_s(\mu^2)) \ln \frac{\mu^2}{\hat{s}} - 2\hat{B}_d(\alpha_s(\mu^2)) \right]. \end{aligned} \quad (6.49)$$

The first integral of both radiative exponents contain the logarithms coming from the splitting function, hence we separate them from the rest. Since we are only interested in additional subleading terms, we replace then $\ln \bar{N}$ with $1/(2N)$, and proceed with the integrations. Solving the integrals at NLL, we receive

$$\begin{aligned} \int_{\sqrt{\hat{s}}/\bar{N}_i}^{\sqrt{\hat{s}}} \frac{d\mu}{\mu} 2 \frac{\alpha_s(\mu^2)}{\pi} A_i^{(1)} \frac{1}{2N_i} &= - \frac{A_i^{(1)} \ln(1-2\lambda)}{2b_0 \pi N_i} + \mathcal{O}\left(\frac{1}{N^2}\right), \\ - \int_{\sqrt{\hat{s}}/\bar{N}_i}^{\sqrt{\hat{s}}/\bar{N}_i} \frac{d\mu}{\mu} 2 \frac{\alpha_s(\mu^2)}{\pi} A_i^{(1)} \frac{1}{2N_i} &= \frac{A_i^{(1)}}{2b_0 \pi N_i} [\ln(1-2\lambda) - \ln(1-\lambda)] + \mathcal{O}\left(\frac{1}{N^2}\right). \end{aligned} \quad (6.50)$$

These are the subleading results from our second consideration. However, they are complementary to the first ones and cancel against each other. This shows that the construction of exponents containing $\ln N/N$ terms is not clearly understood yet. Maybe the cancellation shows that an afterwards adjustment of the exponents is not the end of the story.

However, our last suggestion how to receive subleading contributions uses a slightly other method. We have seen in Sec. 5.3.1 that the exponents contribute with different moments, since we had $N_a = (-\hat{u}/\hat{s})N$, $N_b = (-\hat{t}/\hat{s})N$ and $N_c = N$ for exponents $\Delta_i^{N_i}$. However, in that case we have been interested in NLL exponents without subleading contributions. Now, as Ref. [118] shows, we should regard the full moments including the appropriate

shift, so that we get e.g. for a direct subprocess:

$$\Delta_b^{2N_b+1}, \quad \Delta_c^{2N+3}, \quad J_d^{2N}. \quad (6.51)$$

Thus, by rewriting $N \rightarrow a_i N + b_i$ and expanding the integrals in Eq. (6.38) and (6.39) at NLL accuracy including $\ln N/N$ terms, we get

$$\begin{aligned} \ln \Delta_i^{N \rightarrow a_i N + b_i}(\hat{s}, \mu_{f_i}, \mu_r) &\rightarrow \ln \Delta_i^N(\hat{s}, \mu_{f_i}, \mu_r) - \frac{A_i^{(1)}}{\pi b_0} \left(\frac{b_i}{a_i N} + \ln a_i \right) \ln(1 - 2\lambda) + \mathcal{O}\left(\frac{1}{N^2}\right), \\ \ln J_d^{N \rightarrow a_i N}(\hat{s}, \mu_r) &\rightarrow \ln J_d^N(\hat{s}, \mu_r) - \frac{A_i^{(1)} \ln a_i}{\pi b_0} (\ln(1 - \lambda) - \ln(1 - 2\lambda)) + \mathcal{O}\left(\frac{1}{N^2}\right). \end{aligned} \quad (6.52)$$

However, in what way the final radiative exponents including subleading logarithms are composed is still an open question and has to be further investigated.

We want to explore. We're curious people. [...] Now it's time to go.

Eileen Collins

7

Phenomenological Results for COMPASS

Again, we refer to Refs. [38, 39] where parts of this chapter have already been published in.

We want to apply our theoretical predictions for the resummed polarized cross section and the double-longitudinal spin asymmetries of the photoproduction process $\mu N \rightarrow \mu' h X$ to the COMPASS experiment [18, 19]. The interest in this experiment is based on the following: Since the gluon distribution $\Delta g(x)$ is a key ingredient for solving the proton spin puzzle, one places special emphasis on spin asymmetries which are directly sensitive to Δg . These are examined and measured at the COMPASS experiment, taking place at the *Super Proton Synchrotron* (SPS) at CERN. The process under consideration is semi-inclusive hadron production $\mu N \rightarrow \mu' h X$, for which the theoretical framework was provided in Chap. 5. There and before, we found out that for kinematics like at COMPASS, we are in the threshold region where the resummation of soft logarithms has to be performed.

Hence, we want to investigate the impact of next-to-leading logarithmic threshold resummation on the spin-dependent cross sections and on the corresponding double-longitudinal spin asymmetry in the following.

Using COMPASS kinematics implies a mean beam energy of $E_\mu = 160$ GeV for the longitudinally polarized muon beam corresponding to a center-of-mass energy of $\sqrt{S} = 17.4$ GeV. COMPASS is a fixed-target experiment and we have either a solid-state polarized lithium-deuterid (${}^6\text{LiD}$) target from the run between 2002 to 2006, or an ammonia (NH_3) target from 2007 on. On a more hadronic level, the targets are protons and deuterons and a highly virtual photon is exchanged. Then, a charged hadron is detected at high transverse momentum p_T , which we choose to be equals to the renormalization and factorization scales that means $\mu_r = \mu_{fi} = \mu_{ff} \equiv \mu = p_T$, if not mentioned otherwise. This is the critical point since nearly all of the available center-of-mass energy is used for the

production of a high- p_T parton and its recoiling counterpart. In this threshold region, the phase space for additional parton radiation becomes small and restricts real gluon emission on soft and collinear gluons [26, 27]. The incomplete cancelation of infrared divergences between real and virtual diagrams leave then large logarithmic corrections behind, appearing at every order in perturbation theory. These logarithms may be taken into account by threshold resummation, which leads to large corrections to the NLO calculation. This was shown already for the unpolarized case [22]. As a consequence, an investigation of the longitudinal polarized cross section should follow. With that at hand, we are able to calculate the double-longitudinal spin asymmetries which will then be compared with the COMPASS data. Due to experimental conditions, the maximal virtuality of the exchanged photon used in the Weizsäcker-Williams spectrum in Eq. (5.13), is $Q_{\text{max}}^2 = 1 \text{ GeV}^2$. Furthermore, we introduce the cut for the energy fraction of the virtual photon carried by the hadron, $0.2 \leq z \leq 0.8$ and the cut for the lepton's momentum fraction carried by the photon, $0.1 \leq y \leq 0.9$. Scattered hadrons can be detected within a scattering angle between $10 \leq \theta \leq 120 \text{ mrad}$, corresponding to the pseudorapidity range $-0.1 \leq \eta \leq 2.38$. We consider this full rapidity range as well as several rapidity bins, $[-0.1, 0.45]$, $[0.45, 0.9]$ and $[0.9, 2.4]$, when we come to the asymmetries. For the calculations of the unpolarized NLL resummed cross section, we follow Ref. [22] and use the updated numerical code of that work. Although experimental data are available down to $p_T=0.7 \text{ GeV}$, we require the hadron's transverse momentum to be at least $p_T=1.75 \text{ GeV}$. With that we can ensure our perturbative methods to be valid. We use the DSSV2014 helicity dependent parton distribution functions [62] as well as the unpolarized parton distributions MSTW, see Ref. [119], as standard sets. Calculating the resolved photon processes we adopt the polarized and unpolarized photonic parton distributions of Refs. [87] and [88]. For the helicity dependent ones, we choose the “maximal” set of distributions, as described in Sec. 3.3. This corresponds to the assumption that the spin-dependent and spin-averaged photonic parton distributions start at the same point at some low initial scale. Considering the fragmentation functions, the situation is a bit more involved. The COMPASS data do not distinguish between the different detected hadron species and are specified only by charge. The DSS07 set of Ref. [76] provides fragmentation functions for such “unidentified” hadrons. However, there exist updated sets for pions in [80] (DSS14) and for kaons in [75] (DSS17). An updated proton set is, however, still missing. It is important to keep in mind that in the COMPASS analysis in Ref. [19] only DSS14 was used, neglecting heavier hadrons since there were no further updated sets available like the kaon fragmentation. However, this was expected to catch the dominant effects. In the following we will study the impact of various fragmentation functions on the size and the shape of the predicted spin asymmetries. On the one hand, we will use the set DSS07 for those various unidentified hadrons, on the other hand, we will also adopt the recent sets for combined pions and kaons since those constitute by far the largest fraction of produced charged hadrons. We expect this approximation to be accurate at the 90%-level for absolute cross sections

and even better for spin asymmetries.

7.1. Polarized and Unpolarized Resummed Cross Sections

Investigating the LO and NLO cross sections, polarized and unpolarized, at kinematics used in the COMPASS experiment, it is revealed that there is a huge gap going from the lowest order to the next-leading one. Thus, NLO cannot be the end of the story and we have to find a more precise way to calculate the main contributing parts of the cross sections. This is the point where threshold resummation becomes relevant, giving rise to some further logarithmic corrections. We will verify how these threshold corrections reproduce the main contributions from the fixed-order calculation, as we will compare the first-order expanded resummed results with those at NLO. If the first-order expansion of the next-to-leading logarithmic resummation formula coincides with NLO, our assumptions are confirmed and threshold resummation is a useful method to calculate higher-order corrections precisely without knowing the exact fixed-order contributions like NNLO and higher. If not stated otherwise, the resummed cross section will, in the following, always be with implemented matching, which was introduced in Sec. 5.6.

7.1.1. Polarized Unidentified Hadron Production from a Deuteron

We start with the cross sections for unidentified hadron production, using the DSS07 set, for a first general consideration. Fig. 7.1 shows the direct and resolved photon parts of the spin-dependent cross sections for $\mu d \rightarrow \mu' h^\pm X$ at leading order (LO), next-to-leading order (NLO) and resummed with matching implemented as described in Sec. 5.6. The symbols show the NLO-expansions of the non-matched resummed cross sections. We sum over the charges of the produced hadrons. Going from LO to NLO reveals a large enhancement to the resolved contribution. This can also be perceived when threshold corrections are included. This happens especially at high transverse momentum p_T when the threshold is more closely approached. Furthermore, the matched resolved resummed cross section gives the greatest amount to the full polarized resummed cross section, which means that resolved-photon contributions cannot be neglected. This stands in contrast to the impact of these contributions to the unpolarized calculation, see Fig. 7.2. There, for $p_T \geq 3.25$ GeV, the direct cross sections dominate.

Let us now come to the direct case in Fig. 7.1. Here, the NLO prediction is slightly lower than the LO one at $p_T \lesssim 2.5$ GeV but higher for regions with larger p_T . Including resummation effects only gives a small change of the predictions. The first-order expansions of the resummed cross section reproduces the full NLO result faithfully, especially for the resolved contributions and for the direct ones at high- p_T .

These opposing observations for the direct and resolved cross sections shall be examined in more detail later when the full cross sections are split up into its particular subpro-

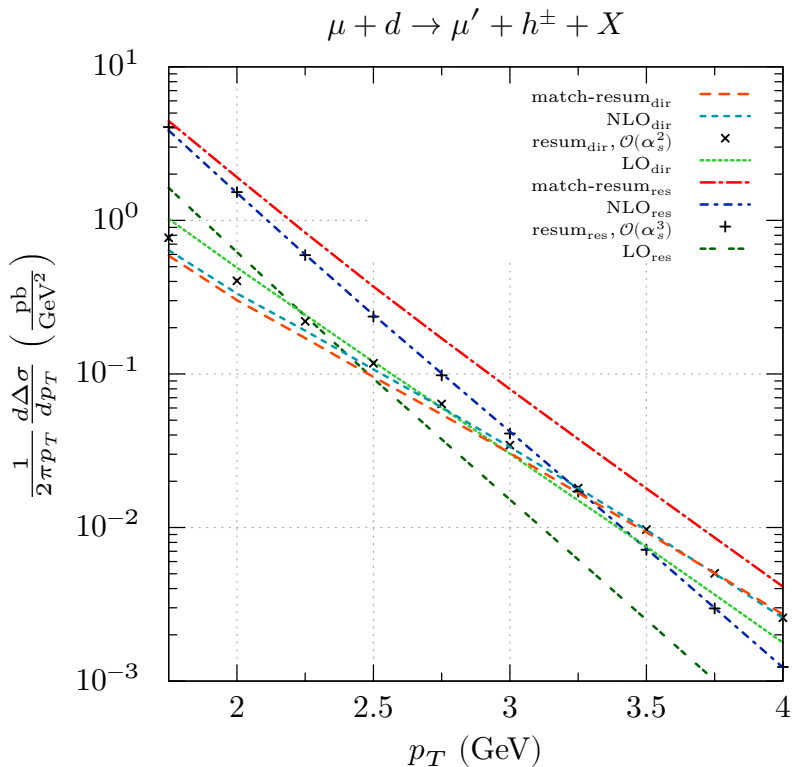


Fig. 7.1.: Direct and resolved parts of the spin dependent LO, NLO and matched resummed differential cross sections for $\mu d \rightarrow \mu' h^\pm X$ with the DSS07 set of fragmentation functions. We also show the NLO expansions of the resummed results (symbols) and consider the full rapidity range $-0.1 \leq \eta \leq 2.38$, here and in the following if not stated otherwise.

cesses. But first we want to compare the polarized with the unpolarized full theoretical predictions, see Fig. 7.3. Going from LO to NLO, both unpolarized, reveals huge corrections. In addition the difference between the NLO and the unpolarized resummed cross section is similarly sizeable. The unpolarized outcome is very similar to the plot shown in [22], except for our use of the more recent parton distribution functions and some kinematic settings. Considering now the polarized cross sections, we again observe that the next-to-leading-order cross section gives a big correction to the LO one in the fully depicted kinematic range. However, logarithmic corrections from threshold resummation only give large adjustments close to threshold limit. The first-order expansions of the resummed cross section reveal in both cases, polarized and unpolarized, that they agree well with the full NLO result. This illustrates that threshold logarithms reproduce the dominant parts of the fixed-order cross section correctly. Just as for the resolved polarized part of the cross section in Fig. 7.1, this happens explicitly at high p_T when the kinematics approach the threshold region. We conclude that although threshold effects are important for the spin-dependent cross sections due to the resolved contributions, the influence of resummation on the spin-averaged prediction is more dominant. This means that threshold corrections do not cancel in the spin asymmetries. We further explore the

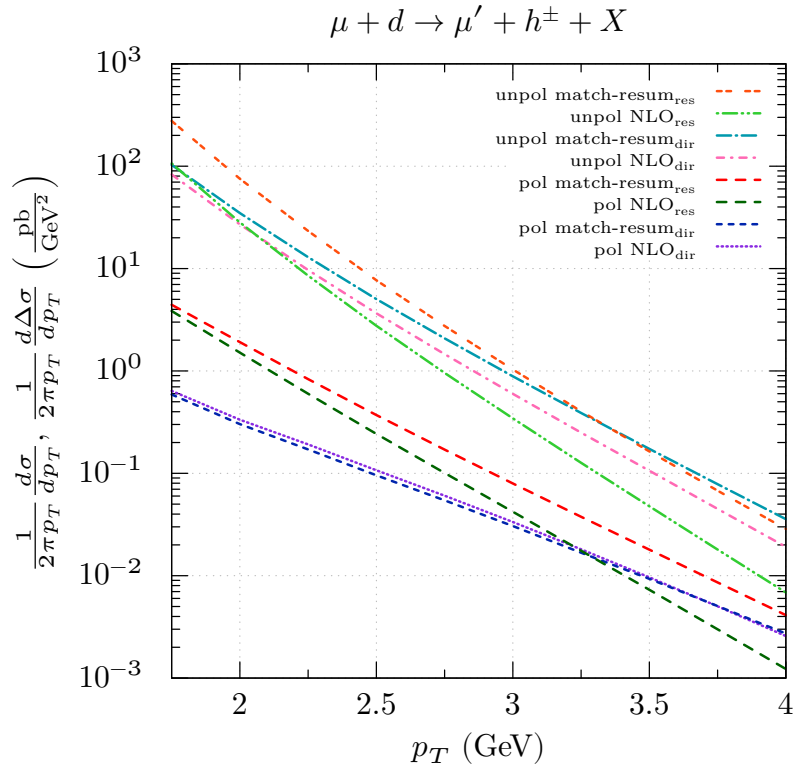


Fig. 7.2.: Comparison of the different impact of direct and resolved photon contributions in the spin-averaged and spin-dependent cross sections.

reliability of perturbative methods by analyzing the dependence of the calculated cross sections on the arbitrary chosen and unphysical factorization and renormalization scales μ_{fi} , μ_{ff} and μ_r . The truncation of perturbation series at some fixed order of α_s results in the dependence on these scales. Thus, one expects these effects to decrease by including higher-order terms. To what extent this can be confirmed is going to be studied in the following. In Fig. 7.4 we examine the scale dependence of the spin-dependent cross section, which contains the full direct and resolved contributions. We vary the scales within the range $p_T/2 \leq \mu_{fi} = \mu_{ff} = \mu_r \leq 2p_T$. However, we note that all scales can be varied independently. A large scale uncertainty can be observed. There is a clear improvement when going from LO to NLO. However, as for the resummed case, one has to consider the results in more detail. At lower p_T and considering the scale at $\mu = p_T/2$, the NLO expansion of the resummed results does not comply with the full NLO result, as it does for the mid-to-high p_T region and for all other scales. Therefore, the matching procedure where we subtract the NLO expanded contributions and add instead the full NLO cross section, yield the small scale dependence for $p_T = 1.75$ GeV. As this problem appears, we intend to compare the scale dependence of the direct and resolved contributions in Fig. 7.5 (a) and (b) independently. In contrast to the resolved case, where the resummed first order expansion is mostly consistent with NLO, except for $\mu = p_T/2$ at low p_T , the

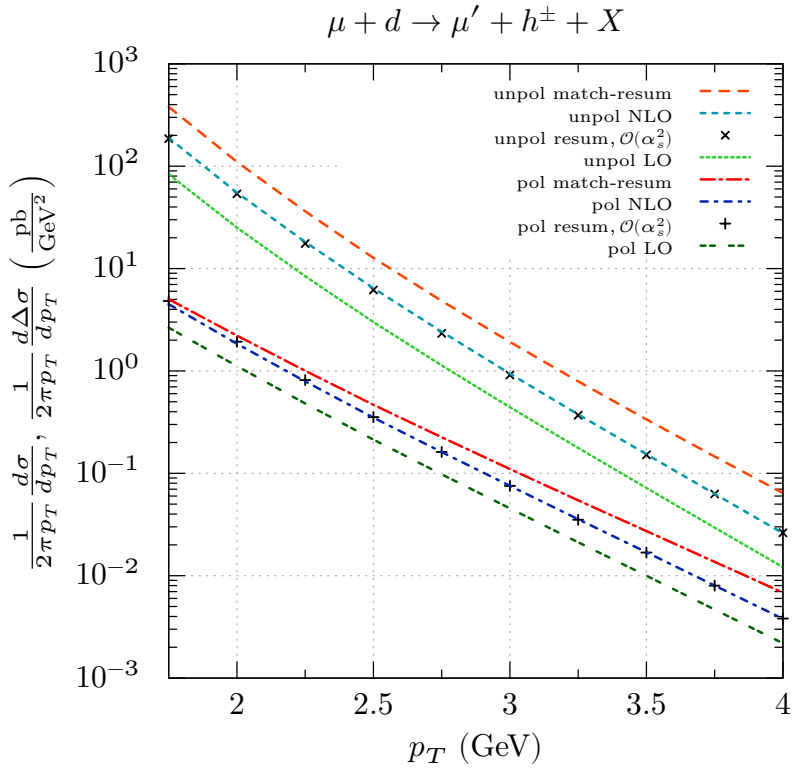


Fig. 7.3.: Spin-dependent and spin-averaged cross sections at LO, NLO and matched resummed cross sections for unidentified hadrons. Again, and as in the following, the symbols denote the NLO expansions of the resummed results.

direct first order expansion does not reproduce the full NLO result at any scale for low- p_T . Nevertheless, the most remarkable deviation can be found again for the upper band with $\mu = p_T/2$. This behaviour diminishes when changing to the mid- p_T range. Again, close to the threshold region, the first order expansions of the resummed resolved and direct cross sections reproduce the NLO-bands perfectly, except for the direct case at $\mu = p_T/2$.

To analyze the improvement of the scale-dependence by including logarithmic corrections, we consider the threshold momentum range where the NLO predictions can be reproduced perfectly by the first order expansion of the resummed cross sections. Contrary to the resolved case, where including threshold logarithms improves the scale dependence considerably, the direct scale dependence is increasing. All these features that we observe in the direct part of the polarized cross section can be understood by investigating the individual subprocesses, which contribute to the full direct cross section, see Fig. 7.6. Thereby, we note that the two competing subprocesses $\gamma q \rightarrow qg$ and $\gamma g \rightarrow q\bar{q}$ enter with opposite sign and thus cancel to some extent. As already observed in the context of the NLO calculation [25], it was discussed that the cancelation may be responsible for the fact that polarized resolved contributions computed with the “maximal” set of [88] are more important for the full amount of the cross section than in the unpolarized case, as is

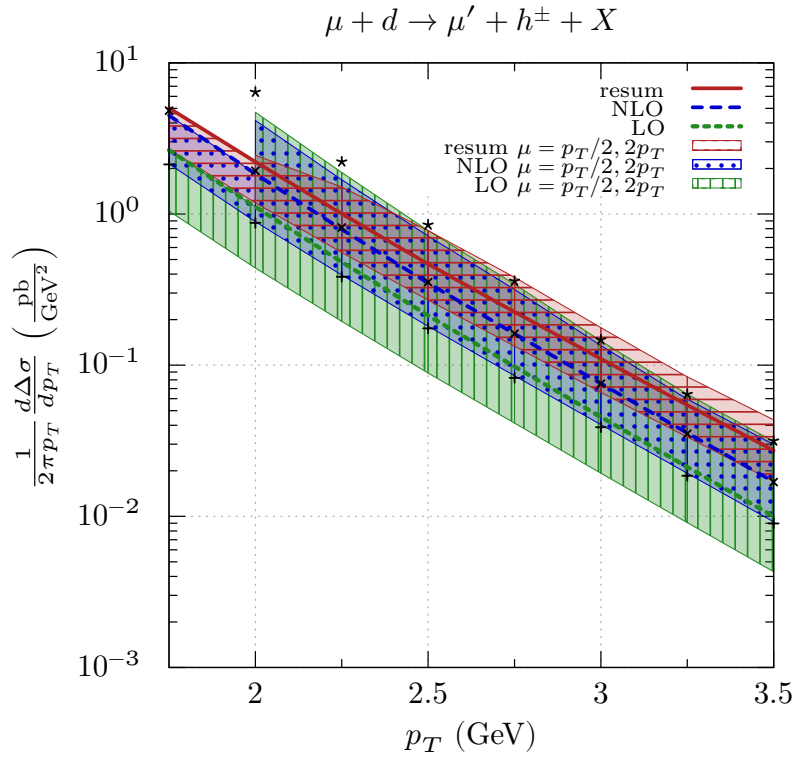


Fig. 7.4.: Scale dependence of the full spin-dependent cross section at LO, NLO, and for the resummed case. We vary the scale $\mu = \mu_r = \mu_{fi} = \mu_{ff}$ in the range $p_T/2 \leq \mu \leq 2p_T$. The upper ends of the bands correspond to $\mu = p_T/2$, the lower ones to $\mu = 2p_T$. To justify perturbative methods, we show results only when the scale μ exceeds 1 GeV.

evident from the curves in Fig. 7.2. Furthermore, also the resolved subprocesses contribute with different sign, see Fig. 7.7. Another feature in terms of the subprocesses is that the resummed first-order expansion of the direct and resolved processes $\gamma g \rightarrow q\bar{q}$, $q_j\bar{q}_j \rightarrow q_k\bar{q}_k$ and $gg \rightarrow q\bar{q}$ cannot reproduce the NLO prediction as exactly as before, especially at low p_T . We notice that we have threshold resummation for some subprocesses not as good under control, as in the unpolarized case. This is due to subleading NLO contributions which are formally suppressed by $1/N$. However, in these subprocesses they are no longer insignificant at low-to-mid transverse momentum. Nevertheless, the numerical amount of these channels is assessable when summing over all subprocesses, over direct and resolved parts. This is confirmed by Fig. 7.3 where the total resummed cross section reveals that the first order expansion perfectly agrees with the NLO prediction. However, we should keep in mind that there are subleading contributions, introduced in Chap. 6, having a larger impact than anticipated.

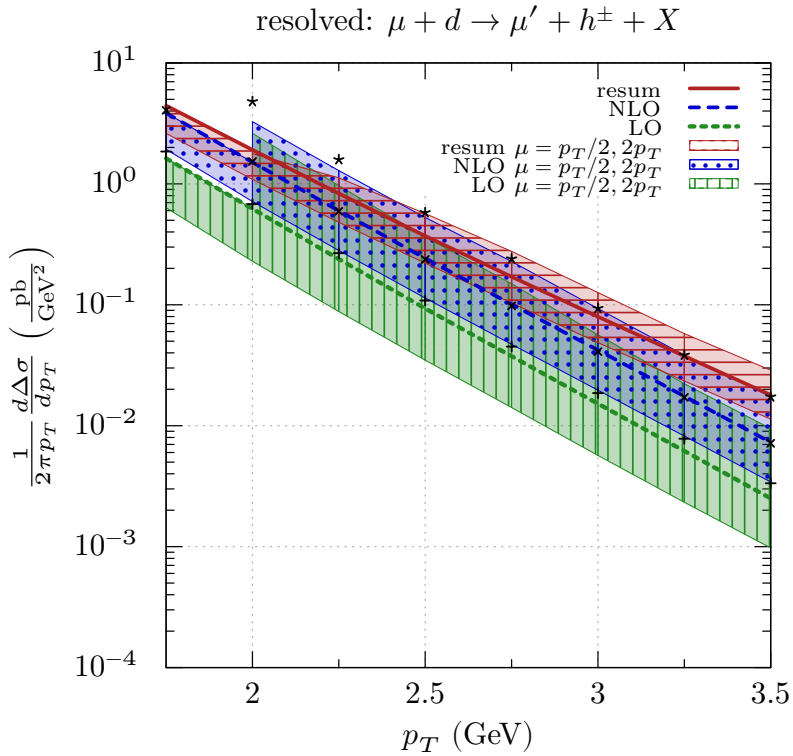
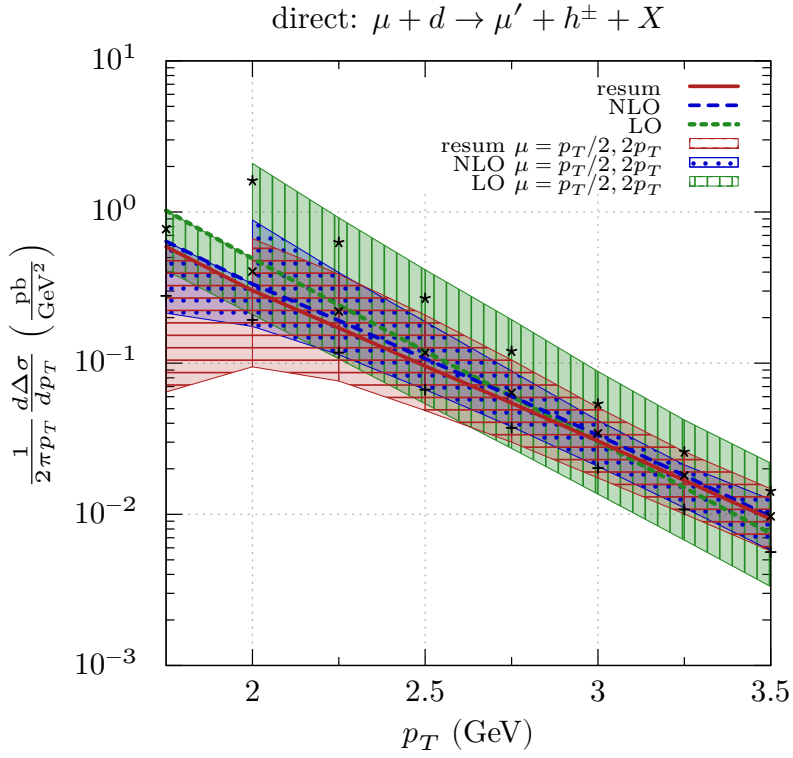


Fig. 7.5.: Scale dependence of (a) the direct and (b) the resolved spin-dependent cross section at LO, NLO, and for the resummed case. We vary the scale $\mu = \mu_r = \mu_{fi} = \mu_{ff}$ in the range $p_T/2$ (upper band) $\leq \mu \leq 2p_T$ (lower band) and show results only for $\mu \geq 1$ GeV.

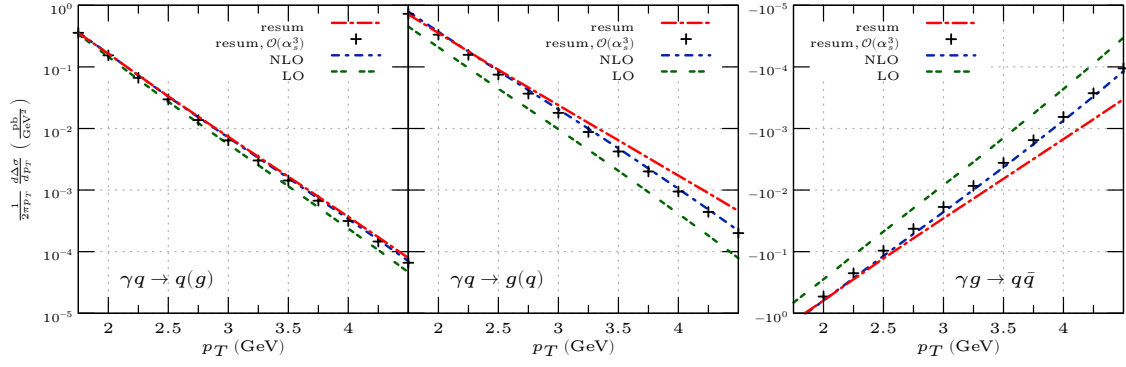


Fig. 7.6.: Contributions to the polarized direct cross section from the individual direct subprocesses.

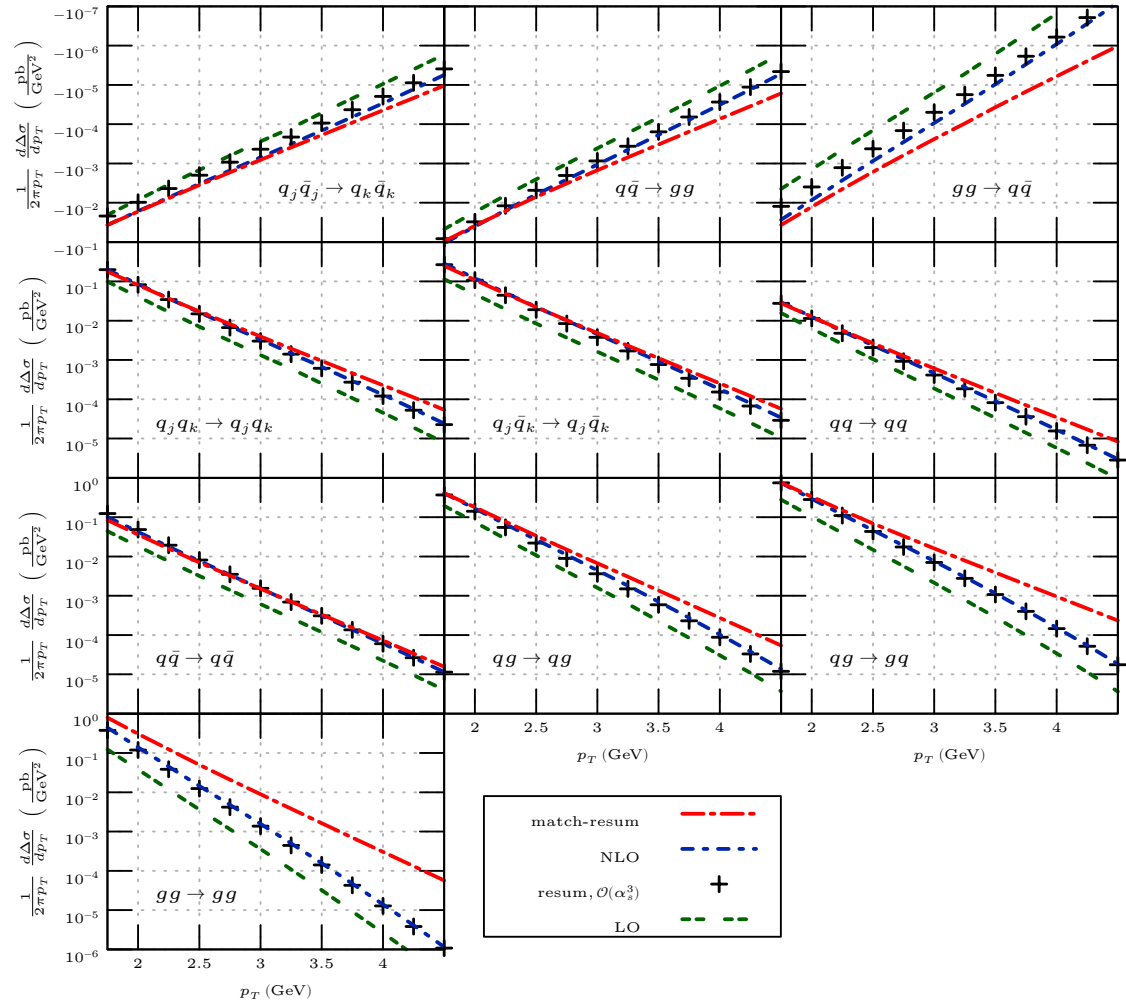


Fig. 7.7.: Contributions to the polarized resolved cross section from the individual resolved subprocesses.

7.1.2. Pion and Kaon Production

As already indicated, we now consider produced kaons and pions. To do so we use the DSS14 and DSS17 fragmentation functions and sum over contributions from produced pions and kaons. Please note that parts of the results are already published in our Ref. [39].

We start with the comparison of the polarized and unpolarized cross sections for $\mu d \rightarrow \mu'(\pi, K)^\pm X$ in Fig. 7.8. Again, we show results at next-to-leading order, the resummed case including the matching procedure as described in Eq. (5.79), and the first order expansions to NLO of the corresponding non-matched resummed cross sections. Considering the spin-averaged cross section, we observe again that the difference between the fixed-order results and the resummed ones are sizeable, especially at high p_T when we are close to kinematic threshold. Comparing the NLO expansion of the resummed cross section with the full NLO one, we detect a very good accordance, illustrating that threshold resummation reproduces the dominant parts of the cross section correctly. Note that the unpolarized plot for unidentified hadrons in Fig. 7.3, decline when the updated fragmentation functions are used so that only kaons and pions are identified in the final state, see Fig. 7.8. However, there are no further apparent changes. In terms of the polarized case, we again detect that the resummed expansions to NLO describe the full NLO cross section somewhat less accurately than in the unpolarized case. Nevertheless it is described still well. Further investigations and explanations for this can be found in Chap. 7.1.1. Additionally, we would like to mention that the shape of the polarized plots have somewhat changed compared to Fig. 7.3. While the logarithmic corrections had a huge influence close to threshold when the fragmentation function DSS07 was used, we now observe only a modest enhancement over NLO for the mid- p_T range up to $p_T \lesssim 3.75$ GeV. Furthermore, we find an approach towards NLO for high p_T . There, the resummed cross section falls slightly below NLO. This clearly demonstrates the impact of the chosen fragmentation functions.

Fig. 7.9 shows the amount of the direct and resolved parts of the spin-dependent resummed cross sections with implemented matching. The resolved plot shows further NLO and the first-order expansions (symbols), however, for the direct part we only show the matched-resummed cross section, since the NLO one starts negative and grows to become positive within the depicted kinematic range. We examine that the full spin-dependent direct resummed cross section is negative when the DSS14 and DSS17 fragmentation functions are used. The resummed resolved contribution turns out to be positive and dominant for our choice of polarized parton distributions of the photon, which yields a positive polarized full cross section. It may perhaps be expected that in the presence of such partial cancellations between the direct and the resolved-photon contributions the expanded resummed cross section will not trace the full NLO one too faithfully. For the same reason, the polarized cross section could be expected to be quite sensitive to higher-order perturbative

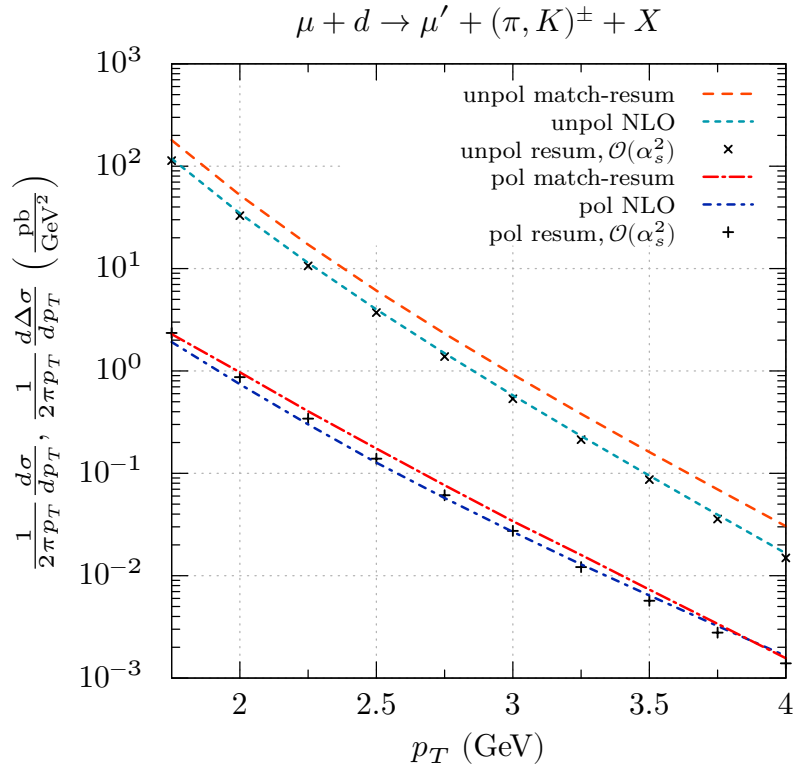


Fig. 7.8.: Unpolarized and polarized NLO and resummed (matched) cross sections for combined pion and kaon production in $\mu d \rightarrow \mu' h X$ in the full rapidity range $-0.1 \leq \eta \leq 2.38$. The symbols compare the NLO expansions of the (non-matched) resummed cross sections to the full NLO results and we sum over the charges of the produced hadron.

corrections. Nonetheless, threshold resummation turns out to offer only relatively small corrections to the polarized NLO results. As a consequence of this different behaviour of polarized and unpolarized higher-order threshold effects, they will not cancel in the double-longitudinal spin asymmetries, as we will discern in the next section. The fact that the various spin-dependent subprocesses conspire to produce overall relatively small QCD corrections is an important outcome of our threshold resummation study.

Analogously to the fragmentation function set DSS07, we intend to estimate the sensitivity of the polarized cross section to the chosen renormalization and factorization scales $\mu \equiv \mu_r = \mu_{fi} = \mu_{ff}$. We vary within the range $p_T/2 \leq \mu \leq 2p_T$ although all scales can be varied independently. In Figs. 7.10 (a) we show our results for the “pion-plus-kaon” fragmentation functions of DSS14 and DSS17 compared to the results for charged-hadron production of DSS07 in (b), which were already shown in Fig. 7.4. Again, the scale dependence for kaon and pion production remains unpleasantly large when including threshold logarithms. Comparing both cases, we see that the first order expansions do neither reproduce the NLO results for kaon and pion production at $\mu = p_T/2$ nor the results for the unidentified-hadron DSS07 fragmentation. This different behaviour at $\mu = 2p_T$ and $\mu = p_T/2$ may be explained by the fact that we are closer to threshold at $\mu = 2p_T$,

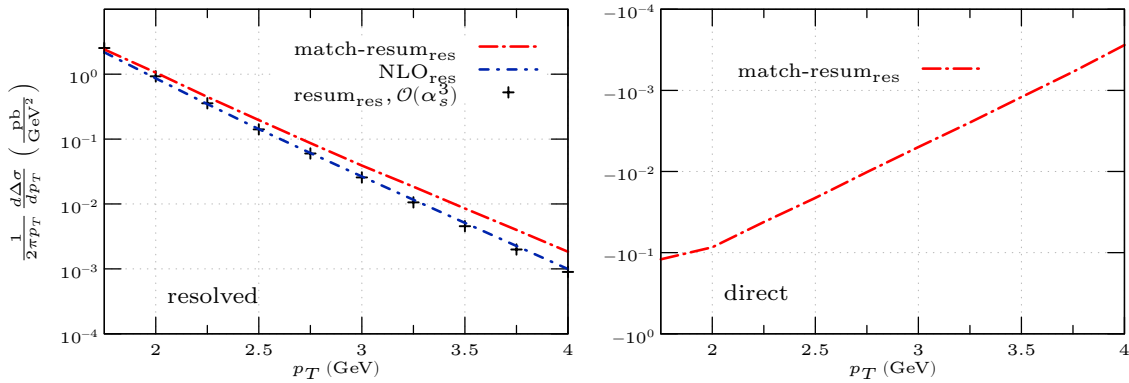


Fig. 7.9.: Direct and resolved parts of the spin-dependent resummed cross sections for $\mu d \rightarrow \mu'(\pi, K)^\pm X$ with implemented matching. For the resolved cross section we also show NLO and the first-order expansions (symbols), however, for the direct part we only show the negative matched-resummed cross section since the NLO one starts negative and grows to become positive within the shown kinematic range.

whereas perturbative methods are less suitable at low p_T . Moreover, we find at LO that the scale uncertainty is larger by one order of magnitude, clearly demonstrating the need for higher-order calculations.

7.2. Double-Spin Asymmetry

In the section before, we have examined the polarized and unpolarized cross sections for semi-inclusive high- p_T photoproduction processes with various fragmentation functions used for the detected hadron. We have compared next-to-leading order results with threshold resummation corrections. We anticipate from the results presented in Fig. 7.3 and Fig. 7.8 that threshold corrections to NLO do not cancel in the double-longitudinal spin asymmetry A_{LL} . Furthermore, we found out that the choice of fragmentation function influences the cross sections considerably. The direct resummed cross section has a positive sign for DSS07 and a negative one for DSS14 and DSS17, combined. Moreover, the logarithmic threshold contribution at high p_T is for DSS07 much more pronounced than for kaon and pion production. These effects of the fragmentation functions we found have been proven in the section before when we examined the deuteron within the full rapidity bin $-0.1 \leq \eta \leq 2.38$. However, we will demonstrate in the following that the choice of the fragmentation function has an increased impact when the three rapidity bins $[-0.1, 0.45]$, $[0.45, 0.9]$ and $[0.9, 2.4]$ are studied and also the process $\mu p \rightarrow \mu' h X$ with a proton as target.

The double-longitudinal spin asymmetry is given by the ratio of the spin-dependent and

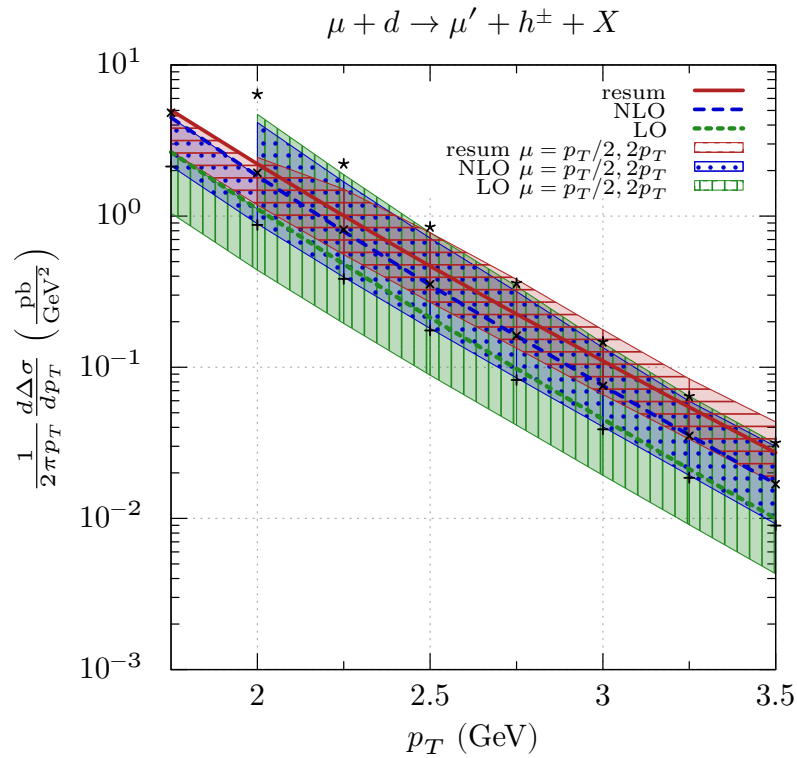
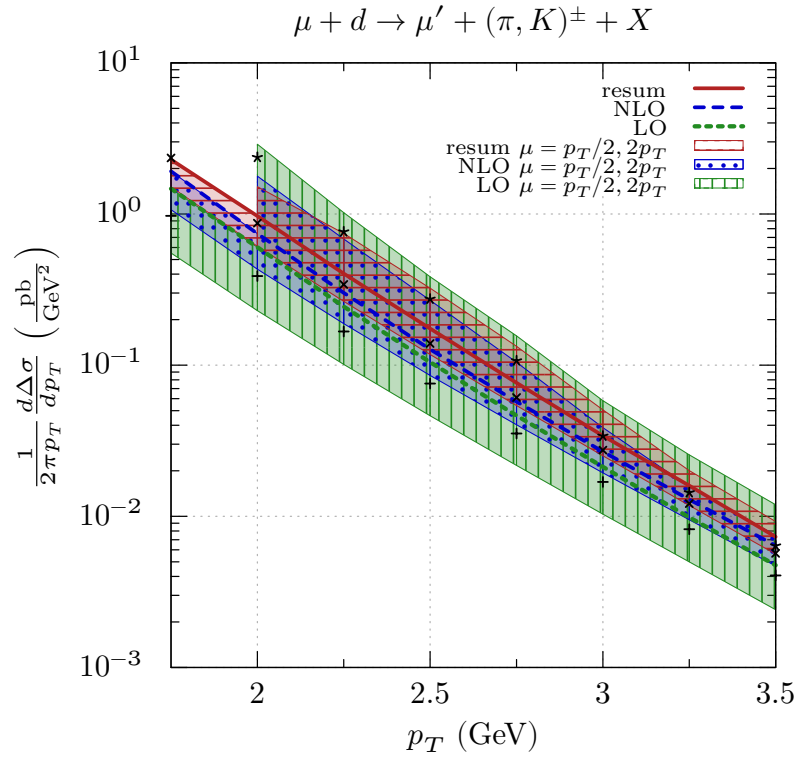


Fig. 7.10.: (a) Scale dependence of the spin-dependent “pion-plus-kaon” production cross section in μd scattering at LO, NLO, and for the resummed case, again matched, using the DSS14+DSS17 fragmentation functions. We vary the scales $\mu = \mu_r = \mu_{fi} = \mu_{ff}$ in the range $p_T/2 \leq \mu \leq 2p_T$. The upper borders of the bands correspond to $\mu = p_T/2$, the lower ones to $\mu = 2p_T$. We only present the results for scales $\mu \geq 1$ GeV. The rapidity lies between the range $-0.1 \leq \eta \leq 2.38$. (b) Due to comparison reasons, we show the plot for unidentified hadrons again using the DSS07 fragmentation functions.

the spin-averaged cross sections,

$$A_{LL} = \frac{d\Delta\sigma}{d\sigma}, \quad (7.1)$$

where these cross sections are defined through

$$d\sigma_{\ell N} \equiv \frac{1}{2} [d\sigma_{\ell N}^{++} + d\sigma_{\ell N}^{+-}], \quad (7.2)$$

$$d\Delta\sigma_{\ell N} \equiv \frac{1}{2} [d\sigma_{\ell N}^{++} - d\sigma_{\ell N}^{+-}], \quad (7.3)$$

with the superscripts $(++)$, $(+-)$ denoting the helicities of the incoming particles. In the following we are going to present results of A_{LL} for single-inclusive charged hadron production for both targets, a deuteron and a proton, compared to the COMPASS data [19]. But first, we intend to investigate the impact of the changes made for the most recent parton-to-pion fragmentation function DSS14. The stand-alone set was used by COMPASS [19] for the comparison of their experimental data with the theoretical NLO prediction. It was stated that asymmetries for hadron production are almost identical to those for pion production, therefore one is safe to use the parton-to-pion fragmentation functions when analyzing hadron production. As the influence of the chosen fragmentation function can be large, especially for protons, we want to proof this statement for COMPASS conditions at NLO and compare thus in Fig. 7.11 the proton asymmetries for DSS07 for positively or negatively charged pions and hadrons. Although the pion clearly dominates the whole DSS07 prediction for unidentified hadrons, we find out that, contrary to the assumptions, there is indeed a discrepancy between the asymmetries with DSS07 pion and hadron sets. In nearly each of the cases this deviation increases with growing p_T . This denotes that calculating hadron production asymmetries with pion fragmentation functions alone may distort the outcome. The next investigation examines to what extent the pion fragmentation set has changed when going from DSS07 to DSS14. Hence, we consider in Fig. 7.12 the NLO asymmetries for pion production, again for a proton target while there is the influence of the choice of fragmentation function at its largest. There is only a minor change between the pion sets for positively charged pions within a range of $\eta \in [0.45, 2.4]$, but when switching to $\eta \in [-0.1, 0.45]$ the difference grows. It increases when negatively charged pions within $\eta \in [0.9, 2.4]$ are considered. Then, when going into lower rapidity ranges, the deviation becomes huge. This indicates that the discrepancy between a possible future updated all-hadron fragmentation set and a from COMPASS used updated pion set DSS14 is smaller than the discrepancy between the older pion fragmentation to the newest one. Additionally our presented theoretical predictions should be much more valid because it also contains the most recent kaon fragmentation set.

Finally, we consider our final NLO and resummed results of A_{LL} for identified pions and kaons by using the updated fragmentation sets of DSS14 [80] and DSS17 [75] in Figure 7.13. We investigate the proton and the deuteron target for the three rapidity bins $[-0.1, 0.45]$,

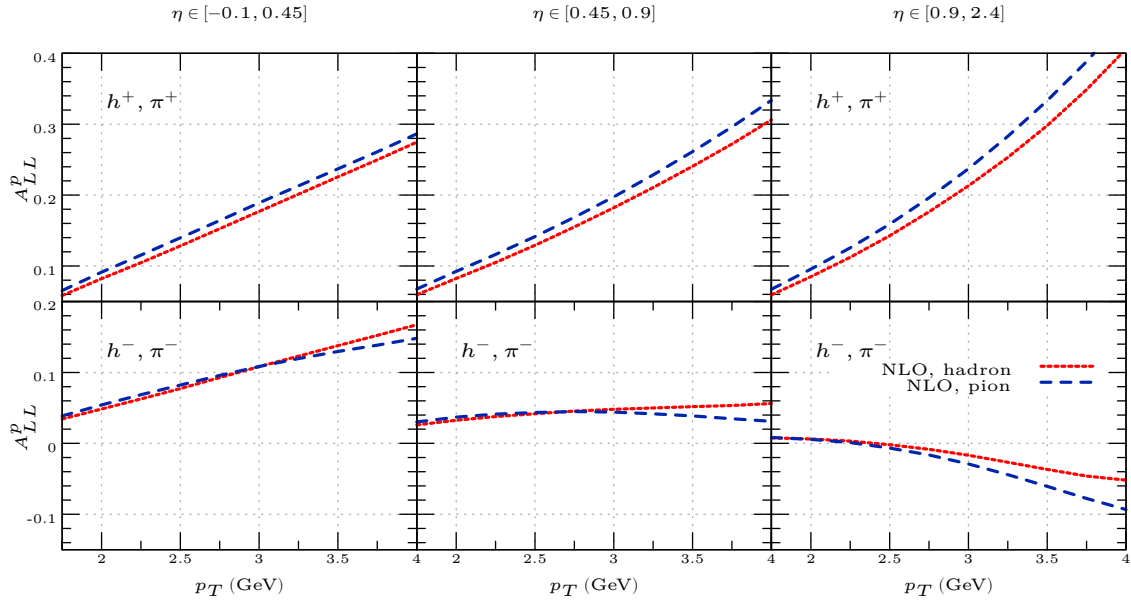


Fig. 7.11.: Comparison of the double-longitudinal spin asymmetries A_{LL}^p at NLO considering an unidentified hadron and an identified pion using the DSS07 fragmentation set for a proton target, splitting up the rapidity range in three bins $[-0.1, 0.45]$, $[0.45, 0.9]$ and $[0.9, 2.4]$. We show positively and negatively charged hadrons.

$[0.45, 0.9]$ and $[0.9, 2.4]$. The symbols in the figure show the results of the asymmetry when the (non-matched) resummed polarized and spin-averaged cross sections are expanded to first order. The resummed cross sections are matched as demonstrated before. While we have summed over the charges of the produced hadrons in Sec. 7.1.1 and Sec. 7.1.2, we intend to study positively and negatively charged hadrons separated from now on. Including logarithmic corrections to NLO, changes the predictions especially for positively charged hadrons. The impact grows accordingly to the increasing of the rapidity range. Comparing the first-order expansions of the non-matched resummed asymmetries to the NLO plots, we discover a very well agreement for positively charged hadrons and a not so well agreement for negatively charged ones, particularly for the proton. In any case, as anticipated, threshold corrections do not cancel out in the asymmetries and rather tend to decrease the asymmetry when going from NLO to the resummed case. This demonstrates clearly that threshold logarithms beyond NLO cannot be ignored and have to be resummed to all orders of perturbation theory. Furthermore, we observe an overall fair agreement between the theoretical resummed results and the COMPASS data within the rather large experimental uncertainties. However, we may find some discrepancy between experiment and theoretical results for the production of positively charged hadrons off a proton target at lower rapidities. Resummation tends to improve the description of the experimental results. As the different fragmentation functions describing the observed hadron influence the cross sections a lot, we are going to investigate now the sensitivity

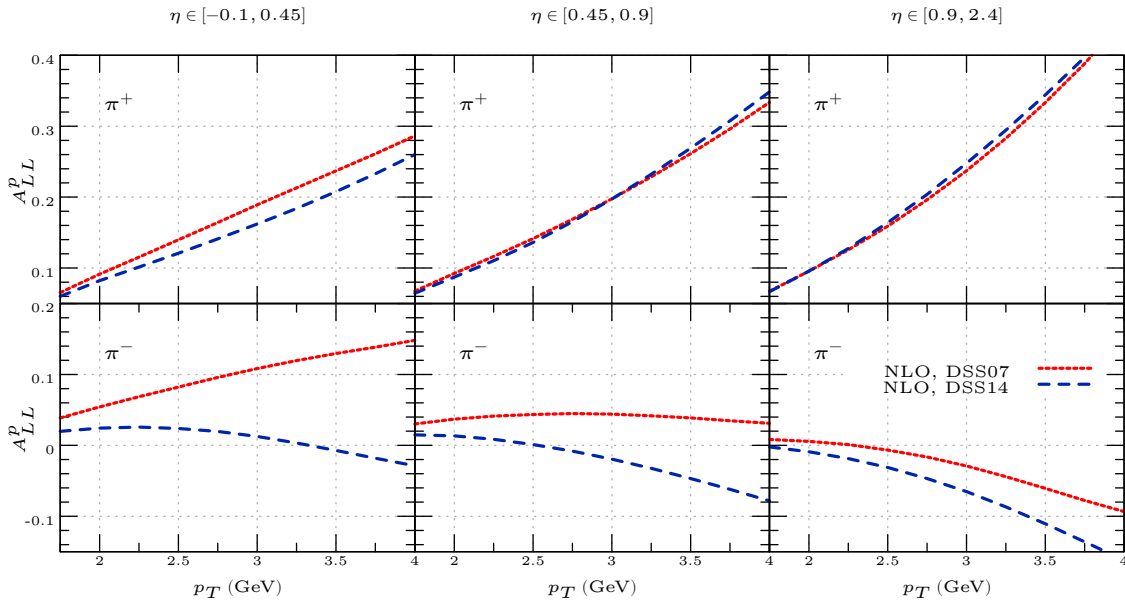


Fig. 7.12.: Comparison of the NLO asymmetries considering pion production with different fragmentation sets, DSS07 and DSS14, again distinguishing within the rapidity bins $[-0.1, 0.45]$, $[0.45, 0.9]$ and $[0.9, 2.4]$ and positive and negative charges.

to the choice of the fragmentation set of the asymmetries. In Figure 7.14, the results from Fig. 7.13 are compared with those obtained for the DSS07 set [76]. The more recent fragmentation functions lead to a significantly better agreement with the COMPASS data, particularly in the case of negatively charged hadrons produced off a proton target. This improvement arises from an interplay between several features. By and large, the cross sections for negatively charged hadrons $\mu p \rightarrow \mu' h^- X$ are expected to be more sensitive to fragmentation functions than the one for positively charged ones. With the help of more data taken from semi-inclusive deep inelastic scattering processes, these functions are now better determined. However, there is still some information missing, for example, an updated fragmentation set for produced protons. Additionally, on the subprocess level, there are several competing cross sections contributing with opposite sign. This leads to sizeable effects for even relatively small differences in the fragmentation functions. Likewise, the gluon fragmentation plays a role here as it is smaller in DSS14 than in DSS07. As a general conclusion, one can say that resummation is vital if high precision is needed. On the theory side, the very significant dependence of the asymmetries on the used fragmentation functions reiterates the need of pinning the latter down with better accuracy, in particularly with respect to future high luminosity experiments at JLab and BNL.

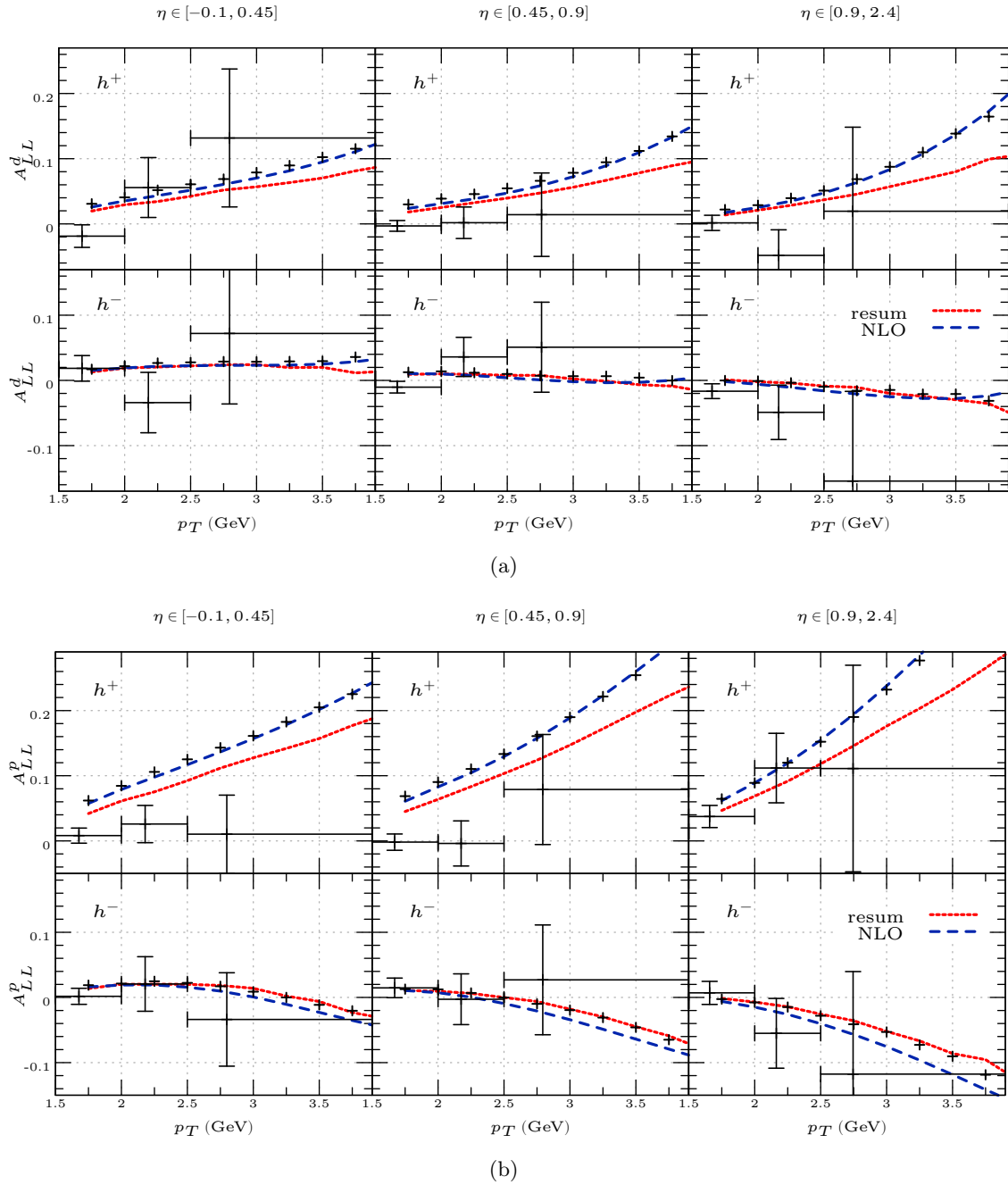


Fig. 7.13.: Double-longitudinal spin asymmetries A_{LL} for (a) $\mu d \rightarrow \mu' h X$ and (b) $\mu p \rightarrow \mu' h X$ in three rapidity bins, compared to the COMPASS data [19]. We show positive and negative charged hadrons and compare the NLO and resummed (matched) results using the combined “pion-plus-kaon” fragmentation functions of DSS14 and DSS17. The symbols denote the results for the asymmetry when the (non-matched) resummed cross sections are expanded to first order.

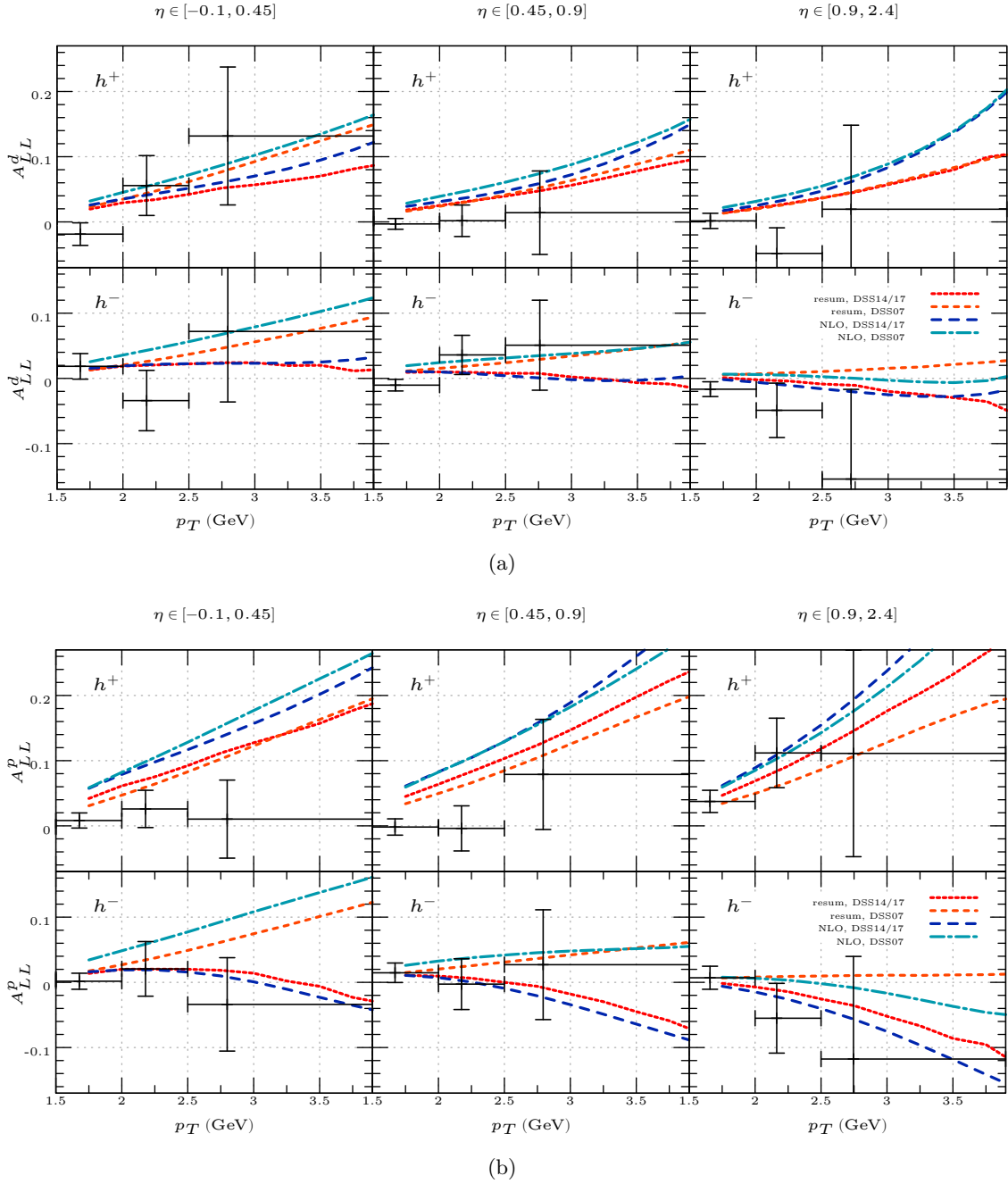


Fig. 7.14.: Same as in Fig. 7.13, but now also showing the results compared to the DSS07 set of charged-hadron fragmentation functions.

I've always been more interested in the future than in the past.

Grace Hopper

8

Conclusion and Outlook

This thesis was focused on threshold resummation studies for high- p_T inclusive-hadron production at COMPASS in longitudinally polarized lepton-nucleon scattering. The aim was to address threshold resummation effects to double-longitudinal spin asymmetries presented in Ref. [19] for which the investigation of spin-dependent cross sections for $\mu N \rightarrow \mu' h X$ at next-to-leading logarithmic accuracy was still missing. The process was studied before at next-to-leading order [25] and for the unpolarized case in the threshold-resummed NLL framework [22]. We have extended the previous studies with the polarized calculation and studied the impact of various fragmentation functions for unpolarized and polarized photoproduction cross sections.

The work was organized as follows. We started with a general introduction of the main ideas of perturbative Quantum Chromodynamics, as a starting point for following calculations. As the calculation of a hadronic cross sections is always a combination of short-distance and long-distance behaviour, we went on with the factorization framework and an examination of the parton distribution and the fragmentation functions. Factorization is a powerful tool with which we were able to separate perturbative from non-perturbative parts. This is necessary to calculate threshold resummation corrections to the perturbative hard-scattering function. We investigated the framework for resolved-photon contributions, where the photon interacts through its partonic structure. For that we discussed various models for the so far unmeasured photonic distribution functions, adopting in our phenomenological results the *maximal* saturated set of distributions. Then we elaborated the techniques of threshold resummation, summing over large logarithmic contributions, which yield huge corrections to the fixed-order calculation. These logarithms appear for the first time at next-to-leading order and can be observed at every higher order in perturbation theory. Their origin lies in an incomplete cancelation of infrared divergences between real and virtual diagrams and at kinematic threshold these logarithms spoil the

perturbative expansion. Therefore, threshold resummation is required at fixed-target energies like at COMPASS kinematics, where nearly all available center-of-mass energy is used for the production of the high- p_T parton fragmenting into the observed hadron and its recoiling counterpart. Using resummation techniques we were able to deal with those logarithmic corrections up to all perturbative orders in α_s at a certain level, choosing for our calculations next-to-leading logarithmic accuracy. To make the idea clear, we had showed explicitly how soft-gluon contributions exponentiate in Mellin momentum space, and afterwards we derived explicitly the radiative exponents for initial- and final-state partons at NLL accuracy. Then we had all relevant theoretical techniques at hand to address soft-gluon resummation to single-inclusive hadron production in spin-dependent lepton-nucleon scattering at COMPASS. This process was chosen due to the still open question, how the nucleon spin is composed of the gluon and quark spins and orbital angular momenta. Results for the double-longitudinal spin asymmetry A_{LL} are directly sensitive to the spin-dependent gluon distribution Δg , which in turn yields information of the proton spin contribution of the gluon. To receive theoretical predictions for the threshold resummed spin asymmetries, we extended the framework for the previous investigated unpolarized resummed cross sections [22] to the case of spin-dependence. While threshold resummation takes place in Mellin- N space, we only transformed the convolution of the partonic hard-scattering cross section with the fragmentation function into Mellin space, keeping the convolution with the parton distribution functions in physical space. This was established in the work of [22], yielding the rapidity-dependent resummed cross section. To make sure that we include the full fixed-order contributions as well as soft-gluon contributions beyond NLO at NLL accuracy, we implemented a matching procedure and calculated matching-coefficients. Further, as our phenomenological results were focused on leading- and next-to-leading logarithmic accuracy neglecting $1/N$ suppressed contributions, we provided additionally $\ln N/N$ subleading NLO contributions and a framework to derive possibly additional subleading threshold contributions. However, this can be useful for a future project.

In our phenomenological results for COMPASS we have presented a detailed study of the impact of next-to-leading logarithmic threshold resummation on the spin-dependent cross section and on the corresponding double-longitudinal spin asymmetry A_{LL} for the high- p_T photoproduction process $\mu N \rightarrow \mu' h X$. We have included resummation for the direct, as well as the resolved-photon contribution. In a comparison of the spin-averaged with the spin-dependent cross sections we found out that the latter receives smaller corrections from resummation than the spin-averaged one. This clearly indicates that threshold corrections do not cancel in the double-spin asymmetry, as anticipated, and rather tend to decrease the asymmetry yielding an overall better agreement between experiment and theory. This contradicts an often claimed assumption, which says that higher order perturbative corrections cancel in ratios of spin-dependent and spin-averaged cross sections, i.e. for spin asymmetries, and in fact, they do not. Therefore, if threshold resummation

is not performed, the systematic uncertainties remain large, which demonstrates clearly that an inclusion of threshold logarithms is vital for phenomenology at COMPASS kinematics. We expect this to remain true also for a future Electron Ion Collider (EIC) where lepton-nucleon scattering could be explored with unprecedented precision and kinematic reach [120]. These processes with polarized beams at an EIC would e.g. yield access to the so far totally unknown polarized photon distributions. Further, larger data samples will provide better statistics, especially in the gluon-dominated regime. At high energies in an upcoming EIC, threshold effects are assumed to be smaller, however, due to the high luminosity also small effects are important to be investigated.

Our present calculation marks the state of the art for theoretical studies of $\ell N \rightarrow \ell' h X$, however, at an EIC an even higher level of theoretical precision will be needed to match experimental accuracy. This may be achieved, for example, by an extension of our resummation studies to next-to-next-to-leading logarithmic accuracy or by an inclusion of subleading $1/N$ logarithms.

Further, we found out that the parton-to-hadron fragmentation functions have a strong impact on the size and shape of the predicted spin asymmetries. Although the most recent sets, which contain much more up-to-date experimental information than the previous ones, help to improve the theoretical description of the COMPASS data, they arguably remain a primary source of systematic theoretical uncertainties. With that, continued improvements of these distributions are necessary. Promising avenues in this direction are perhaps offered by studies of hadron fragmentation inside jets [121–125].

Finally all these efforts will surely shed light on the unsolved questions of the proton spin to reach a further key point in the knowledge about the proton.

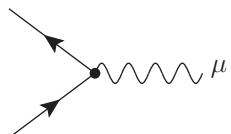
A

Feynman Rules

Feynman rules are diagrams visualizing mathematical expressions which describe the behaviour of bosons and fermions intuitively, and have been introduced in 1948 by Richard Feynman. As they are necessary to calculate matrix elements in perturbative QCD, we provide them in this Appendix, however, for more details we refer to standard text books like Ref. [40].

As usual, solid, curly and dashed lines represent quarks, gluons and ghosts. Momentum conservation is imposed at each vertex and we integrate over undetermined loop momenta. Fermion loops are supposed to receive an additional factor of (-1) . Further, we have implemented the notation $p_\mu \gamma^\mu = p^\mu \gamma_\mu \equiv \not{p}$.

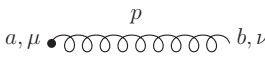
Feynman Rules for Quantum Electrodynamics:

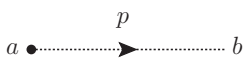
photon propagator	$\mu \overset{q}{\sim} \nu$	$= \frac{-i}{q^2 + i\epsilon} \left(g^{\mu\nu} - (1 - \xi) \frac{q^\mu q^\nu}{q^2} \right)$
fermion propagator	$a \overset{p}{\longrightarrow} b$	$= i \frac{\not{p} + m}{p^2 - m^2 + i\epsilon} \delta_{ab}$
photon vertex		$= -ie_q e \gamma^\mu$

Note that ξ labels the chosen gauge, hence for Feynman gauge we have $\xi = 1$ and for Landau gauge we have $\xi = 0$. $e_q e$ labels the charge of the considered fermion given in units of the electron charge e . The Feynman rules for the vertices describe the interaction between the fermions with photons (in QED), gluons and ghosts (in QCD).

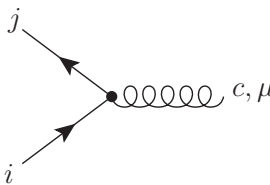
Feynman Rules for Quantum Chromodynamics:

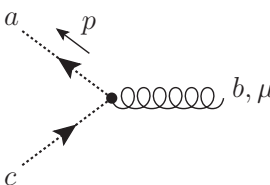
Propagators

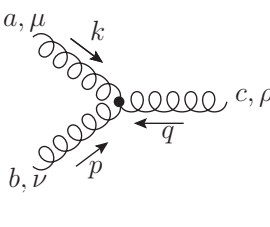
gluon propagator  $= \frac{-i}{p^2 + i\epsilon} \left(g^{\mu\nu} - (1 - \xi) \frac{p^\mu p^\nu}{p^2} \right) \delta_{ab}$

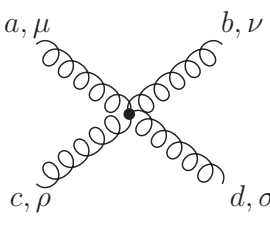
ghost propagator  $= \frac{i}{p^2 + i\epsilon} \delta_{ab}$

Vertices

quark-gluon vertex  $= i g \gamma^\mu t_{ij}^c$

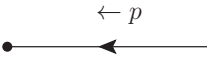
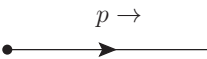
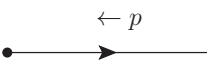
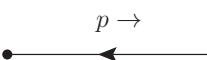


ghost-gluon vertex  $= -g f^{abc} p^\mu$

3-gluon vertex  $= g f^{abc} \left[g^{\mu\nu} (k - p)^\rho + g^{\nu\rho} (p - q)^\mu + g^{\rho\mu} (q - k)^\nu \right]$

4-gluon vertex  $= -i g^2 \left[f^{abe} f^{cde} (g^{\mu\rho} g^{\nu\sigma} - g^{\mu\sigma} g^{\nu\rho}) + f^{ace} f^{bde} (g^{\mu\nu} g^{\rho\sigma} - g^{\mu\sigma} g^{\nu\rho}) + f^{ade} f^{bce} (g^{\mu\nu} g^{\rho\sigma} - g^{\mu\rho} g^{\nu\sigma}) \right]$

We follow with the rules describing external particles, expressing them through spinors like $u^s(p)$ in dependence of the momentum p and the spin s :

Dirac Spinor Rules for External Lines:

incoming fermion		$= u^s(p)$
outgoing fermion		$= \bar{u}^s(p)$
incoming antifermion		$= \bar{v}^s(p)$
outgoing antifermion		$= v^s(p)$
incoming vector		$= \epsilon_\lambda^{\mu*}(k)$
outgoing vector		$= \epsilon_\lambda^\mu(k)$

Quarks are described by the fermion-rules, and photons and gluons by the vector-rules. Note that the spinors $u^s(p)$ and $v^s(p)$ obey the Dirac equation:

$$\begin{aligned} 0 &= (\not{p} - m)u^s(p) = \bar{u}^s(p)(\not{p} - m) \\ &= (\not{p} + m)v^s(p) = \bar{v}^s(p)(\not{p} + m), \end{aligned} \quad (\text{A.1})$$

and describe fermions and antifermions with mass m . The energy is positive and reads $p_0 \equiv E_p = \sqrt{\mathbf{p}^2 + m^2}$ and the normalization of the spinors and antispinors is such that

$$\bar{u}^r(p)u^s(p) = 2m\delta^{rs}, \quad (\text{A.2})$$

$$\bar{v}^r(p)v^s(p) = -2m\delta^{rs}. \quad (\text{A.3})$$

In the evaluation of Feynman diagrams, we often need to sum over spin polarizations, for example when calculating unpolarized cross sections. Then, the relevant completeness

relations are given by:

$$\sum_s u^s(p) \bar{u}^s(p) = \not{p} + m, \quad (\text{A.4})$$

$$\sum_s v^s(p) \bar{v}^s(p) = \not{p} - m. \quad (\text{A.5})$$

The projection operators are defined through

$$\left(\frac{1 + \gamma^5}{2} \right), \quad \left(\frac{1 - \gamma^5}{2} \right), \quad (\text{A.6})$$

and project onto right- and left-handed spinors. In the basis of

$$\gamma^\mu = \begin{pmatrix} 0 & \sigma^\mu \\ \bar{\sigma}^\mu & 0 \end{pmatrix}, \quad \gamma^5 = \begin{pmatrix} -1 & 0 \\ 0 & 1 \end{pmatrix}, \quad (\text{A.7})$$

with $\sigma^\mu = (1, \vec{\sigma})$ and ξ, η being two-component spinors, the normalized Dirac spinors can be written:

$$u^s(p) = \begin{pmatrix} \sqrt{p \cdot \sigma} \xi^s \\ \sqrt{p \cdot \bar{\sigma}} \xi^s \end{pmatrix}, \quad v^s(p) = \begin{pmatrix} \sqrt{p \cdot \sigma} \eta^s \\ -\sqrt{p \cdot \bar{\sigma}} \eta^s \end{pmatrix}. \quad (\text{A.8})$$

B

Hard, Soft and Γ -Matrices

In this Appendix all the matrices needed for the polarized calculation of the resummed cross section are collected from Refs. [27, 32, 33, 105, 113, 114]. In the following we are using the notation of [105],

$$T \equiv \ln \frac{-\hat{t}}{\hat{s}} + \pi i, \quad U \equiv \ln \frac{-\hat{u}}{\hat{s}} + \pi i. \quad (\text{B.1})$$

Further we have $C_A N_c = 3$ and $C_F = (N_c^2 - 1)/(2N_c) = 4/3$. When writing a process with q and q' , as in $q\bar{q} \rightarrow q'\bar{q}'$ we have a different flavor constellation of both quarks.

B.1. Soft Matrices

The soft matrices are lowest-order expanded, so that

$$S_{ab \rightarrow cd}(\hat{\eta}, \alpha_s) = S_{ab \rightarrow cd}^{(0)} + \mathcal{O}(\alpha_s). \quad (\text{B.2})$$

The first soft matrix reads,

$$S_{q\bar{q} \rightarrow q\bar{q}} = \begin{pmatrix} N_c^2 & 0 \\ 0 & \frac{N_c^2 - 1}{4} \end{pmatrix}. \quad (\text{B.3})$$

This soft matrix is valid for $q\bar{q} \rightarrow q\bar{q}$, $q\bar{q} \rightarrow q'\bar{q}'$ and $q\bar{q}' \rightarrow q\bar{q}'$. Valid for the subprocesses $qq \rightarrow qq$ and $qq' \rightarrow qq'$ is

$$S_{qq \rightarrow qq} = \begin{pmatrix} \frac{N_c^2 - 1}{4} & 0 \\ 0 & N_c^2 \end{pmatrix}, \quad (\text{B.4})$$

further we have for $q\bar{q} \rightarrow gg$ and $gg \rightarrow q\bar{q}$:

$$S_{q\bar{q} \rightarrow gg} = S_{gg \rightarrow q\bar{q}} = \begin{pmatrix} N_c(N_c^2 - 1) & 0 & 0 \\ 0 & \frac{(N_c^2 - 4)(N_c^2 - 1)}{2N_c} & 0 \\ 0 & 0 & \frac{N_c(N_c^2 - 1)}{2} \end{pmatrix}. \quad (\text{B.5})$$

For $qg \rightarrow qg$ we have the same,

$$S_{qg \rightarrow qg} = \begin{pmatrix} N_c(N_c^2 - 1) & 0 & 0 \\ 0 & \frac{(N_c^2 - 4)(N_c^2 - 1)}{2N_c} & 0 \\ 0 & 0 & \frac{N_c(N_c^2 - 1)}{2} \end{pmatrix}. \quad (\text{B.6})$$

and finally for $gg \rightarrow gg$:

$$S_{gg \rightarrow gg} = \begin{pmatrix} S_{gg \rightarrow gg}^{3 \times 3} & 0^{3 \times 5} \\ 0^{5 \times 3} & S_{gg \rightarrow gg}^{5 \times 5} \end{pmatrix}, \quad (\text{B.7})$$

consisting of

$$S_{gg \rightarrow gg}^{3 \times 3} = \begin{pmatrix} 5 & 0 & 0 \\ 0 & 5 & 0 \\ 0 & 0 & 5 \end{pmatrix}, \quad \text{and} \quad S_{gg \rightarrow gg}^{5 \times 5} = \begin{pmatrix} 1 & 0 & 0 & 0 & 0 \\ 0 & 8 & 0 & 0 & 0 \\ 0 & 0 & 8 & 0 & 0 \\ 0 & 0 & 0 & 20 & 0 \\ 0 & 0 & 0 & 0 & 27 \end{pmatrix}. \quad (\text{B.8})$$

B.2. Anomalous Dimension Matrices

The Γ -matrices are expanded regarding to the perturbative expansion of Eq. (5.36). The corresponding matrix for the subprocesses $q\bar{q} \rightarrow q\bar{q}$, $q\bar{q} \rightarrow q'\bar{q}'$ and $q\bar{q}' \rightarrow q\bar{q}'$ reads:

$$\Gamma_{q\bar{q} \rightarrow q\bar{q}} = \frac{\alpha_s}{\pi} \begin{pmatrix} 2C_F T & -\frac{C_F U}{N_c} \\ -2U & -\frac{T - 2U}{N_c} \end{pmatrix}. \quad (\text{B.9})$$

Next we have for $qq \rightarrow qq$ and $qq' \rightarrow qq'$

$$\Gamma_{qq \rightarrow qq} = \frac{\alpha_s}{\pi} \begin{pmatrix} -\frac{T+U}{N_c} + 2C_F U & 2U \\ \frac{C_F U}{N_c} & 2C_F T \end{pmatrix}, \quad (\text{B.10})$$

and for $q\bar{q} \rightarrow gg$ and $gg \rightarrow q\bar{q}$:

$$\Gamma_{q\bar{q} \rightarrow gg} = \Gamma_{gg \rightarrow q\bar{q}} = \frac{\alpha_s}{\pi} \begin{pmatrix} 0 & 0 & U - T \\ 0 & \frac{C_A}{2}(T + U) & \frac{C_A}{2}(U - T) \\ 2(U - T) & \frac{N_c^2 - 4}{2N_c}(U - T) & \frac{C_A}{2}(T + U) \end{pmatrix}. \quad (\text{B.11})$$

For $qg \rightarrow qg$ the anomalous dimension gets

$$\Gamma_{qg \rightarrow qg} = \frac{\alpha_s}{\pi} \begin{pmatrix} (C_F + C_A)T & 0 & U \\ 0 & C_F T + \frac{C_A U}{2} & \frac{C_A U}{2} \\ 2U & \frac{N_c^2 - 4}{2N_c} U & C_F T + \frac{C_A U}{2} \end{pmatrix}, \quad (\text{B.12})$$

and finally the matrix reads for the last subprocess, $gg \rightarrow gg$:

$$\Gamma_{gg \rightarrow gg} = \frac{\alpha_s}{\pi} \begin{pmatrix} \Gamma_{gg \rightarrow gg}^{3 \times 3} & 0^{3 \times 5} \\ 0^{5 \times 3} & \Gamma_{gg \rightarrow gg}^{5 \times 5} \end{pmatrix}, \quad (\text{B.13})$$

consisting of

$$\Gamma_{gg \rightarrow gg}^{3 \times 3} = \begin{pmatrix} 3T & 0 & 0 \\ 0 & 3U & 0 \\ 0 & 0 & 3(T+U) \end{pmatrix}, \quad (\text{B.14})$$

and

$$\Gamma_{gg \rightarrow gg}^{5 \times 5} = \begin{pmatrix} 6T & 0 & -6U & 0 & 0 \\ 0 & 3T + \frac{3U}{2} & -\frac{3U}{2} & -3U & 0 \\ -\frac{3U}{4} & -\frac{3U}{2} & 3T + \frac{3U}{2} & 0 & -\frac{9U}{4} \\ 0 & -\frac{6U}{5} & 0 & 3U & -\frac{9U}{5} \\ 0 & 0 & -\frac{2U}{3} & -\frac{4U}{3} & -2T + 4U \end{pmatrix}. \quad (\text{B.15})$$

B.3. Hard Matrices

Let us consider now the hard matrices for longitudinally polarized scattering. Remember that color-connected Born cross sections given for a color basis appear as a matrix, called ‘‘hard matrix. To receive them we combine the color structure of a diagram with the color-decomposition of the complex conjugated amplitude, average over the color of the incoming partons and include also the kinematics. The techniques to gain the color structure are described in Ref. [126]. Then we have for the lowest order expansion of Eq. (5.33) the following matrices:

$$\Delta H_{q\bar{q} \rightarrow q\bar{q}} = \alpha_s^2 \begin{pmatrix} h_{11} & h_{12} \\ h_{12} & h_{22} \end{pmatrix}, \quad \text{with} \quad \begin{aligned} h_{11} &= -\frac{2C_F^2}{N_c^4} \frac{\hat{t}^2 + \hat{u}^2}{\hat{s}^2}, \\ h_{12} &= -\frac{2C_F}{N_c^3} \left(-\frac{\hat{t}^2 + \hat{u}^2}{N_c \hat{s}^2} + \frac{\hat{u}^2}{\hat{s}\hat{t}} \right), \\ h_{22} &= \frac{1}{N_c^2} \left(-\frac{2}{N_c^2} \frac{\hat{t}^2 + \hat{u}^2}{\hat{s}^2} + 2 \frac{\hat{s}^2 - \hat{u}^2}{\hat{t}^2} + \frac{4}{N_c} \frac{\hat{u}^2}{\hat{s}\hat{t}} \right), \end{aligned} \quad (\text{B.16})$$

$$\Delta H_{q\bar{q} \rightarrow q'\bar{q}'} = -\alpha_s^2 h \begin{pmatrix} \frac{C_F^2}{N_c^2} & -\frac{C_F}{N_c^2} \\ -\frac{C_F}{N_c^2} & \frac{1}{N_c^2} \end{pmatrix}, \quad \text{with} \quad h = \frac{2}{N_c^2} \frac{\hat{t}^2 + \hat{u}^2}{\hat{s}^2}. \quad (\text{B.17})$$

Furthermore we have for $q\bar{q}' \rightarrow q\bar{q}'$ the hard matrix,

$$\Delta H_{q\bar{q}' \rightarrow q\bar{q}'} = \alpha_s^2 \begin{pmatrix} 0 & 0 \\ 0 & 2 \frac{\hat{s}^2 - \hat{u}^2}{N_c^2 \hat{t}^2} \end{pmatrix}. \quad (\text{B.18})$$

Going on with those matrices contributing to $qq \rightarrow qq$, we have

$$\Delta H_{qq \rightarrow qq} = \alpha_s^2 \begin{pmatrix} h_{11} & h_{12} \\ h_{12} & h_{22} \end{pmatrix}, \quad \text{with} \quad \begin{aligned} h_{11} &= \frac{2}{N_c^2} \left(\frac{\hat{s}^2 - \hat{u}^2}{\hat{t}^2} + \frac{1}{N_c^2} \frac{\hat{s}^2 - \hat{t}^2}{\hat{u}^2} - \frac{2}{N_c} \frac{\hat{s}^2}{\hat{t}\hat{u}} \right), \\ h_{12} &= \frac{2C_F}{N_c^4} \left(N_c \frac{\hat{s}^2}{\hat{t}\hat{u}} - \frac{\hat{s}^2 - \hat{t}^2}{\hat{u}^2} \right), \\ h_{22} &= \frac{2C_F^2}{N_c^4} \frac{\hat{s}^2 - \hat{t}^2}{\hat{u}^2}, \end{aligned} \quad (\text{B.19})$$

and

$$\Delta H_{qq' \rightarrow qq'} = \alpha_s^2 \begin{pmatrix} 2 \frac{\hat{s}^2 - \hat{u}^2}{N_c^2 \hat{t}^2} & 0 \\ 0 & 0 \end{pmatrix}. \quad (\text{B.20})$$

Let us now come to those subprocesses where also gluons are involved. We have for $q\bar{q} \rightarrow gg$ and $gg \rightarrow q\bar{q}$:

$$\Delta H_{q\bar{q} \rightarrow gg} = -\alpha_s^2 \begin{pmatrix} h_{11} & h_{12} & h_{13} \\ h_{12} & h_{22} & h_{23} \\ h_{13} & h_{23} & h_{33} \end{pmatrix}, \quad \text{and} \quad \Delta H_{gg \rightarrow q\bar{q}} = -\frac{N_c^2}{N_c^2 - 1} \alpha_s^2 \begin{pmatrix} h_{11} & h_{12} & h_{13} \\ h_{12} & h_{22} & h_{23} \\ h_{13} & h_{23} & h_{33} \end{pmatrix} \quad (\text{B.21})$$

with

$$\begin{aligned} h_{11} &= \frac{1}{2N_c^4} \left(\frac{\hat{u}}{\hat{t}} + \frac{\hat{t}}{\hat{u}} \right), \\ h_{12} &= N_c h_{11}, \\ h_{22} &= N_c^2 h_{11}, \\ h_{13} &= -\frac{1}{2N_c^3} \frac{\hat{u}^2 - \hat{t}^2}{\hat{t}\hat{u}} - \frac{1}{N_c^3} \frac{\hat{u} - \hat{t}}{\hat{s}}, \\ h_{23} &= N_c h_{13}, \\ h_{33} &= \frac{1}{2N_c^2} \frac{\hat{s}^2}{\hat{t}\hat{u}} + \frac{4}{N_c^2} \frac{\hat{t}\hat{u}}{\hat{s}^2} - \frac{3}{N_c^2}. \end{aligned} \quad (\text{B.22})$$

Further we have quark-gluon scattering with

$$\Delta H_{qg \rightarrow qg} = \frac{\hat{s}^2 - \hat{u}^2}{\hat{s}^2 + \hat{u}^2} \alpha_s^2 \begin{pmatrix} h_{11} & h_{12} & h_{13} \\ h_{12} & h_{22} & h_{23} \\ h_{13} & h_{23} & h_{33} \end{pmatrix}, \quad \text{with} \quad \begin{aligned} h_{11} &= -\frac{1}{2N_c^3(N_c^2 - 1)} \left(\frac{\hat{t}^2}{\hat{s}\hat{u}} - 2 \right), \\ h_{12} &= N_c h_{11}, \\ h_{22} &= N_c^2 h_{11}, \\ h_{13} &= \frac{1}{N_c^2(N_c^2 - 1)} \left(-1 - \frac{2\hat{s}}{\hat{t}} + \frac{\hat{u}}{2\hat{s}} - \frac{\hat{s}}{2\hat{u}} \right), \\ h_{23} &= N_c h_{13}, \\ h_{33} &= \frac{1}{N_c(N_c^2 - 1)} \left(3 - \frac{4\hat{s}\hat{u}}{\hat{t}^2} - \frac{\hat{t}^2}{2\hat{s}\hat{u}} \right). \end{aligned} \quad (\text{B.23})$$

Finally we end up with the last process, gluon-gluon scattering $gg \rightarrow gg$, and as this matrix is rather lengthy, we directly set $N_c = 3$, so that we get

$$\Delta H_{gg \rightarrow gg} = \frac{\hat{s}^4 - \hat{t}^4 - \hat{u}^4}{\hat{s}^4 + \hat{t}^4 + \hat{u}^4} \alpha_s^2 \begin{pmatrix} 0_{3 \times 3} & 0_{3 \times 5} \\ 0_{5 \times 3} & h_{5 \times 5} \end{pmatrix}, \quad (\text{B.24})$$

with the 5×5 matrix

$$h_{5 \times 5} = \frac{1}{16} \begin{pmatrix} 9h_1 & \frac{9}{2}h_1 & \frac{9}{2}h_2 & 0 & -3h_1 \\ \frac{9}{2}h_1 & \frac{9}{4}h_1 & \frac{9}{4}h_2 & 0 & -\frac{3}{2}h_1 \\ \frac{9}{2}h_2 & \frac{9}{4}h_2 & h_3 & 0 & -\frac{3}{2}h_2 \\ 0 & 0 & 0 & 0 & 0 \\ -3h_1 & -\frac{3}{2}h_1 & -\frac{3}{2}h_2 & 0 & h_1 \end{pmatrix}, \quad (\text{B.25})$$

where we have:

$$\begin{aligned} h_1 &= 1 - \frac{\hat{t}\hat{u}}{\hat{s}^2} - \frac{\hat{s}\hat{t}}{\hat{u}^2} + \frac{\hat{t}^2}{\hat{s}\hat{u}}, \\ h_2 &= \frac{\hat{s}\hat{t}}{\hat{u}^2} - \frac{\hat{t}\hat{u}}{\hat{s}^2} + \frac{\hat{u}^2}{\hat{s}\hat{t}} - \frac{\hat{s}^2}{\hat{t}\hat{u}}, \\ h_3 &= \frac{27}{4} - 9 \left(\frac{\hat{s}\hat{u}}{\hat{t}^2} + \frac{1}{4} \frac{\hat{t}\hat{u}}{\hat{s}^2} + \frac{1}{4} \frac{\hat{s}\hat{t}}{\hat{u}^2} \right) + \frac{9}{2} \left(\frac{\hat{u}^2}{\hat{s}\hat{t}} + \frac{\hat{s}^2}{\hat{t}\hat{u}} - \frac{1}{2} \frac{\hat{t}^2}{\hat{s}\hat{u}} \right). \end{aligned} \quad (\text{B.26})$$

C

Coefficients

In this part we want to present only polarized coefficients for direct-photon subprocesses. We calculated and presented them already in Ref. [38]. To give our results for the coefficients $\Delta C_{\gamma b \rightarrow cX}$ in a compact form, we define

$$\begin{aligned}
\rho_{q\gamma}^{(A)} &= 4\gamma_E + 4 \ln 2, \\
\rho_{q\gamma}^{(F)} &= -3 + 4\gamma_E + 4 \ln(2(1-v)), \\
\rho_{g\gamma}^{(A)} &= 4\gamma_E + 4 \ln(2(1-v)), \\
\rho_{g\gamma}^{(F)} &= -3 + 4\gamma_E + 4 \ln 2,
\end{aligned} \tag{C.1}$$

with γ_E as the Euler constant. For the Compton process $\gamma q \rightarrow qq$ we then have

$$\begin{aligned}
\Delta C_{\gamma q \rightarrow qq} &= b_0 \pi \ln \frac{\mu_r^2}{\hat{s}} + \frac{C_F}{4} \ln \frac{\mu_{ff}^2}{\hat{s}} \left(\rho_{q\gamma}^{(A)} - 3 \right) + \frac{C_F}{4} \ln \frac{\mu_{fi}^2}{\hat{s}} \rho_{q\gamma}^{(F)} + \frac{1}{18} (2C_A - 5N_f) + \frac{7}{4C_A} \\
&+ \frac{1}{4} b_0 \pi \rho_{q\gamma}^{(A)} + \frac{C_A^2 - 2}{32C_A} \left(\rho_{q\gamma}^{(A)} \right)^2 + \frac{\ln v}{4C_A} \left(\rho_{q\gamma}^{(A)} - \ln v \right) + \frac{\pi^2}{4C_A} \frac{2v - 1}{v(v-2)} + \frac{\pi^2 C_F}{3} \\
&+ \frac{\ln(1-v)}{2C_A v(v-2)} \left\{ \ln \left(\frac{\sqrt{1-v}}{v} \right) (4v - v^2 - 1) \right. \\
&\quad \left. + \frac{1}{2} \left[1 - 3C_A^2 + 2v + \rho_{q\gamma}^{(A)} (2v - v^2) \right] \right\},
\end{aligned} \tag{C.2}$$

where $C_F = 4/3$, $C_A = 3$. For the process $\gamma q \rightarrow gq$ with an observed gluon, the coefficient reads

$$\begin{aligned}
\Delta C_{\gamma q \rightarrow gq} &= b_0 \pi \ln \frac{\mu_r^2}{\hat{s}} + \ln \frac{\mu_{ff}^2}{\hat{s}} \left(\frac{C_A}{4} \rho_{q\gamma}^{(A)} - b_0 \pi \right) + \frac{C_F}{4} \rho_{q\gamma}^{(F)} \ln \frac{\mu_{fi}^2}{\hat{s}} + \left(\frac{C_F}{2} + C_A \right) \left(\frac{\rho_{q\gamma}^{(A)}}{4} \right)^2 \\
&+ \frac{\pi^2 (v^2 - 6v + 2)}{12C_A (v^2 - 1)} + \frac{1}{12} \left\{ \frac{3C_F}{4} (3\rho_{q\gamma}^{(A)} - 28) + \pi^2 (4C_A + C_F) \right\} \\
&+ \frac{\ln v}{4} \left\{ C_F (2 \ln v + 3) - C_A (2 \ln(1-v) + \rho_{q\gamma}^{(A)}) - \frac{1}{C_A (v^2 - 1)} \left[-v(v-2) \ln v \right. \right. \\
&\quad \left. \left. + 3C_A C_F (v^2 + 1) + 2 \ln(1-v)(1-2v) + 2v \right] \right\} \\
&+ \frac{C_A}{4} \ln(1-v) \left[\rho_{q\gamma}^{(A)} + \ln(1-v) \right].
\end{aligned} \tag{C.3}$$

Finally, for photon-gluon fusion $\gamma g \rightarrow q\bar{q}$, we find

$$\begin{aligned}
\Delta C_{\gamma g \rightarrow q\bar{q}} = & b_0 \pi \ln \frac{\mu_r^2}{\mu_{fi}^2} + \ln \frac{\mu_{fi}^2}{\hat{s}} \frac{C_A}{4} \rho_{g\gamma}^{(A)} + \frac{C_F}{4} \ln \frac{\mu_{ff}^2}{\hat{s}} \rho_{g\gamma}^{(F)} + \frac{C_A}{6} \left[\frac{3}{8} \left(\rho_{g\gamma}^{(F)} + 3 \right)^2 + \pi^2 \right] \\
& + \frac{C_F}{6} \left[\frac{9}{8} \left(\rho_{g\gamma}^{(F)} - \frac{19}{3} \right) + \frac{5}{2} \pi^2 \right] - \frac{\ln^2 v}{4C_A} \left\{ \frac{1+v^2}{v^2+(1-v)^2} - C_A^2 \right\} \\
& + \frac{\ln v}{8C_A} \left\{ \frac{3C_A^2(1-2v) + 2v(1+2v) - 3}{v^2+(1-v)^2} - 2C_A^2 \rho_{g\gamma}^{(A)} + 6C_A C_F \right\} \\
& + \ln(1-v) \left\{ \frac{3C_A^2 v^2 - v(v+2)}{v^2+(1-v)^2} + C_A^2 \left(\rho_{g\gamma}^{(F)} + 3 \right) \right\} \\
& - \frac{\ln^2(1-v)}{4C_A} \left\{ \frac{1+(1-v)^2}{v^2+(1-v)^2} - C_A^2 \right\}. \tag{C.4}
\end{aligned}$$

We note that $\Delta C_{\gamma g \rightarrow q\bar{q}}$ is identical to the corresponding coefficient $C_{\gamma g \rightarrow q\bar{q}}$ in the unpolarized subprocess, which was already given in [22].

The polarized coefficients for resolved-photons are rather lengthy and one can obtain them on request, as we have noted in our Ref. [39].

Bibliography

- [1] “Physics at the British Association,” *Nature* **106**, 357 (1920), ISSN 1476-4687.
- [2] W. Gerlach and O. Stern, “Der experimentelle Nachweis der Richtungsquantelung im Magnetfeld,” *Zeitschrift für Physik* **9**, 349 (1922).
- [3] W. Gerlach and O. Stern, “Das magnetische Moment des Silberatoms,” *Zeitschrift für Physik* **9**, 353 (1922).
- [4] D. Dennison, “A Note on the Specific Heat of the Hydrogen Molecule,” *Proceedings of the R. Soc. Lond.* **A115**, 483 (1927).
- [5] R. W. McAllister and R. Hofstadter, “Elastic Scattering of 188 MeV Electrons from Proton and the Alpha Particle,” *Phys. Rev.* **V102**, 851 (1956).
- [6] Y. Ne’emann, “Derivation of strong interactions from gauge invariance,” *Nucl. Phys.* **26**, 222 (1961).
- [7] M. Gell-Mann, “A Schematic Model of Baryons and Mesons,” *Phys. Lett.* **8**, 214 (1964).
- [8] G. Zweig, “An SU(3) Model for Strong Interaction Symmetry and its Breaking,” CERN Report No.8182/TH.401 (1964).
- [9] J. Ashman et al. (European Muon), “A Measurement of the Spin Asymmetry and Determination of the Structure Function $g(1)$ in Deep Inelastic Muon-Proton Scattering,” *Phys. Lett.* **B206**, 364 (1988).
- [10] P. Hagler, “Hadron structure from lattice quantum chromodynamics,” *Phys. Rept.* **490**, 49 (2010), 0912.5483.
- [11] E. Aschenauer et al., “The RHIC SPIN Program: Achievements and Future Opportunities,” (2015), 1501.01220.
- [12] T. Lin (STAR), in *22nd International Symposium on Spin Physics (SPIN 2016) Urbana, IL, USA, September 25-30, 2016* (2017), 1705.02655.
- [13] R. L. Jaffe and A. Manohar, “The G(1) Problem: Fact and Fantasy on the Spin of the Proton,” *Nucl. Phys.* **B337**, 509 (1990).
- [14] X.-D. Ji, “Gauge-Invariant Decomposition of Nucleon Spin,” *Phys. Rev. Lett.* **78**, 610 (1997), hep-ph/9603249.
- [15] M. Wakamatsu, “On Gauge-Invariant Decomposition of Nucleon Spin,” *Phys. Rev.* **D81**, 114010 (2010), 1004.0268.

-
- [16] S. Panebianco (COMPASS Collaboration), “The COMPASS spin physics program,” p. 247 (2005), [hep-ex/0505005](#).
- [17] A. Magnon (COMPASS Collaboration), “The Compass experiment at CERN,” AIP Conf.Proc. **747**, 72 (2005).
- [18] C. Adolph et al. (COMPASS), “Measurement of the cross section for high- p_T hadron production in the scattering of 160-GeV/c muons off nucleons,” Phys. Rev. **D88**, 091101 (2013), [1207.2022](#).
- [19] C. Adolph et al. (COMPASS), “Longitudinal double spin asymmetries in single hadron quasi-real photoproduction at high p_T ,” Phys. Lett. **B753**, 573 (2016), [1509.03526](#).
- [20] M. Levillain, “ $A_{LL}(p_T)$ for single hadron photoproduction at high p_T ,” Proceedings, 12th Conference on the Intersections of Particle and Nuclear Physics (CIPANP 2015), Vail, Colorado, USA, May 19-24, 2015 (2015), [1509.01419](#).
- [21] M. Klasen, “Theory of hard photoproduction,” Rev. Mod. Phys. **74**, 1221 (2002), [hep-ph/0206169](#).
- [22] D. de Florian, M. Pfeuffer, A. Schäfer, and W. Vogelsang, “Soft-gluon Resummation for High- p_T Inclusive-Hadron Production at COMPASS,” Phys.Rev. **D88**, 014024 (2013), [1305.6468](#).
- [23] D. de Florian and W. Vogelsang, “Next-to-leading order QCD corrections to inclusive hadron photoproduction in polarized lepton-proton collisions,” Phys.Rev. **D57**, 4376 (1998), [hep-ph/9712273](#).
- [24] B. Jäger, M. Stratmann, and W. Vogelsang, “Longitudinally polarized photoproduction of inclusive hadrons beyond the leading order,” Phys.Rev. **D68**, 114018 (2003), [hep-ph/0309051](#).
- [25] B. Jäger, M. Stratmann, and W. Vogelsang, “Longitudinally polarized photoproduction of inclusive hadrons at fixed-target experiments,” Eur.Phys.J. **C44**, 533 (2005), [hep-ph/0505157](#).
- [26] G. F. Sterman and W. Vogelsang, “Threshold resummation and rapidity dependence,” JHEP **0102**, 016 (2001), [hep-ph/0011289](#).
- [27] D. de Florian, W. Vogelsang, and F. Wagner, “Single-Inclusive Hadron Production in Polarized pp Scattering at Next-to-Leading Logarithmic Accuracy,” Phys.Rev. **D76**, 094021 (2007), [0708.3060](#).
- [28] D. de Florian and W. Vogelsang, “Threshold resummation for the inclusive-hadron cross-section in pp collisions,” Phys.Rev. **D71**, 114004 (2005), [hep-ph/0501258](#).

- [29] G. F. Sterman, “Summation of Large Corrections to Short Distance Hadronic Cross-Sections,” Nucl.Phys. **B281**, 310 (1987).
- [30] S. Catani and L. Trentadue, “Resummation of the QCD Perturbative Series for Hard Processes,” Nucl. Phys. **B327**, 323 (1989).
- [31] E. Laenen, G. Oderda, and G. F. Sterman, “Resummation of threshold corrections for single particle inclusive cross-sections,” Phys. Lett. **B438**, 173 (1998), hep-ph/9806467.
- [32] N. Kidonakis, G. Oderda, and G. Sterman, “Threshold resummation for dijet cross-sections,” Nucl.Phys. **B525**, 299 (1998), hep-ph/9801268.
- [33] N. Kidonakis, G. Oderda, and G. F. Sterman, “Evolution of color exchange in QCD hard scattering,” Nucl.Phys. **B531**, 365 (1998), hep-ph/9803241.
- [34] R. Bonciani, S. Catani, M. L. Mangano, and P. Nason, “Sudakov resummation of multiparton QCD cross-sections,” Phys. Lett. **B575**, 268 (2003), hep-ph/0307035.
- [35] S. Catani, M. Grazzini, and A. Torre, “Soft-gluon resummation for single-particle inclusive hadroproduction at high transverse momentum,” Nucl. Phys. **B874**, 720 (2013), 1305.3870.
- [36] T. Becher and M. D. Schwartz, “Direct photon production with effective field theory,” JHEP **02**, 040 (2010), 0911.0681.
- [37] L. Almeida, G. F. Sterman, and W. Vogelsang, “Threshold Resummation for Di-hadron Production in Hadronic Collisions,” Phys.Rev. **D80**, 074016 (2009), 0907.1234.
- [38] C. Uebler, A. Schäfer, and W. Vogelsang, “Threshold resummation for polarized high- p_T hadron production at COMPASS,” Phys. Rev. **D92**, 094029 (2015), 1510.01058.
- [39] C. Uebler, A. Schäfer, and W. Vogelsang, “Direct- and Resolved-Photon Threshold Resummation for Polarized High- p_T Hadron Production at COMPASS,” Phys. Rev. **D96**, 074026 (2017), 1708.08284.
- [40] M. E. Peskin and D. V. Schroeder, *An Introduction to Quantum Field Theory* (Westview Press, 1995).
- [41] C. Itzykson and J. B. Zuber, *International Series In Pure and Applied Physics* (McGraw-Hill, 1980).
- [42] S. Weinberg, *The Quantum theory of fields. Vol. 1: Foundations* (Cambridge University Press, 2005).

- [43] J. E. Bjorken and S. D. Drell, *Relativistic quantum fields* (McGraw-Hill, 1965).
- [44] M. Tanabashi et al. (Particle Data Group), “Review of Particle Physics,” *Phys. Rev.* **D98**, 030001 (2018).
- [45] S. Bethke, “Determination of the qcd Coupling $\alpha(s)$,” *J. Phys.G26* **R27** (2000), 0004021v1.
- [46] A. Deur, S. J. Brodsky, and G. F. de Teramond, “The QCD Running Coupling,” *Prog. Part. Nucl. Phys.* **90**, 1 (2016), 1604.08082.
- [47] W. Siegel, “Fields,” (1999), [hep-th/9912205](#).
- [48] C. G. Bollini and J. J. Giambiagi, “Dimensional Renormalization: The Number of Dimensions as a Regularizing Parameter,” *II Nuovo Cimento* **12**, 20 (1972).
- [49] G. t’ Hooft and M. Veltman, “Regularization and renormalization of gauge fields,” *Nucl. Phys.* **B44**, 189 (1972).
- [50] W. A. Bardeen, A. J. Buras, D. W. Duke, and T. Muta, “Deep Inelastic Scattering Beyond the Leading Order in Asymptotically Free Gauge Theories,” *Phys. Rev.* **D18**, 3998 (1978).
- [51] R. K. Ellis, H. Georgi, M. Machacek, H. D. Politzer, and G. G. Ross, “Perturbation Theory and the Parton Model in QCD,” *Nucl. Phys.* **B152**, 285 (1979).
- [52] D. Amati, R. Petronzio, and G. Veneziano, “Relating Hard QCD Processes Through Universality of Mass Singularities. 2.,” *Nucl. Phys.* **B146**, 29 (1978).
- [53] J. C. Collins, D. E. Soper, and G. F. Sterman, “Factorization for Short Distance Hadron - Hadron Scattering,” *Nucl. Phys.* **B261**, 104 (1985).
- [54] J. C. Collins, D. E. Soper, and G. F. Sterman, “Factorization of Hard Processes in QCD,” *Adv. Ser. Direct. High Energy Phys.* **5**, 1 (1989), [hep-ph/0409313](#).
- [55] J. C. Collins, “Hard scattering in QCD with polarized beams,” *Nucl. Phys.* **B394**, 169 (1993), [hep-ph/9207265](#).
- [56] D. de Florian, R. Sassot, M. Stratmann, and W. Vogelsang, “Global Analysis of Helicity Parton Densities and Their Uncertainties,” *Phys. Rev. Lett.* **101**, 072001 (2008), 0804.0422.
- [57] Y. L. Dokshitzer, “Calculation of the Structure Functions for Deep Inelastic Scattering and $e^+ e^-$ Annihilation by Perturbation Theory in Quantum Chromodynamics.,” *Sov. Phys. JETP* **46**, 641 (1977).
- [58] V. N. Gribov and L. N. Lipatov, “Deep inelastic $e p$ scattering in perturbation theory,” *Sov. J. Nucl. Phys.* **15**, 438 (1972).

- [59] G. Altarelli and G. Parisi, “Asymptotic Freedom in Parton Language,” Nucl. Phys. **B126**, 298 (1977).
- [60] G. Altarelli, S. Forte, and G. Ridolfi, “On positivity of parton distributions,” Nucl. Phys. **B534**, 277 (1998), [hep-ph/9806345](#).
- [61] E. Leader and C. Lorcé, “The angular momentum controversy: What’s it all about and does it matter?,” Phys. Rept. **541**, 163 (2014), [1309.4235](#).
- [62] D. de Florian, R. Sassot, M. Stratmann, and W. Vogelsang, “Evidence for polarization of gluons in the proton,” Phys. Rev. Lett. **113**, 012001 (2014), [1404.4293](#).
- [63] K. V. Dharmawardane et al. (CLAS), “Measurement of the x - and Q^{*2} -dependence of the asymmetry $A(1)$ on the nucleon,” Phys. Lett. **B641**, 11 (2006), [nucl-ex/0605028](#).
- [64] A. Airapetian et al. (HERMES), “Precise determination of the spin structure function $g(1)$ of the proton, deuteron and neutron,” Phys. Rev. **D75**, 012007 (2007), [hep-ex/0609039](#).
- [65] R. Gray et al. (CLEO), “A Study of Exclusive Charmless Semileptonic B Decays and Extraction of $|V_{ub}|$ at CLEO,” Phys. Rev. **D76**, 012007 (2007).
- [66] V. Yu. Alexakhin et al. (COMPASS), “The Deuteron Spin-dependent Structure Function $g_1(d)$ and its First Moment,” Phys. Lett. **B647**, 8 (2007), [hep-ex/0609038](#).
- [67] M. Alekseev et al. (COMPASS), “The Polarised Valence Quark Distribution from semi-inclusive DIS,” Phys. Lett. **B660**, 458 (2008), [0707.4077](#).
- [68] A. Adare et al. (PHENIX), “Inclusive cross-section and double helicity asymmetry for π^0 production in $p + p$ collisions at $s^{*2} = 200\text{-GeV}$: Implications for the polarized gluon distribution in the proton,” Phys. Rev. **D76**, 051106 (2007), [0704.3599](#).
- [69] B. I. Abelev et al. (STAR), “Longitudinal double-spin asymmetry for inclusive jet production in $p+p$ collisions at $s^{*2} = 200\text{-GeV}$,” Phys. Rev. Lett. **100**, 232003 (2008), [0710.2048](#).
- [70] P. Djawotho (STAR), “Gluon polarization and jet production at STAR,” Nuovo Cim. **C036**, 35 (2013), [1303.0543](#).
- [71] A. Adare et al. (PHENIX), “Inclusive double-helicity asymmetries in neutral-pion and eta-meson production in $\vec{p} + \vec{p}$ collisions at $\sqrt{s} = 200\text{ GeV}$,” Phys. Rev. **D90**, 012007 (2014), [1402.6296](#).

- [72] J. C. Collins and D. E. Soper, “Back-To-Back Jets in QCD,” Nucl. Phys. **B193**, 381 (1981).
- [73] J. C. Collins and D. E. Soper, “Parton Distribution and Decay Functions,” Nucl. Phys. **B194**, 445 (1982).
- [74] A. Metz and A. Vossen, “Parton Fragmentation Functions,” Prog. Part. Nucl. Phys. **91**, 136 (2016), 1607.02521.
- [75] D. de Florian, M. Epele, R. J. Hernandez-Pinto, R. Sassot, and M. Stratmann, “Parton-to-Kaon Fragmentation Revisited,” Phys. Rev. **D95**, 094019 (2017), 1702.06353.
- [76] D. de Florian, R. Sassot, and M. Stratmann, “Global analysis of fragmentation functions for pions and kaons and their uncertainties,” Phys.Rev. **D75**, 114010 (2007), hep-ph/0703242.
- [77] A. Airapetian et al. (HERMES), “Multiplicities of charged pions and kaons from semi-inclusive deep-inelastic scattering by the proton and the deuteron,” Phys. Rev. **D87**, 074029 (2013), 1212.5407.
- [78] C. Adolph et al. (COMPASS), “Multiplicities of charged kaons from deep-inelastic muon scattering off an isoscalar target,” Phys. Lett. **B767**, 133 (2017), 1608.06760.
- [79] G. Agakishiev et al. (STAR), “Identified hadron compositions in p+p and Au+Au collisions at high transverse momenta at $\sqrt{s_{NN}} = 200$ GeV,” Phys. Rev. Lett. **108**, 072302 (2012), 1110.0579.
- [80] D. de Florian, R. Sassot, M. Epele, R. J. Hernández-Pinto, and M. Stratmann, “Parton-to-Pion Fragmentation Reloaded,” Phys. Rev. **D91**, 014035 (2015), 1410.6027.
- [81] J. P. Lees et al. (BaBar), “Production of charged pions, kaons, and protons in e^+e^- annihilations into hadrons at $\sqrt{s}=10.54\text{GeV}$,” Phys. Rev. **D88**, 032011 (2013), 1306.2895.
- [82] M. Leitgab et al. (Belle), “Precision Measurement of Charged Pion and Kaon Differential Cross Sections in e^+e^- Annihilation at $s=10.52\text{GeV}$,” Phys. Rev. Lett. **111**, 062002 (2013), 1301.6183.
- [83] Y.-Q. Ma and J.-W. Qiu, “Extracting Parton Distribution Functions from Lattice QCD Calculations,” Phys. Rev. **D98**, 074021 (2018), 1404.6860.
- [84] E. J. Williams, “Nature of the high-energy particles of penetrating radiation and status of ionization and radiation formulae,” Phys. Rev. **45**, 729 (1934).

- [85] M. Glück and E. Reya, “Boundary Conditions for the Photon Structure Function in the Leading and Subleading Order,” *Phys. Rev.* **D28**, 2749 (1983).
- [86] M. Stratmann, “Parton content of polarized photons: Theoretical status and experimental prospects,” Proceedings, Photon interactions and the photon structure, Workshop, Lund, Sweden, September 10-13, 1998 pp. 135–146 (1998), [hep-ph/9810481](#).
- [87] M. Glück, E. Reya, and A. Vogt, “Photonic parton distributions,” *Phys. Rev.* **D46**, 1973 (1992).
- [88] M. Glück and W. Vogelsang, “Current conservation and the parton structure of the longitudinally polarized photon,” *Z. Phys.* **C57**, 309 (1993).
- [89] M. Glück, M. Stratmann, and W. Vogelsang, “Polarized photon structure at e^+e^- colliders,” *Phys. Lett.* **B337**, 373 (1994).
- [90] G. A. Schuler and T. Sjostrand, “A Scenario for high-energy gamma gamma interactions,” *Z. Phys.* **C73**, 677 (1997), [hep-ph/9605240](#).
- [91] G. A. Schuler and T. Sjostrand, “Parton distributions of the virtual photon,” *Phys. Lett.* **B376**, 193 (1996).
- [92] M. Stratmann and W. Vogelsang, “Spin dependent parton distributions of the longitudinally polarized photon beyond the leading order,” *Phys. Lett.* **B386**, 370 (1996), [hep-ph/9606346](#).
- [93] M. Glück, E. Reya, and I. Schienbein, “Radiatively generated parton distributions of real and virtual photons,” *Phys. Rev.* **D60**, 054019 (1999).
- [94] V. V. Sudakov, “Vertex parts at very high-energies in quantum electrodynamics,” *Sov. Phys. JETP* **3**, 65 (1956).
- [95] J. G. Gatheral, “Exponentiation of Eikonal Cross-sections in Nonabelian Gauge Theories,” *Phys.Lett.* **B133**, 90 (1983).
- [96] J. Frenkel and J. Taylor, “Nonabelian Eikonal Exponentiation,” *Nucl.Phys.* **B246**, 231 (1984).
- [97] C. Berger, “Higher orders in $A(\alpha(s))/[1-x]^+$ of nonsinglet partonic splitting functions,” *Phys.Rev.* **D66**, 116002 (2002), [hep-ph/0209107](#).
- [98] W. Vogelsang, “Large-x resummations in QCD,” *AIP Conf.Proc.* **747**, 9 (2005).
- [99] S. Catani, M. Mangano, P. Nason, and L. Trentadue, “The Resummation of soft gluons in hadronic collisions,” *Nucl.Phys.* **B478**, 273 (1996), [hep-ph/9604351](#).

- [100] N. Kidonakis and G. F. Sterman, “Subleading logarithms in QCD hard scattering,” *Phys.Lett.* **B387**, 867 (1996).
- [101] S. Catani, M. Mangano, and P. Nason, “Sudakov resummation for prompt photon production in hadron collisions,” *JHEP* **9807**, 024 (1998), [hep-ph/9806484](#).
- [102] P. Hinderer, F. Ringer, G. F. Sterman, and W. Vogelsang, “Toward NNLL Threshold Resummation for Hadron Pair Production in Hadronic Collisions,” (2014), [1411.3149](#).
- [103] E. Laenen and S.-O. Moch, “Soft gluon resummation for heavy quark electroproduction,” *Phys. Rev.* **D59**, 034027 (1999), [hep-ph/9809550](#).
- [104] N. Kidonakis, “Resummation for heavy quark and jet cross-sections,” *Int.J.Mod.Phys.* **A15**, 1245 (2000), [hep-ph/9902484](#).
- [105] N. Kidonakis and J. F. Owens, “Effects of higher order threshold corrections in high E(T) jet production,” *Phys.Rev.* **D63**, 054019 (2001), [hep-ph/0007268](#).
- [106] P. Hinderer, F. Ringer, G. F. Sterman, and W. Vogelsang, “Toward NNLL Threshold Resummation for Hadron Pair Production in Hadronic Collisions,” *Phys. Rev.* **D91**, 014016 (2015), [1411.3149](#).
- [107] D. de Florian and S. Frixione, “Jet cross-sections in polarized photon hadron collisions,” *Phys. Lett.* **B457**, 236 (1999), [hep-ph/9904320](#).
- [108] B. Jäger, A. Schäfer, M. Stratmann, and W. Vogelsang, “Next-to-leading order QCD corrections to high p(T) pion production in longitudinally polarized pp collisions,” *Phys.Rev.* **D67**, 054005 (2003), [hep-ph/0211007](#).
- [109] F. Aversa, P. Chiappetta, M. Greco, and J. P. Guillet, “QCD Corrections to Parton-Parton Scattering Processes,” *Nucl. Phys.* **B327**, 105 (1989).
- [110] L. E. Gordon, “Next-to-leading order corrections to inclusive hadron photoproduction,” *Phys. Rev.* **D50**, 6753 (1994).
- [111] P. Hinderer, M. Schlegel, and W. Vogelsang, “Single-Inclusive Production of Hadrons and Jets in Lepton-Nucleon Scattering at NLO,” *Phys. Rev.* **D92**, 014001 (2015), [1505.06415](#).
- [112] N. Kidonakis and J. F. Owens, “Soft gluon resummation and NNLO corrections for direct photon production,” *Phys. Rev.* **D61**, 094004 (2000), [hep-ph/9912388](#).
- [113] M. Sjö Dahl, “Color structure for soft gluon resummation: A General recipe,” *JHEP* **0909**, 087 (2009), [0906.1121](#).

-
- [114] N. Kidonakis and G. F. Sterman, “Resummation for QCD hard scattering,” Nucl.Phys. **B505**, 321 (1997), [hep-ph/9705234](#).
- [115] S. Catani, M. L. Mangano, P. Nason, and L. Trentadue, “The Resummation of soft gluons in hadronic collisions,” Nucl. Phys. **B478**, 273 (1996).
- [116] S. Catani, D. de Florian, M. Grazzini, and P. Nason, “Soft gluon resummation for Higgs boson production at hadron colliders,” JHEP **07**, 028 (2003).
- [117] A. Kulesza, G. F. Sterman, and W. Vogelsang, “Joint resummation in electroweak boson production,” Phys. Rev. **D66**, 014011 (2002), [hep-ph/0202251](#).
- [118] D. de Florian and W. Vogelsang, “Threshold resummation for the inclusive-hadron cross-section in pp collisions,” Phys. Rev. **D71**, 114004 (2005), [hep-ph/0501258](#).
- [119] A. D. Martin, W. J. Stirling, R. S. Thorne, and G. Watt, “Parton distributions for the LHC,” Eur. Phys. J. **C63**, 189 (2009), [0901.0002](#).
- [120] X. Chu, E.-C. Aschenauer, J.-H. Lee, and L. Zheng, “Photon structure studied at an Electron Ion Collider,” Phys. Rev. **D96**, 074035 (2017), [1705.08831](#).
- [121] T. Kaufmann, A. Mukherjee, and W. Vogelsang, “Hadron Fragmentation Inside Jets in Hadronic Collisions,” Phys. Rev. **D92**, 054015 (2015), [1506.01415](#).
- [122] Y.-T. Chien, Z.-B. Kang, F. Ringer, I. Vitev, and H. Xing, “Jet fragmentation functions in proton-proton collisions using soft-collinear effective theory,” JHEP **05**, 125 (2016), [1512.06851](#).
- [123] D. P. Anderle, T. Kaufmann, M. Stratmann, F. Ringer, and I. Vitev, “Using hadron-in-jet data in a global analysis of D^* fragmentation functions,” Phys. Rev. **D96**, 034028 (2017), [1706.09857](#).
- [124] M. Procura and I. W. Stewart, “Quark Fragmentation within an Identified Jet,” Phys. Rev. **D81**, 074009 (2010), [Erratum: Phys. Rev.D83,039902(2011)], [0911.4980](#).
- [125] M. Procura and W. J. Waalewijn, “Fragmentation in Jets: Cone and Threshold Effects,” Phys. Rev. **D85**, 114041 (2012), [1111.6605](#).
- [126] S. Keppeler and M. Sjodahl, “Orthogonal multiplet bases in $SU(N_c)$ color space,” JHEP **09**, 124 (2012).

Acknowledgements

An dieser Stelle möchte ich mich bei all jenen bedanken, die maßgeblich zur Entstehung dieser Arbeit beigetragen haben.

An erster Stelle gilt mein Dank meinem Doktorvater Prof. Dr. Andreas Schäfer, der mir überhaupt erst die Möglichkeit gab, mich in diesem Forschungsgebiet zu vertiefen und darin zu promovieren. Über viele Jahre hinweg unterstützte er mich, hatte stets ein offenes Ohr und hielt gute Ratschläge für mich bereit. Von seiner Betreuung konnte ich schon bei meiner Bachelor- und Masterarbeit profitieren und möchte mich dafür herzlichst bedanken.

Des Weiteren danke ich Prof. Dr. Werner Vogelsang vielmals für die gemeinsame Zusammenarbeit. Ohne seine fachliche Expertise und seine nie erschöpften Ideen wäre diese Arbeit nie möglich gewesen. Stets hatte er Antworten auf meine Fragen parat und wurde nie müde, mir zu helfen, diese Arbeit zu meistern.

Außerdem danke ich Dr. Melanie Pfeuffer für die Bereitstellung ihres numerischen Codes und für die Zeit, die sie sich zu Beginn meiner Promotion genommen hat, mich in dieses Thema einzuführen. Daneben danke ich Dr. Maxime Levillain für die Bereitstellung der COMPASS-Daten.

All meinen Kolleginnen und Kollegen, die zu Freund*innen wurden, möchte ich für die gemeinsam verbrachte Zeit danken. Vor allem seien hier Felix Hofmann, Jakob Simeth, Dr. Maximilian Emmerich und Dr. Jacob Wellnhofner für all das gemeinsam Erlebte gedankt. Für die Korrektur meiner Arbeit danke ich ihnen ebenso, zusätzlich auch Maxi Vilser, Michael Kerscher, Peter Plößl und Matthias Strohmaier.

Auch Daniel Miehling, Johanna Ertl und Anika Kup möchte ich meinen herzlichen Dank aussprechen. Dafür, dass sie mir immer meinen Rücken gestärkt haben, immer an mich glaubten, mir mit ihrer Geduld und Zuversicht stets meine Sorgen nahmen und mich in meinem Tun zu jeder Zeit bestärkten.

Und ganz besonders möchte ich mich bei meiner Familie bedanken, für all ihre Liebe und ihre Unterstützung. Meinen Eltern, Edeltraud und Lothar Uebler, die mir dieses Studium erst ermöglicht haben, mich förderten und unterstützten, und bei all meinen Entscheidungen immer hinter mir standen. Auch meinen Geschwistern, Susanne, Monika und Christian möchte ich danken. Dafür, dass sie mir als Vorbilder dienten, meinen Wissensdurst und meine Neugierde förderten und stets und in allen Lebenslagen für mich da waren.

Euch allen, vielen Dank!